Thermodynamic Controls on the Global Ocean Overturning Circulation

Emily Rose Newsom

A dissertation submitted in partial fulfillment of the requirements for the degree of

Doctor of Philosophy

University of Washington
2016

Reading Committee:

Cecilia Bitz, Chair
Edwin Waddington, Co-Chair
Peter Rhines

Program Authorized to Offer Degree:

Earth and Space Sciences

University of Washington

Abstract

Thermodynamic Controls on the Global Ocean Overturning Circulation

Emily Rose Newsom

Chair of the Supervisory Committee:
Professor Cecilia Bitz
Department of Atmospheric Sciences

This dissertation explores the fundamental relationship between the spatial distribution of air-sea flux and the structure of the ocean's Global Overturning Circulation (GOC). The GOC describes the circulation of ocean waters from the surface ocean at high latitudes to the deep and abyssal ocean, through the interior ocean, and ultimately back to ocean surface. In steady-state, this GOC persists even while the ocean density structure, which differs greatly with location, remains steady in time. To sustain the density structure, flow through the ocean must encounter sources and sinks of density at the ocean surface. The input of heat and freshwater fluxes at the surface supply the surface sources and sinks of density. Here, this thermodynamic requirement to maintain a steady state is exploited using an established framework — the Water Mass Transformation Framework — in a novel application: to arrive at a quantitative exploration of the relationship between the three-dimensional GOC and the distribution of surface heat and freshwater fluxes on global scale.

This global analysis is approached in several steps. First, the downwelling branch of the

GOC is explored. Specifically, the WMT framework is applied to examine how the dense-water formation in the Southern Ocean relates to regional surface fluxes in a fully coupled climate model. This study demonstrates that the surface processes mediating heat loss from the ocean have a fundamental influence on how dense-water is circulated through the Southern Ocean. In the following study, the upwelling branch of the GOC (required to compensate for the formation of dense waters at polar surfaces) is considered. Specifically, to complete an overturning circulation, dense waters must form at the surface, circulate downward, and then return to the surface in a manner that maintains a steady global density structure. This study explores, from a theoretical perspective, how water can circulate between regions of the ocean surface in a thermodynamically consistent manner. A theoretical set of governing relationships between interior flow, surface density flux, and interior density transport are derived to reveal an important coupling between the spatial pattern of surface density flux and interior dynamics. In the final study of this dissertation, these theoretical relationships are tested in a fully-coupled global climate model. This global scale analysis reveals that the GOC transports buoyancy from the Indo-Pacific Oceans, through the Southern Ocean, and into the Atlantic Ocean; this transport is sustained by regional differences in surface heat and freshwater fluxes. To close, this dissertation offers an explanation for why the system may be organized into its current structure. Specifically, a hypothesis is advanced that argues for a preconditioning in the climate system towards an ocean circulation which conveys buoyancy out of the Indo-Pacific, through the Southern Ocean, and towards the North Atlantic. This preconditioning, it is suggested, arises from the location of these major ocean basins relative to the distribution of incoming solar radiation, two constrained features of the currently climate system.

Table of Contents

Acknowledgments

It is impossible to imagine my graduate school experience without the incredible group of mentors, friends, and collaborators that have supported me along the way. Before presenting my work, I want to express my sincere gratitude to this community. Above all, I am grateful to my adviser, Cecilia Bitz. Cecilia embodies a rare combination of qualities: she is a world-class scientist, one who has taught me invaluable lessons about how to define and scope scientific questions, has strengthened my curiosity in the physical world, and who's expertise and insights have been fundamental to my research. Yet, despite her personal success as a scientist, Cecilia simultaneously supports her students to follow their own instincts and build their own intuition. I owe my excitement for new, yet-unanswered questions to her. I'd also like to thank the members of my reading committee — Professor Ed Waddington and Professor Peter Rhines. Both Ed and Peter have offered me their time, wisdom, and support. I've learned so much from each of them over the course of my education, and I am confident I have had the fortune of learning about the ocean and cryosphere from the world's experts. I'm also grateful to the other members of my PhD committee: Dargan Frierson, Gerard Roe, Gregory Johnson, and LuAnne Thompson. Each has a unique and fascinating way of seeing the climate system, and I am lucky to have been exposed to each of their perspectives. Beyond my committee, I want to acknowledge the amazing group of scientists with whom I've had the privilege of collaborating; many thanks to Kyle Armour, Frank Bryan, Peter Gent, and Ryan Abernathey.

I feel immensely grateful for the group of students in Earth and Space Sciences, Atmospheric Sciences, and Oceanography, who have made my time at UW significantly more fun. I am particularly grateful for my friends Kyle Armour, Stuart Evans, Kat Huybers, Brad Markle, Ed Blanchard-Wrigglesworth, Elizabeth Maroon, Judy Twedt, Max Stevens, David Shean, and Ashley Maloney, though there are many many more to thank as well. Thanks to LuAnne Thompson and Terrie Klinger for championing the UW Program on Climate Change and the UW IGERT Program on Ocean Change, two programs which have greatly enriched my experience at UW and broadened my perspective as a scientist. The faculty, students, and staff at UW have created a singularly collaborative and supportive community. I am truly grateful to have been a part of it.

Dedication

To my family, without whom this, and most everything, would have been impossible.

Chapter 1

Introduction

Over the last century, oceanographers have grappled with the implications of dense-water formation. Specifically, vigorous heat loss and salinity changes in the high latitudes make surface waters very dense, driving them to sink from the surface to great depths in several specific regions. This dense-water formation implies a cycle, or an "overturning circulation," by which, after sinking into the ocean's abyss, these waters can gain buoyancy within the ocean's interior, and be drawn back to the surface again. The deep-water mass formed in the Northern Hemisphere, North Atlantic Deep Water (NADW), is produced in several localized regions in the North Atlantic Ocean. Similarly, the formation of the the dense water in the Southern Hemisphere, known as Antarctic Bottom Water (AABW), occurs in several distinct locations in the ocean surrounding Antarctica. The "coming up" component of this circulation is far harder to define with such precision. The upwelling of deep waters involves a myriad of processes that occur over a range of spatial scales and are distributed across many locations in the vast global ocean. Decades of study have led to an emerging, though incomplete, understanding of how oceanic processes perpetuate the cycling or seawater through the global ocean.

Much of this work owes its foundation to a seminal speculation that upwelling was accomplished through the breaking of internal waves across interior stratification in the ocean's interior (Munk, 1966). Sufficient mixing, Munk reasoned, could account for the gradual

upwelling and warming (and thus, lightening) of the dense, cold waters occupying the deep ocean. Broecker (1991) argued that this mixing occurred gradually as dense NADW flowed from the deep Atlantic, through the Southern Ocean, and into the Pacific— a "Great Ocean Conveyor." However, the magnitude of mixing required to sustain this process far exceeded mixing rates that were observed *in situ*. This internal mechanism of upwelling, as required by Munk's hypothesis, became known as the ocean's "missing mixing" (Munk, 1966; Broecker, 1991).

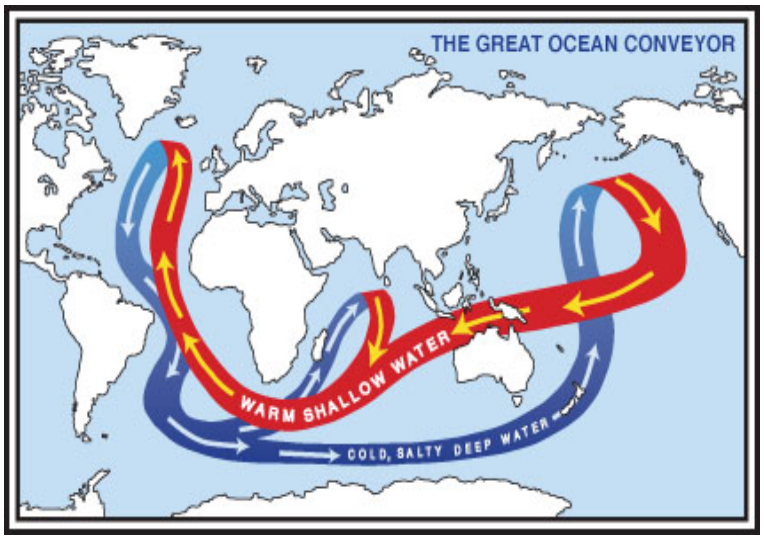

Figure 1.0.1: An early schematic depicting the "Great Ocean Conveyor," as proposed by Broeker, 1991.

Toggweiler and Samuels (1995) made what is arguably the second seminal leap forward in our understanding of the ocean overturning circulation. They argued that the zonally unbounded geometry of the Southern Ocean, and the strong zonal winds that blow across its surface, provided a pathway by which the majority of waters above 2000 meters can be pumped up to the ocean surface along density surfaces, with little to no mixing whatsoever (via "adiabatic" upwelling). This Southern Ocean wind-driven pathway largely circumvented the need for non-physical mixing rates to close the global ocean overturning circulation; this pathway thus rectified, in part, the "missing mixing" dilemma. This insight shifted the

paradigm by which ocean overturning was commonly described and studied. A "two-celled" picture of overturning emerged, supported quantitatively by a stream function of volume transport, calculated from the zonal sum of velocity along each latitude circle. This stream function, by construction, highlights key features of *meridional*, zonally-averaged structures in ocean overturning. This streamfunction clearly depicts two deep, global-scale, counter-rotating overturning cells- the "Upper" and "Lower" cells, which sit under two shallow, but vigorous Equatorial Cells that diverge at the Equator. Together, these circulation features imply important meridional structure in the pathways water takes as it circulates from the surface to depth; a multitude of subsequent studies have endeavored to understand this structure, and the dynamics of this "Meridional Overturning Circulation" (MOC), as it has come to be called.

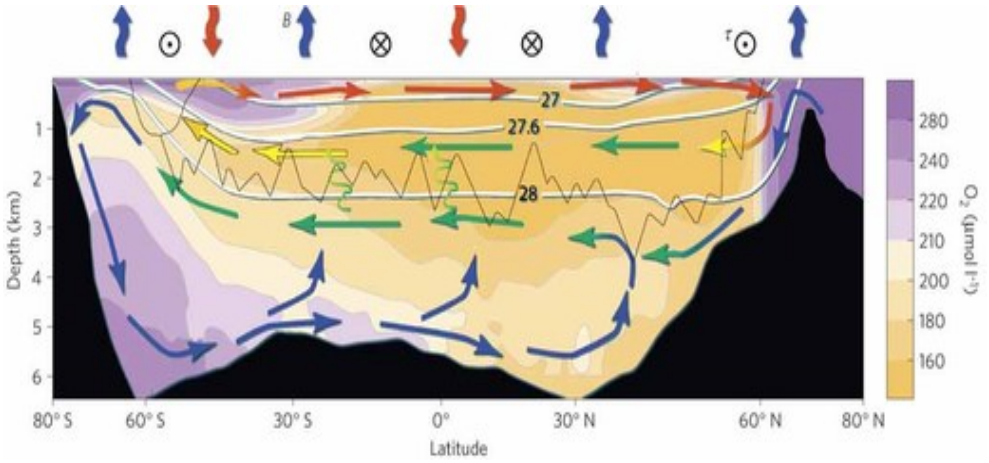

Figure 1.0.2: A schematic of the the MOC from Marshall and Speer, 2012. Arrows depicting direction of circulation are superimposed over the distribution of dissolved oxygen. Arrow colors represent average water temperature from colder (blue) to warmer (red) waters. Positive and negative surface fluxes, as well as wind-stress directions, are represented at the surface. Note that this description of the MOC is characterized by two major cells, emanating from each pole and each outcropping in the Southern Ocean.

A great many studies of MOC dynamics approached the problem from a zonal-mean perspective, either theoretically (Marshall and Radko, 2003), or using idealized ocean models described by simple geometries, particularly that of a zonally re-entrant "Southern Ocean"

channel, appended onto a single northern basin, or "basin and channel models" (e.g. Abernathey et al., 2011; Wolfe and Cessi, 2011; Nikurashin and Vallis, 2011, 2012). Such an idealized approach was taken by studies that resolved ocean dynamics across a spectrum of complexities, ranging from those that parameterized ocean eddies (Nikurashin and Vallis, 2011, 2012), to those that permitted or resolved transient eddies (Morrison et al., 2011; Munday et al., 2013; Abernathey et al., 2011; Wolfe and Cessi, 2011). Together, these studies probed the interaction among NADW formation rates, Southern Ocean wind and buoyancy flux, transient eddies, and the mean flow. They tended to focus attention on the strength and dynamics of the Upper Cell because of its direct connection to downwelling in the Atlantic (Marshall and Radko, 2003; Radko and Kamenkovich, 2011), even probing the system's dynamics in the complete adiabatic limit (which eradicates the Lower Cell component of the MOC completely) (Wolfe and Cessi, 2011, 2015). Interactions with shallow Equatorial Cells are either ignored in these studies, or highly simplified; further, the relationship between the deep MOC cells and low-latitude changes in surface flux are rarely explored. In sum, a conclusion that could be drawn from this literature is that global MOC dynamics are primarily sensitive to surface processes in the Southern Ocean (the location of descending and ascending branches of the MOC) and the North Atlantic (the location of the second descending branch of the MOC).

While this body of work has advanced understanding of ocean dynamics substantially, a recent study has drawn attention to the limitations inherent in the two-celled MOC paradigm that these studies reinforce. Talley (2013) argued, based on the global distribution of water mass properties and heat budgets, that the actual overturning of ocean waters has a rich, three-dimensional structure. Instead of two distinct cells, Talley argued, the circulation is better described as a continuous pathway that (on average) transits all ocean basins, or a "Global Overturning Circulation" (GOC). Talley's three-dimensional description acknowledges the key role of the Southern Ocean, which mediates exchanges among all ocean basins,

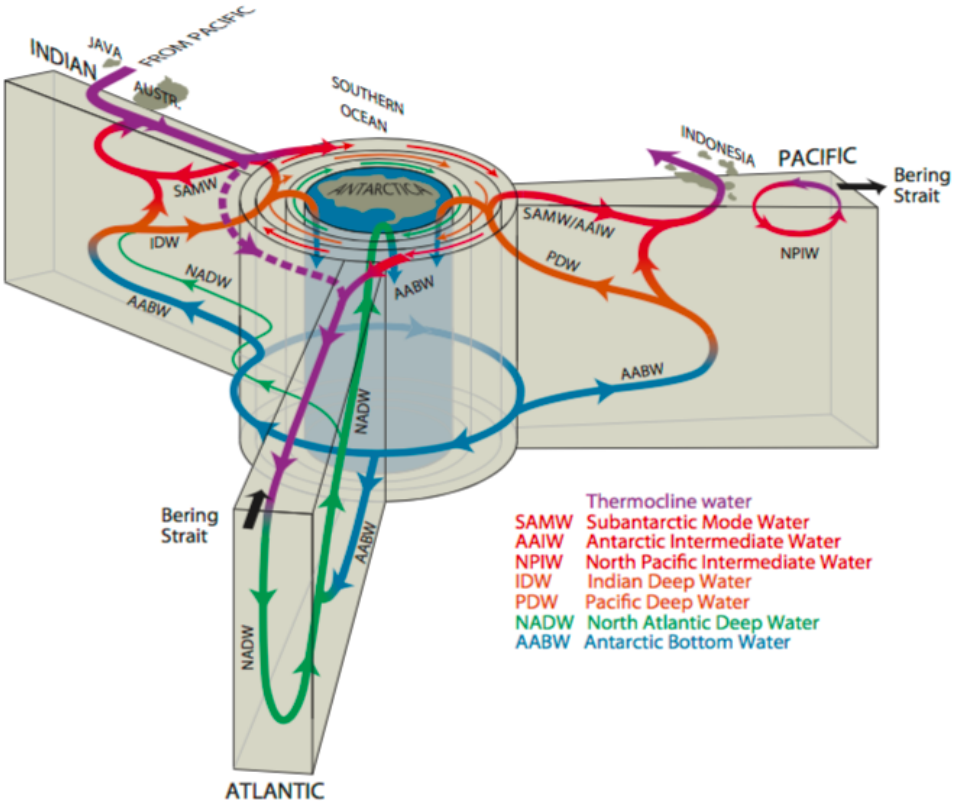

Figure 1.0.3: Schematic of the GOC from Talley [2013] illustrating the flow, and water-mass transformation, between key water masses in each major ocean basin.

both by lateral flows in its vigorous circumpolar currents, and via flows along isopycnals (surfaces of constant density), which are drawn to the surface by the intense westerly winds. This wind-driven process enables both meridional and vertical transport, with little mixing. In addition, Tally's paradigm re-emphasizes the vital role of deep mixing in the Indian and Pacific Oceans, which diffusively enables dense water to be pulled upwards towards lighter-density seawater classes (e.g. Munk, 1966; Broecker, 1991).

These important dynamical regimes (the Indo-Pacific and Southern Oceans) are coupled by the dominant export of AABW into the Indian and Pacific Oceans, where it is converted into lighter waters that are exported back into the Southern Ocean. This Indo-Pacific AABW circulation is essential in sustaining the three-dimensional circulation, though its structure is obscured in the zonal average. This thesis addresses this fundamental, and under-explored,

component of the climate system. I will do so by viewing the problem through a mostly thermodynamic lens. Each chapter will exploit, in differing ways, a theory that relates the ocean's physical circulation to the spatial distribution of heat and freshwater fluxes, or the Water Mass Transformation (WMT) Framework (Walin, 1982). This framework, and theory underlying it, will be discussed, and interpreted, in differing ways in each chapter.

In Chapter 2, I apply the WMT Framework to investigate high-latitude processes that sustain the formation of AABW and drive its descent into the abyssal ocean. While this water mass is an essential component of the overturning circulation, its formation is often oversimplified in process studies and under-emphasized in many theories of larger-scale ocean dynamics, as will be discussed. In Chapter 2 I make the case that Antarctic sea ice processes have a vital role in the formation of AABW; as a result, these processes also exert important controls on the system's response to a climate perturbation.

In Chapter 3, I consider the opposing branch of the circulation — the interior pathways by which dense waters are returned to the ocean surface. This study is a theoretical discussion of how upwelling and the structure of the ocean circulation can be related to thermodynamics. There, I reexamine the theory underlying the WMT Framework to develop a set of governing equations that are intended to shed new light into the circulation and its adiabatic and diffusive components. These theoretical relationships suggest that the spatial distribution of surface heat and freshwater fluxes (through their combined effect on ocean density, or the "surface density flux") has a fundamental impact on the organization of the interior ocean circulation.

In Chapter 4, I investigate the relationship between the interior circulation and the distribution of surface density flux in a more complex and realistic system— a fully coupled Global Climate Model. The primary focus of the study is to assess how the three-dimensional

structure of the GOC corresponds to differences in surface processes in the Atlantic, Indo-Pacific, and Southern Oceans. Inspired by my findings, I propose a conceptual model to explain why the GOC has developed its current structure.

In Chapter 5, I synthesize the results of these studies to advance a new perspective on the role of the Global Overturning Circulation in the global climate system.

Chapter 2

Southern Ocean Deep Circulation and Heat Uptake in a High-Resolution Climate Model

2.1 Introduction

The vast majority of the energy gained by the climate system during periods of global radiative imbalance is stored within the global ocean (Levitus et al., 2001; Abraham et al., 2013). The effective volume of ocean available to warm at a given time is set by the rate at which heat can be moved from the surface mixed layer into the deep ocean Hansen et al. (1985), redirecting heat that would otherwise warm the surface. Therefore, deep ocean heat uptake plays a critical role in slowing the pace of global surface warming in response to greenhouse gas forcing (Gregory, 2000; Held et al., 2010; Raper et al., 2002; Kostov et al., 2014).

The deep and abyssal ocean is filled by water masses formed at the high-latitudes; deep ocean heat uptake proceeds through the warming and redistribution of these polar-sourced water masses. The deep water mass formed at the Southern Ocean surface, Antarctic Bottom Water (AABW), comprises a large fraction of the oldest waters found in the global abyssal ocean (Johnson, 2008; Gebbie and Huybers, 2012). Consequently, the heat content

of the global abyssal ocean is directly influenced by Southern Ocean processes. Indeed, the estimated 0.1 Wm-2 rate of global ocean heat uptake below 2000 m over the last 30 years was driven primarily by the warming of AABW. This warming is likely linked to changes in the surface ocean and climate around Antarctica (Purkey and Johnson, 2010, 2013). Further, the impact of ocean heat uptake is particularly high within the Southern Ocean, where it acts to curb surface warming that would otherwise be strongly amplified by the combined effects of the sea-ice albedo feedback and a stably stratified atmosphere Armour et al. (2013).

While the Southern Ocean plays a fundamental role in climate change, the unique influence of small-scale processes on its circulation presents modeling challenges. Processes such as mesoscale eddy mixing, internal wave breaking, turbulent overflows, and convection have first order effects on the overturning circulation. Because these processes are often sub-grid scale in modern general circulation models (GCMs), they are either parameterized or under-resolved. The simplest and most ubiquitous parameterization is simply grid-scale diffusion and viscosity, which is often prescribed by numerical considerations rather than physical ones. Deep ocean circulation and stratification are quite sensitive to diapycnal diffusion (Bryan, 1987; Cummins et al., 1990), and diffusion (including spurious numerical diffusion) itself is resolution dependent (Griffies et al., 2000; Hill et al., 2012; Urakawa and Hasumi, 2014). Coarse resolution models employ mesoscale eddy transport schemes, comprised of isopycnal diffusion (Redi, 1982)) and eddy-induced advection (Gent and McWilliams, 1990) (hereafter GM). These parameterizations involve tuning parameters that strongly influence the circulation (Danabasoglu and McWilliams, 1995; Gnanadesikan, 1999; Pradal and Gnanadesikan, 2014; Gnanadesikan et al., 2015). Overflow parameterizations have been employed with limited success (Danabasoglu et al., 2012; Snow et al., 2015), as have abyssal tidal mixing schemes (Jayne, 2009). The recent advent of global mesoscale resolving/permitting ocean models allows some such parameterizations and other scale-dependent processes to be

evaluated against more direct explicit simulation, especially with respect to the mesoscale (Griffies et al., 2015).

The potential for inadequate model resolution to bias Southern Ocean dynamics has garnered substantial attention in the literature. The focus has been mostly directed towards the behavior of the upper cell of the meridional overturning circulation (MOC) (see e.g. Henning and Vallis, 2005; Hallberg and Gnanadesikan, 2006; Gent and Danabasoglu, 2011; Bryan et al., 2014; Farneti et al., 2010; Abernathey et al., 2011; Farneti et al., 2014; Gent, 2015). In contrast, the impact of model resolution on lower cell of the MOC and its relationship to Southern Ocean abyssal heat uptake is relatively unexplored. This is the aim of our paper.

The lower MOC is sustained by processes that make surface water denser, "pushing" water into the abyssal ocean, and processes that reduce the density of dense water in the interior, "pulling" it upwards again. In the abyssal ocean, water is "pulled" up via diapycnal mixing, the magnitude of which is likely a key control on abyssal overturning strength (Nikurashin and Vallis, 2011, 2012). Such mixing is accomplished by the breaking of locally generated internal waves over bathymetric features, geothermal heating, remote tidal dissipation and entrainment across strong density gradients in localized overflows (Garabato et al., 2004, 2007; Nikurashin and Vallis, 2012; Lavergne et al., 2014). Transient eddy fluxes, which redistribute potential energy and result in the northward transport of dense water in the abyss, have also been linked to mixing rates and overturning strength because of their influence on abyssal stratification (Ito and Marshall, 2008). A misrepresentation of these abyssal diapycnal mixing processes could introduce biases into the lower cell dynamics.

The descending branch of the lower cell is sustained by buoyancy loss at high latitudes via the interaction of cold, salty water that is rejected during sea ice growth (especially in

coastal polynyas and leads); extremely cold, fresh water formed from sub ice-shelf melting; and comparatively warm, salty Lower Circumpolar Deep Water (LCDW) that upwells near the coast (Orsi et al., 1999; Jacobs, 2004; Gordon, 2001). Polynyas and leads, which are key moderators of heat loss and brine rejection, form on spatial and temporal scales below the resolution of the current generation of GCMs (Stössel et al., 2007; Willmott et al., 2007). Additionally, recent studies have suggested that transient eddies are key to the transport of AABW across the continental shelf front (where the deformation radius is on order 1-10 km), as is the input of momentum from coastal easterly winds (Stewart and Thompson, 2012, 2015; Thompson and Naveira Garabato, 2014). In sum, sea ice formation, the formation of dense plumes, transient cross-shelf flow, and sub ice-shelf processes all occur on scales smaller than the grid spacing of most GCMs; as a result, most models misrepresent the volume and formation rate of AABW. Indeed, Heuzé et al. (2013) found that no model participating in phase 5 of the Coupled Model Intercomparison Project (CMIP5; Taylor et al., 2012) formed AABW via the sinking of shelf waters. Instead the majority of models formed bottom waters by (possibly spurious) open ocean convection, leading to large biases in the abyssal ocean density simulated in most of the CMIP5 models analyzed in their study.

Here, we explore how increasing model resolution in the ocean and sea ice components influences the dynamics of the lower cell of the MOC. We are motivated by the questions: does resolution alter the lower cell in the mean state? And, does resolution affect the rate of Southern Ocean heat uptake under greenhouse warming? Ours is, to the best of our knowledge, the first study to investigate the resolution dependence of this circulation in a coupled model. We use a GCM configured at resolution high enough to capture coastal polynyas and to explicitly resolve transient eddies throughout much of the global ocean, and compare the results to a lower resolution counterpart, configured at a resolution typical of CMIP5 models.

2.2 Model setup and analysis

2.2.1 Model and Experiments

We use the Community Climate System Model version 3.5 (CCSM3.5), with ocean and sea ice at two resolutions, while maintaining identically configured atmosphere and land components. The high-resolution version (HR) is run with 0.1° resolution in the sea ice and ocean components. The comparatively low-resolution version (LR) is run at 1° resolution in the ocean and sea ice. The atmospheric component has a finite-volume dynamical core and is run in both cases at identical resolution: 26 vertical levels, with horizontal resolution of 0.47° x 0.63° (as in Gent et al., 2010). The horizontal resolution of the land model is the same as for the atmosphere. The HR and LR setups are identical to those used in Kirtman et al. (2012); Bitz and Polvani (2012) and Bryan et al. (2014).

HR has a sufficiently fine ocean horizontal grid to be deemed eddy resolving at low and mid latitudes and eddy permitting at very high latitudes (south of 50°S), following Smith et al. (2000). Grid spacing near the Antarctic coast is 3-5 km, which we will show improves the resolution of sea ice dynamics. In contrast, LR is non-eddy resolving, and relies on the GM eddy parameterization with a spatially and temporally varying GM coefficient that depends on the square of the local buoyancy frequency (see Danabasoglu and Marshall, 2007; Gent and Danabasoglu, 2011). No overflow parameterizations were employed in this model, and neither of the resolutions examined here exhibits grid-scale-size, full-depth open-ocean convection (a problem endemic to some GCMs, i.e., Heuzé et al. (2013). Control integrations of HR and LR were run with 1990âĂŹs carbon dioxide mixing ratios for 167 yr. Kirtman et al. (2012) describe in depth the configuration and climate of the control integrations.

Perturbed runs were branched from the control integrations of each resolution (LR and

HR) at year 77. Each perturbed run was subject to a 1 percent increase in the carbon dioxide mixing ratio of the atmosphere until carbon dioxide doubling was reached at year 147; thereafter, carbon dioxide mixing ratios were held fixed for the next twenty years. To minimize the impact of possible climate drift, we define the âĂIJresponseâĂİ or âĂIJanomalyâĂİ of a given field in a perturbed run as the difference between its average during the 20-year period after carbon dioxide doubling and its average during the contemporaneous 20 years in the control integration. Because of the computational expense at high resolution, our control runs are necessarily short relative to the equilibration timescale of the deep ocean, and there is still a small drift in deep ocean temperatures from the branch point to the end of the control runs at either resolution (see Kirtman et al. (2012)). We find this drift has a minimal effect on isopycnal inflation (explained subsequently) in our control simulations. However, we cannot conclusively rule out that the features we diagnose are transient.

One limitation of this model, of particular relevance to this study, is the absence of interactive ice shelves. Instead, the mass balance of Antarctica is enforced by uniformly freshening and cooling the ocean at the continental margin by any precipitation reaching the Antarctic continent that causes the snow depth to exceed a maximum value of 1m, termed âĂIJice runoffâĂİ. Raising carbon dioxide results in an increase in ice runoff owing to higher snowfall rates over Antarctica from increased poleward moisture transport. However, in this model, the reduction in sea ice formation and increase in precipitation over the ocean near Antarctica are a much greater source of anomalous freshwater than Antarctic ice or meltwater runoff (see Kirkman IV and Bitz (2011).

2.2.2 Isopycnal Overturning and Water Mass Transformation

A challenge to understanding the impact of model resolution on circulation is the certainty that increasing resolution will affect multiple processes simultaneously. We try to assess the relative importance of different processes in altering the circulation by employing the water-

mass-transformation framework, first introduced by Walin (1982) and further developed in many subsequent studies (e.g., Speer and Tziperman, 1992, Marsh et al., 2000, Bryan et al., 2006, Iudicone et al., 2008). We consider the ocean circulation most directly related to stratification by calculating an overturning streamfunction along surfaces of constant density [D*öös* and Webb, 1994]. We refer to the time average of this field,

$$\Psi^{\sigma}(\sigma, y) = -\frac{1}{t_1 - t_0} \int_{t_0}^{t_1} \int_{x_W}^{x_E} \int_{-B(x,y)}^{z(x,y,\sigma,t)} v(x, y, \sigma, t) dz dx dt \tag{2.1}$$

as the isopycnal MOC, where v is the total meridional velocity (including the bolus velocity in LR), σ is potential density, x is longitude (positive eastward), y is latitude (positive northward), z is depth (positive upward), B is the ocean bottom depth, and t is time. The component of the MOC from Eq. 2.1 with v equal to the time-mean velocity and σ equal to the time-mean isopycnal depth is the mean isopycnal MOC, Ψ^{σ}_{m}. The impact of transient eddies on the isopycnal MOC (or the transient eddy-induced isopycnal MOC, Ψ^{σ}_{E} can be expressed as the difference between the total and mean MOC components:

$$\Psi^{\sigma}_{E} = \Psi^{\sigma} - \Psi^{\sigma}_{m} \tag{2.2}$$

The transient eddy-induced MOC emerges as a result of explicitly resolved eddies in HR, while in LR, it is computed from the GM parameterized bolus velocity field using Eq. 2.1 with $v = v_{bolus}$. At either resolution, the impact of standing eddies and gyres as well as any steady correlations between density and non-zonally uniform flow can be expressed as the difference between the mean isopycnal MOC and a depth-space MOC, Ψ_z (Dufour et al., 2012), the latter of which is calculated in the more traditional method relative to surfaces of constant depth.

The isopycnal circulation Ψ^{σ} persists on a global scale because of the continual redistribution of seawater between density classes. As illustrated in Fig. 2.2.1, the volume of a

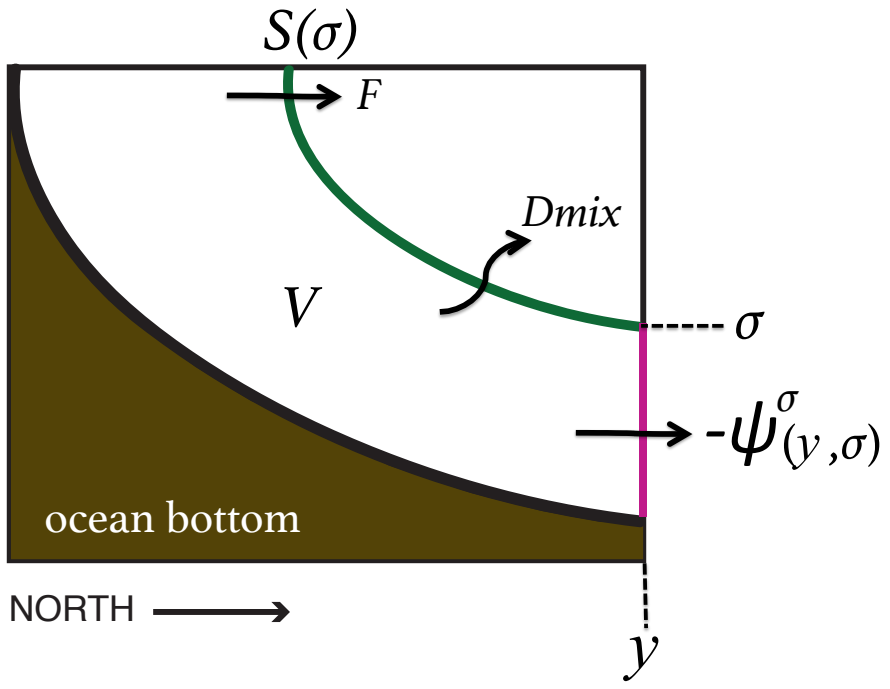

Figure 2.2.1: Schematic to demonstrate processes controlling the volume V poleward of an isopycnal surface s and latitude y in Eq. (3). Volume fluxes into V include contributions of surface transformation induced by surface fluxes south of the outcrop at $S(\sigma)$ (component F), contributions from diapycnal mixing across the isopycnal surface σ (component D_{mix}), and total southward flow across y and below σ (component Ψ^{σ}). Colors are added to the lines denoting the isopycnal surface (green), ocean surface (black), and latitude transect (pink) to orient the reader to the components of diapycnal volume flux illustrated in Figs. 2.3.6 and 2.4.3

region of the ocean, V, below and southward of isopycnal σ and latitude y varies with the volume flux across its boundaries. Considering the volume, V, south of any given σ and y, the volume inflation can be expressed as:

$$\frac{\partial}{\partial t}(V(\sigma, y, t)) = \Psi^{\sigma}(\sigma, y, t) - [F(\sigma, y, t) + D_{mix}(\sigma, y, t)] \tag{2.3}$$

where the latter two terms together represent water mass transformation, with $F(\sigma, y, t)$ induced by air-sea fluxes at the sea surface (surface transformation) and $D_{mix}(\sigma, y, t)$ induced by mixing across density surfaces in the interior (interior transformation). A general definition of surface transformation, F_{gen}, is:

$$F_{gen}(\sigma,t) = -\frac{\partial}{\partial\sigma}\int\int_{A([\sigma^*>\sigma]} \lambda_{surf}(x,y,t)dA \tag{2.4}$$

where λ_{surf} is the spatial distribution of surface density flux, a function of heat and freshwater fluxes (f_{heat} and f_{water}, defined positive downward):

$$\lambda_{surf}(x,y,t) = \frac{\alpha}{c_p} f_{heat}(x,y,t) - \frac{\rho_0}{\rho_{fw}}\beta S_0 f_{water}(x,y,t) \tag{2.5}$$

Here, α and β are the coefficients of thermal expansion and saline contraction, respectively, c_p is the specific heat of seawater, ρ_0 is a reference seawater density, ρ_{fw} is the density of freshwater, and S_0 is a reference salinity. To directly compare surface transformation to the circulation at a given latitude y, as in Eq. 2.3, we must consider only the net surface transformation occurring south of y, which we call simply F. This can be calculated as

$$F(\sigma,y,t) = F_{gen}(\sigma,t)\mathcal{H}[\sigma - \sigma_{min}(y,t)] \tag{2.6}$$

where $\mathcal{H}$ is the Heaviside function and σ_{min} is the lowest density to outcrop at latitude y. The flux F is positive toward lighter densities for direct comparison with the MOC in the Southern Hemisphere. The interior transformation D_{mix} can be defined similarly to F; however, doing so requires knowledge of time-varying, three-dimensional diffusive fluxes, which were not saved for these simulations because of data storage limitations. Instead, we follow Marsh et al. (2000) and calculate D_{mix} at latitude y as a residual of the other terms in Eq. 2.3. This effectively measures the path integrated interior transformation at each density between the surface and y. With this method, we cannot identify the specific mixing processes responsible for interior diapycnal volume fluxes, though we can gain insight into the relative importance of surface and interior transformation on MOC strength.

It is important to note two caveats to our analysis. First, we use a reference pressure of 2000 dbar (1 dbar = 10^4 Pa) to calculate potential density, known as σ_2, for both our sur-

face transformation and MOC calculations, since our focus is on the deep ocean; however, the choice of reference pressure may affect our results (Iudicone et al., 2008; Stewart and Thompson, 2015). Second, because of prohibitive amounts of data generated in HR, we were restricted to saving monthly data, meaning that higher-frequency transient behavior is not captured in our analysis. Ballarotta et al. (2013) explored the temporal and spatial scales at which transient behavior was most influential: though daily time scales were important to the upper MOC cell, their impact was much smaller in the lower MOC cell. Furthermore, in a spectral analysis of eddy heat fluxes in the same class of eddy- resolving model, Abernathey and Wortham (2015) found that sub-monthly variability makes a negligible contribution to the total heat flux. Thus, we expect to capture the majority of transient fluctuations most relevant for our analysis.

2.3 Control State Results

It is essential to understand the mean state of the Southern Ocean at each resolution to interpret how resolution affects the response to carbon dioxide forcing. Compared to LR, HR produces consistently saltier and colder waters on the continental shelf and throughout the deep Southern Ocean (Fig. 2.3.1a-f). In the abyssal ocean (below 4000 meters) waters are colder by approximately 0.45°C and saltier by approximately 0.016 psu on average. Near the surface, HR forms a fresher branch of Antarctic Intermediate Water (AAIW) and warmer surface water. In comparison to World Ocean Circulation Experiment (WOCE: publically available at http://seahunt.ucsd.edu/find.html) hydrographic data, both model resolutions form deep waters that are too saline. This salinity bias is more pronounced in HR, which may be the result of non-local processes impacting the salinity of upwelling circumpolar deep water (CDW), such as by brine rejection from sea ice in the Northern Hemisphere [Kirtman et al., 2012]. Bottom waters formed in HR are too cold in some regions, while bottom waters in LR are consistently too warm. An example of these large-scale properties is shown along

an Indian Ocean transect (WOCE identification IO8 in Fig. 2.3.1g-l), though we note that the comparison between each model and observations varies significantly with region.

These zonally averaged properties arise from rich spatial structures. Irrespective of resolution, the densest waters in the abyssal ocean (Fig. 2.3.2c-d) outcrop in the coastal regions of the Ross and Weddell Seas (Fig. 2.3.2a-b). The waters extending from the high latitude surface into the abyssal ocean are notably denser in HR. The densest of these bottom waters emanate from the Ross and Weddell continental shelves, as is illustrated by the distribution of ocean bottom temperature and salinity (Fig. 2.3.3). Both the density and the density response to increased resolution are highest in these shelf regions, and both decrease with distance from the shelf following topographically driven AABW export pathways. These distributions imply that differences in surface properties propagate into the deep ocean from these locations.

To understand how differences in stratification and abyssal properties are manifested in the large-scale circulation, we examine the MOC south of the equator. In Fig. 2.3.4 we show the relative contributions towards the circulation Ψ^σ from each of the components in Eq. 2.2. In our control simulation, the volume inflation contributes only a small term (on order 1 Sv) and thus we ignore it in this calculation. To visualize the spatial distribution of the large-scale isopycnal circulation, we have projected each component onto the depth of each mean isopycnal in Fig. 2.3.4.

We focus our analysis on differences in the lower cell, which emerge more robustly when the circulation is defined along isopycnals Ψ^σ. In light of the recent focus on model resolution in the upper cell, as mentioned in the introduction, it is noteworthy that in this model, features of the lower cell vary significantly with resolution. There are two distinct local minima in Ψ^σ (see Fig. 2.3.4a-d). One minimum is associated with the export of dense surface waters

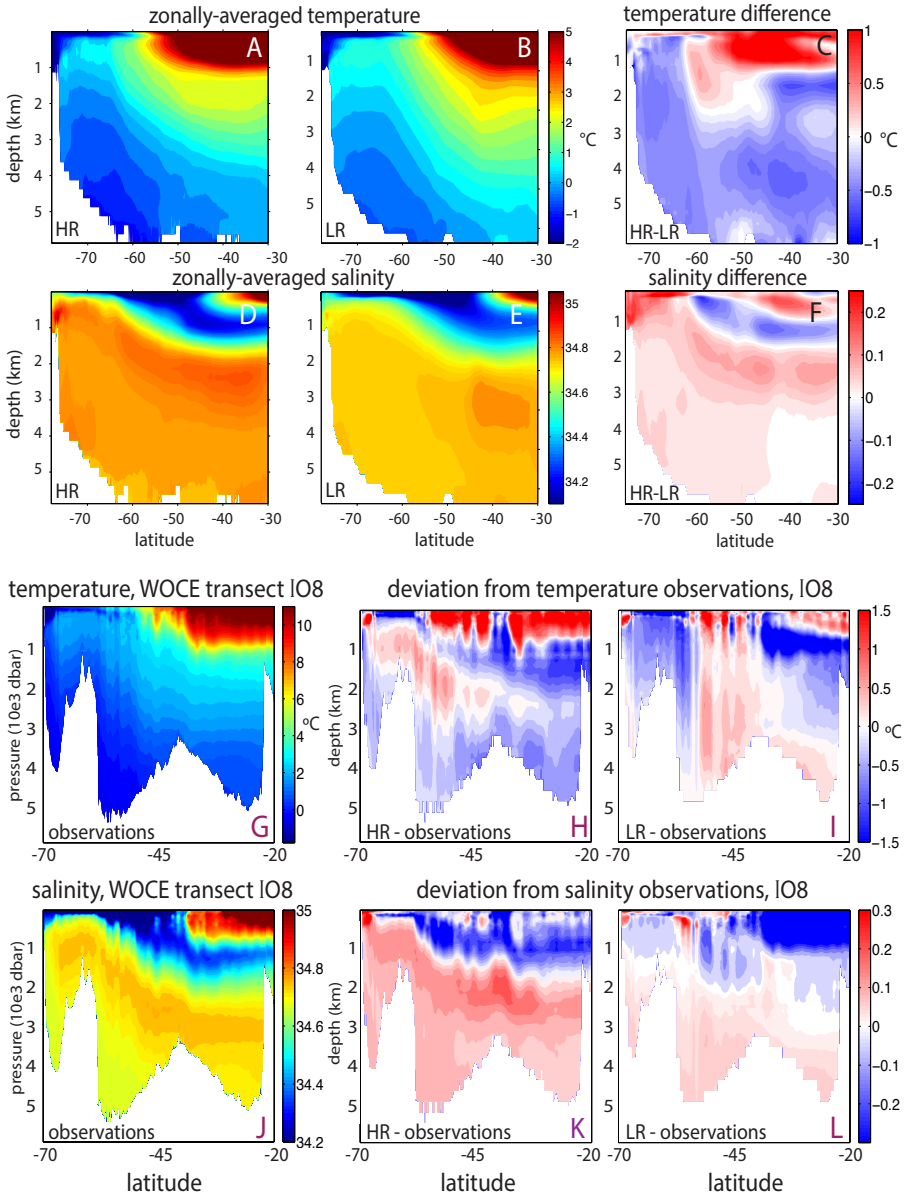

Figure 2.3.1: Zonally averaged properties in the Southern Ocean for (a)âĂŞ(c) potential temperature and (d) through (f) salinity in (a),(d) HR; (b),(e) LR; and (c),(f) HR minus LR. (g)âĂŞ(i) Potential temperature and (j)âĂŞ(l) salinity along the WOCE transect IO8 (longitude varies from 828 to 958E) from (g),(j) observations; (h),(k) HR minus observations; and (i),(l) LR minus observations.

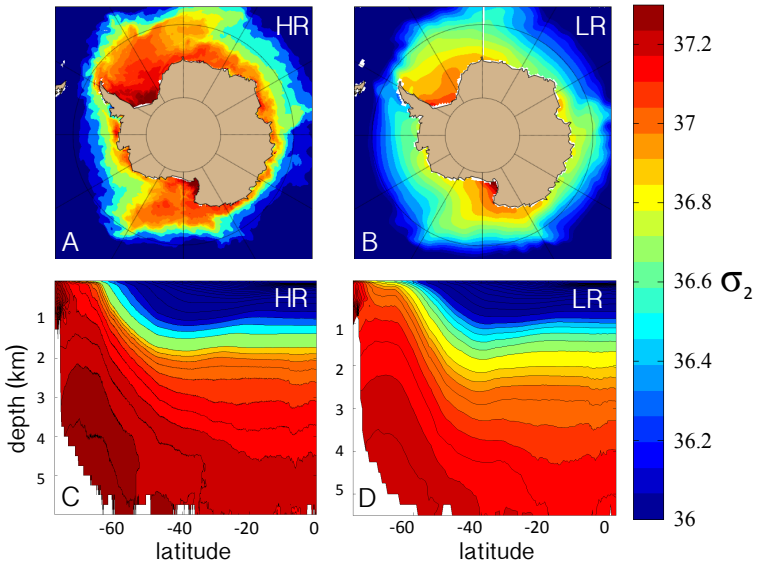

Figure 2.3.2: Potential density referenced to 2000 dbar (σ_2) (kgm^3). (a),(b) Annual-average surface σ_2 and (c),(d) annual-average, zonal-average σ_2 in (a),(c) HR and (b),(d) LR. Color scale is chosen to highlight density variations in the deep and polar surface ocean.

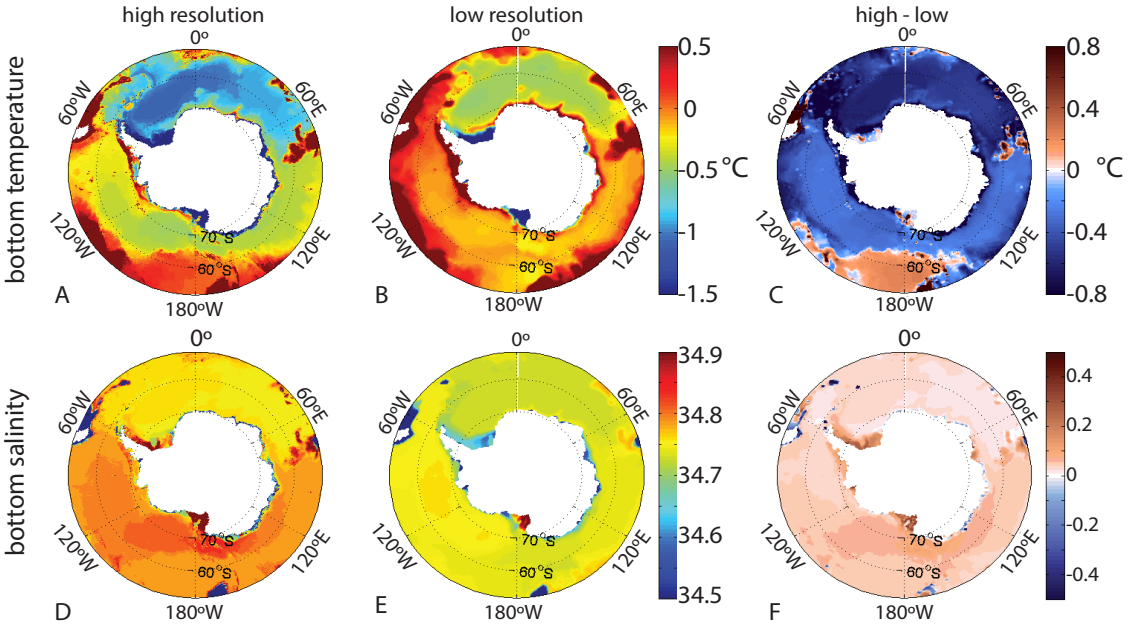

Figure 2.3.3: Ocean bottom properties south of 508 S for (a)âĂŞ(c) temperature and (d)âĂŞ(f) salinity in (a),(d) HR; (b),(e) LR; and (c),(d) HR minus LR. The ocean bottom is defined as the deepest ocean grid cell.

into the abyssal ocean and their return flow, contained south of 55°S, which we define as the "sub-polar range" of the lower cell. This feature is weak in the depth-space overturning, likely because much of the export of dense water occurs in the Ross and Weddell Gyres, as is suggested by the distribution of bottom temperature and salinity. The second minimum, in what we refer to as the "abyssal range" of the lower cell to describe overturning north of 55°S and south of the equator, is associated with the circulation of dense waters north of the ACC. Across this latitude range, bottom waters must mix sufficiently with lighter waters to upwell at the polar surface. The apparent spatial separation of these circulation minima, seen in most climate models (Farneti et al., 2015), derives from the partial recirculation of Weddell and Ross Sea waters at high latitudes. This separation is much reduced by density transport achieved by eddy fluctuations (resolved or parameterized), evident in the transient eddy-induced streamfunctions shown in Fig. 2.3.4. This counterclockwise transient eddy-induced cell, ${\Psi_E}^\sigma$, is strongest between $45^\circ - 60^\circ$ S and reaches from the upper ocean to the full depth (Fig. 2.3.4 e and f). The lack of resolution dependence in the structure of ${\Psi_E}^\sigma$ suggests that the eddy parameterization in LR is well calibrated, though${\Psi_E}^\sigma$ is stronger near the ocean bottom in HR, indicating that resolved eddies may alter the northward export of very dense AABW. Further, it is possible that we underestimate the strength of the HR eddy-induced cell by using monthly velocities in Eq. 1, particularly in the upper cell where daily correlations between velocity and temperature may become more important [Ballarotta et al, 2013].

In contrast to ${\Psi_E}^\sigma$, there are striking resolution-dependent differences in the mean isopycnal overturning, ${\Psi_M}^\sigma$ (Fig 5 c versus d); these differences dominate the resolution-dependence of the total overturning,Ψ^σ. Mean transport in the sub-polar range is stronger in HR (26 Sv versus 22 Sv in LR) and occurs on isopycnals that are deeper in the zonal average, corresponding to the production of more and relatively denser AABW in HR, consistent with the abyssal temperature and salinity fields. Mean overturning in the abyssal range extends

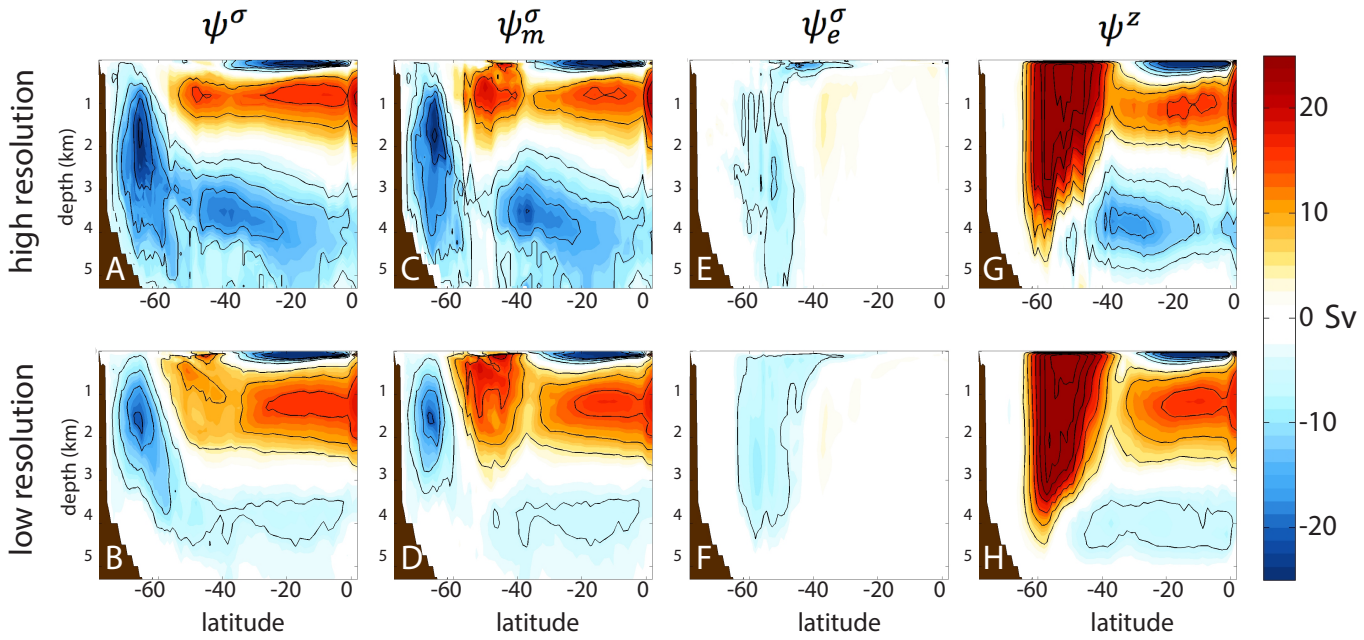

Figure 2.3.4: Components of the MOC: (a) through (f) isopycnal overturning remapped to depth-latitude space using the zonal and time-mean isopycnal depths in the Southern Hemisphere and (g), (h) overturning calculated in level coordinates; (top) HR and (bottom) LR. (a),(b) The total isopycnal overturning is broken into components of the (c),(d) mean isopycnal overturning and (e),(f) transient eddy-induced isopycnal overturning. Contour intervals of 5 Sv are overlaid in black.

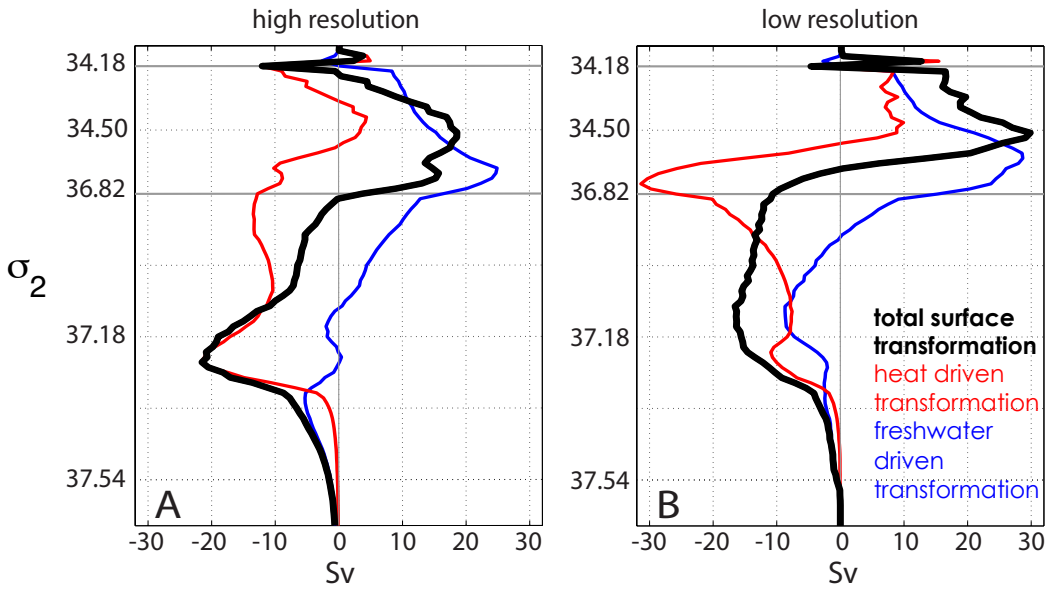

Figure 2.3.5: Total surface water-mass transformation rate F in the Southern Ocean. The contributions from heat fluxes (red) and freshwater fluxes (blue) add up to the total (black) for (a) HR and (b) LR. The density spacing is increased for waters denser than 36.82 kgm^3, which outcrop over a small area at the surface but occupy 70% of the ocean volume south of 30 S.

further northward and remains stronger throughout the abyssal ocean in HR, with an overturning maximum of 20 Sv around 40° S. In contrast, the majority of lower cell overturning occurs south of 50° S in LR, north of which abyssal overturning becomes relatively weak (with a maximum of 6 Sv).

The influence of resolution on surface and interior processes driving diapycnal volume exchange can be compared via Eq. 3. Implicit to this analysis is the notion that both surface fluxes and interior mixing processes can change the density of seawater on a given isopycnal, and in turn, any change in density must drive a volume flux of seawater across isopycnals; the transformation (separated into components F and D_{mix}) describes these induced volume fluxes. The sign of the transformation denotes the direction of this volume flux, where a positive transformation is a volume flux towards lighter isopycnals. Any slope in the transformation rate indicates that the diapycnal volume flux differs across neighboring isopycnals,

thus inducing a convergence or divergence of seawater volume into or out of a given density class. In steady state, the convergence [divergence] of volume into a density class will necessitate export [import] of water at that density, i.e. its formation [destruction].

The surface transformation function ($F(\sigma, y, t)$ in Eq. 3) at 30° S captures the surface regeneration of the major water masses of the Southern Ocean, specifically, the regions of net positive transformation and net negative transformation associated with the upper cell and lower cell, respectively (see Fig. 2.3.5). Waters in the small density range of the lower cell (which differs slightly between models: $36.82 \leq \sigma \leq 37.2$ in HR and $36.2 \leq \sigma \leq 37.54$ in LR) occupies 70 percent of the volume of the Southern Ocean; we focus our analysis on a shared density range which encompasses the majority of this cell at both resolutions ($\sigma_{lowercell}$ defined as $36.72 \leq \sigma \leq 37.72$). Downwelling AABW is formed across the range of net volume flux convergence (≥ 37.25 in HR and ≥ 37.12 in LR), so transformation across this density range is of particular importance to understanding what "drives" descent from the surface.

To diagnose the distribution of interior transformation, D_{mix}, we consider how Ψ_σ varies with density at a given latitude y_o. We then compare Ψ_σ to the other terms in Eq. 3 (recalling that volume inflation is negligible) at several latitudes over the density range of the lower cell; the degree to which Ψ_σ and F differ will indicate the impact diapycnal mixing has had on the circulation at each latitude. Fig. 2.3.6 illustrates the relative strength of $\Psi_\sigma(\sigma_{lowercell}, y_0)$, $F(\sigma_{lowercell}, y_0)$, and $D_{mix}(\sigma_{lowercell}, y_0)$ at $y_0) = 64°$ S, 38° S, and 30° S.

We first examine $y_0 = 64°$ S, chosen as a compromise between the northern extent of the Ross and Weddell shelves to capture how flow from the continental shelf into the abyssal ocean transforms water masses. Here,Ψ^σ bears a close connection to F (Fig. 2.3.6a and b). Vigorous surface transformation leads to a peak in Ψ^σ at $\sigma \sim 37.25$, in HR and $\sigma \sim 37.15$

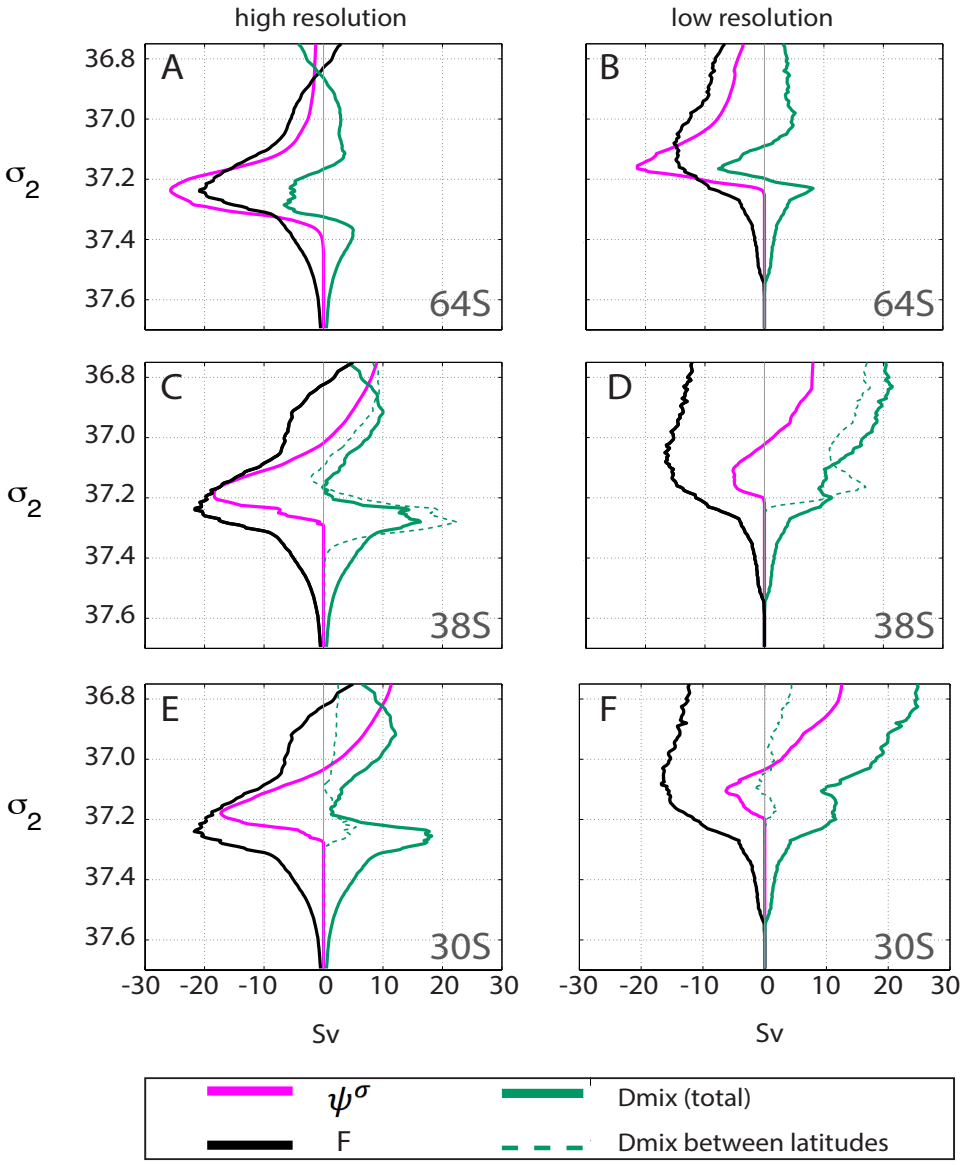

Figure 2.3.6: Isopycnal overturning streamfunction Ψ^{σ} (magenta) and its components from the total surface transformation F (black) and total implied mixing at each latitude D_{mix} (in green) at (top) 65 S, (middle) 38 S, and (bottom) 30 S in (left)HR and (right) LR. For convenience, the total mixing between latitude pairs (dashed green) is included (i.e., between 908 and 64 S, 64 S and 38 S, and 38 S and 30 S).

in LR; this peak is modestly increased by the diapycnal mixing of very dense waters along their descent from the shelf into the abyss (i.e., D_{mix} drives a volume flux of 6 Sv in HR and 8 Sv in LR from the densest waters into the peak flow in Ψ^σ). Somewhat surprisingly, the magnitude and relative distribution across density classes of this D_{mix} is similar between resolutions, though it is translated to slightly denser classes in HR because of the higher densities of waters formed at the surface. So, while a number of ocean processes may depend on resolution, together these processes don't result in significant resolution dependence in diapycnal volume transport, and thus large-scale circulation patterns, south of this latitude. Though some export off the Weddell continental shelf may occur northward of 64° S, Fig. 2.3.4 and b indicates that much of the total descent has occurred by this latitude. We conclude that the flux of dense water into the high latitude abyssal ocean differs with resolution primarily because more of it is being made at higher densities at the surface in HR.

A similar breakdown of the streamfunction in the abyssal range of the lower cell can be made at 38° S (Fig. refTRANSECTS1c and d). At either resolution, there is significant diapycnal mixing and associated adjustment of the isopycnal circulation between $64° - 38°$ S. The mixing between $64° - 38°$ S (dashed green line in Fig. refTRANSECTS1c and d) destroys waters denser than $\sigma \sim 37.3$ in HR and $\sigma \sim 37.2$ in LR by 38° S. The impact of this mixing on the circulation differs markedly between models. By 38° S, mixing redistributes volume from very dense water ($\sigma \geq 37.15$) into the $37.15 \leq \sigma \leq 37.27$ range in HR, shifting the peak in Ψ^σ towards $\sigma \approx 37.2$ but maintaining substantial northward flow. In contrast, mixing in LR lightens waters across the entire density range of the lower cell by 38° S, inducing volume fluxes towards lighter isopycnals and greatly reducing the northward flow across all density levels evident in Fig. 2.3.4. At both resolutions, D_{mix} overcomes F in waters lighter than $\sigma \sim 37.0$, reversing the direction of flow and the sign of Ψ^σ.

Examination of the streamfunction components at 30° S reveals that little additional mixing

occurs from $38^\circ - 30^\circ$ S at either resolution. There is a small volume flux towards lighter density classes across much of this density range at both resolutions, further reducing the magnitude of counterclockwise (negative) overturning in denser waters, and increasing the magnitude of clockwise (positive) overturning for lighter waters in $\sigma_{lowercell}$. In sum, both surface transformation and interior transformation are key to sustaining the circulation across the latitudes sampled here, as is anticipated in an (approximate) steady state. However, the relative importance of surface and interior transformation processes, and resolution dependence therein, has a consistent spatial structure, one which may have important effects on the pattern and mechanisms of ocean heat uptake, as discussed in the next section.

To uncover the actual oceanic processes responsible for the distribution of water mass transformation, we first consider surface transformation in more depth. Fig. 2.3.5 illustrates the relative roles of heat and freshwater fluxes in transforming surface waters. Somewhat surprisingly, in light of the strong control salinity variations exert on the density of polar waters, heat loss contributes most significantly to buoyancy loss across $\sigma_{lowercell}$ at both resolutions (but especially so in HR). Salt input contributes significantly only at very high densities in this density range, again particularly so in HR, though sea ice melt and precipitation are important to the transformation of lighter waters. The spatial distribution of surface transformation per unit area, over several key density classes in $\sigma_{lowercell}$ elucidates why this is so (Fig. 2.3.7).

These "transformation maps," or distributions of diapycnal velocity, are constructed from the 20-year mean of monthly estimates and capture the covariance of isopycnal migration and surface fluxes. These distributions demonstrate the important control isopycnal surface area has on total transformation rates (recall Eq. 4). Both heat and salt fluxes induce strong density gain at very high densities in the coastal polynyas of the Weddell and Ross Seas (and the entire coastal Antarctic region at decreasing densities) because of the intensity of brine

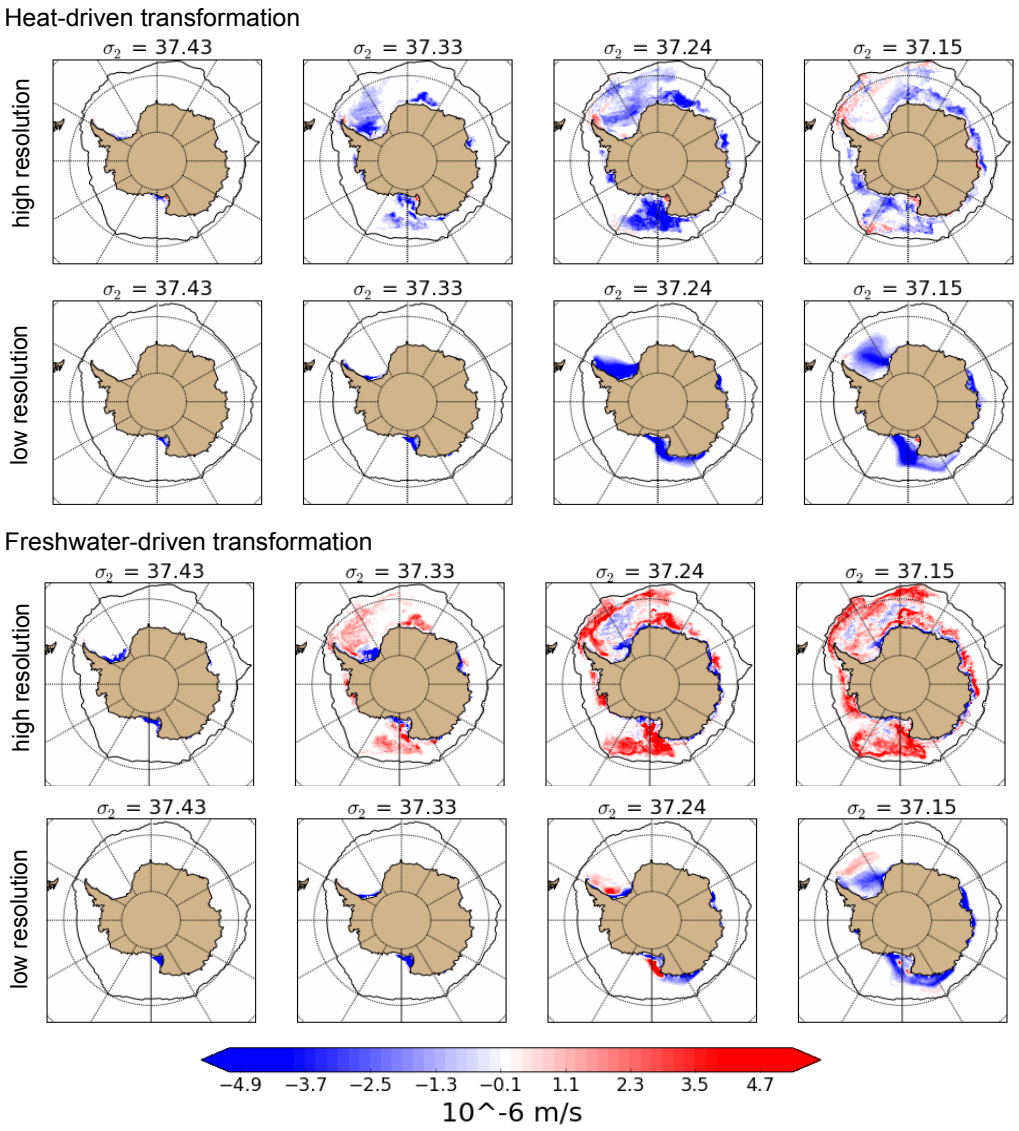

Figure 2.3.7: Distribution of transformation per unit area (positive toward lower densities) across density surfaces (roughly spanning the density range of net volume convergence and thus surface-forced downwelling). Shown are the following: heat-driven buoyancy flux in (top) HR and (upper middle) LR and freshwater-induced buoyancy flux in (lower middle) HR and (bottom) LR.

rejection and the reduced control of heat fluxes on the density of very cold water. However, the total area of these coastal polynyas is relatively small, especially in HR, so the associated transformation is not substantial. The greater impact of salt rejection in LR follows from the larger spatial scale over which sea ice is formed. Perhaps counter-intuitively, relatively lower surface density fluxes associated with heat loss over broader regions of the sea ice pack account for more total transformation because they act over a larger area. In LR, dense isopycnal outcrops migrate over a smaller area than in HR, such that even extreme heat losses near the coast drive less total transformation at equivalent densities. At either resolution, the Ross and Weddell Sea regions are of particular importance in part because of their southward extent: they host large areas of continental shelf and sea ice, through which dense isopycnals can maintain contact with the surface over much of the year.

Elevated rates of heat-loss induced transformation in dense waters in HR imply larger rates of diapycnal heat convergence into these density classes. Waters in the upper 1000 m are generally colder in HR under most of the ice pack in the Ross and Weddell Seas, aside from a small region of warmer sub-surface temperatures in the Ross Sea. The resolution dependency of heat transport likely results from changes in the regional circulation and diapycnal temperature gradients, though it is difficult to attribute such changes to one particular process. In both regions, the standard deviation of wintertime temperature is slightly greater in HR, which may be key to sustaining intermittent high heat loss. Variations in temperature may arise from transient features in the flow as well as fluctuations the sea ice cover above.

Sea ice is well known to mediate rates of surface heat loss (Maykut, 1982). In HR, the sea ice is thinner and less extensive than in LR, in better agreement with observations, as discussed in depth by Bryan et al. (2014). While ice thickness is likely sensitive to ocean heat transport into the ice-zone, the resolution of ice dynamics also plays a central role in regulating ice thickness, and thus heat loss. In HR, finely-spaced grid cells allow sea ice

to respond to more localized atmosphere and ocean conditions, leading to more pervasive and smaller-scale coastal polynyas. This leads to higher rates of brine rejection hugging the coast, in better agreement with observations (Willmott et al., 2007). In the pack ice, higher resolution enables a greater magnitude of divergence/convergence and shear, which creates the "leads" that are endemic to the observed Antarctic ice pack (Willmott et al., 2007). Lead opening exposes the ocean surface to the cold atmosphere in winter, driving enormous heat loss and rapid new ice formation. The resulting "frazil ice" only forms in open water (in our model), and is thus a proxy for the continuous exposure of the ocean surface. The rate of frazil ice formation has a broad peak, spanning austral fall through spring in HR (Fig. 2.3.7a.). In contrast, frazil ice formation in LR is sharply peaked in austral fall and is relatively weak in winter. The timing in LR is consistent with the northward expansion of the sea ice extent in fall, while the prolonged frazil ice production in HR indicates the consistent opening of polynyas and leads throughout the winter. These dynamics maintain more thin ice throughout the ice-covered waters in winter in HR (not shown), which drives areas of intense heat loss, as illustrated in Fig. 2.3.7a and 2.3.8b. The extremity of heat loss experienced through the sea ice in HR contributes to the northerly transit of dense isopycnal outcrops in winter; the outcrops in LR migrate less due to the insulating effects of its thicker ice pack and less frequent leads and polynyas.

Diagnosing the processes inducing different rates of diapycnal-mixing driven transformation is more difficult, given our methods of calculation. Generally, models must homogenize properties like temperature and salinity over the grid scale, a consequence of discretizing a continuum; simply reducing grid-cell size reduces this spurious diffusion and enables the formation of smaller-scale density gradients. This likely improves the scale of dense overflows resolved in HR, especially because bathymetry is better resolved. However, as is evident in Fig. 2.3.6, these processes have a minimal effect on altering the circulation south of 64° S, which may in part be a consequence of the small volume of the high latitude ocean, since

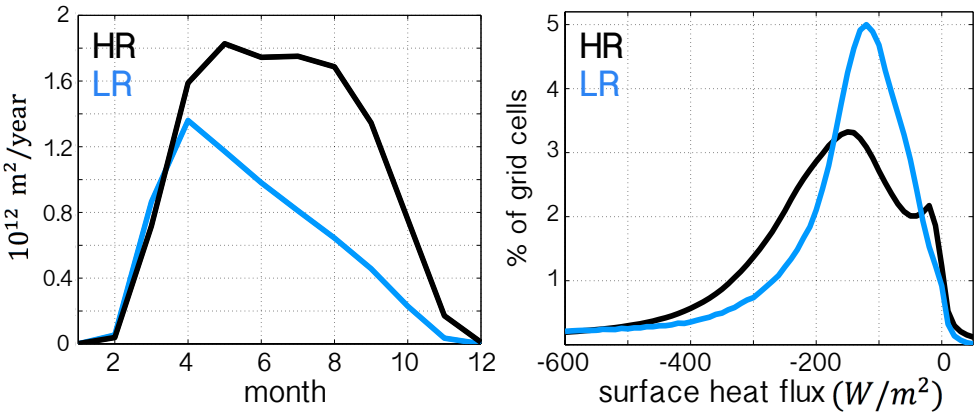

Figure 2.3.8: (left) Monthly rates of total frazil ice formation (m^2yr^{-1}) in HR (black) and LR (blue). (right) Distribution of area-weighted winter surface heat flux (Wm^2) in HR (black) and LR (blue). This distribution is calculated from monthly values during the period in which the majority of negative surface transformation occurs (June − September), within a region bounded at the north by the contour of 5% ice concentration on average for this period, though the relationship is insensitive to choice of domain. Note the skew toward more negative (out of the ocean) values in HR.

volume has a strong control on transformation rates.

North of 64° S, an increase in resolution significantly impacts the magnitude of mixing. The meridional flow of dense water towards the subtropics likely occurs via transient mass fluxes (Ito and Marshall, 2008; Lozier, 2010), and in deep western boundary currents (DWBC) where bathymetry allows (Orsi et al., 1999; Fukamachi et al., 2010). These boundary currents are particularly susceptible to real and numerical mixing because of their association with strong density gradients and shearing rates (Griffies et al., 2000). Mesoscale turbulence, acting to either erode or intermittently increase density gradients, likely depends on resolution, even without altering Ψ_E^σ. Further, there may be different levels of numerical mixing induced across these currents; this spurious diffusion likely decreases with increasing resolution (to a degree, akin to the numerics discussed by Griffies et al., 2000), though it persists in eddying models (Urakawa and Hasumi, 2014)). A representative example of the differences in DWBC characteristics between resolutions is shown at 30°S (Fig. 2.3.9), at a latitude chosen due to the large contrast in abyssal circulation strength apparent in both the

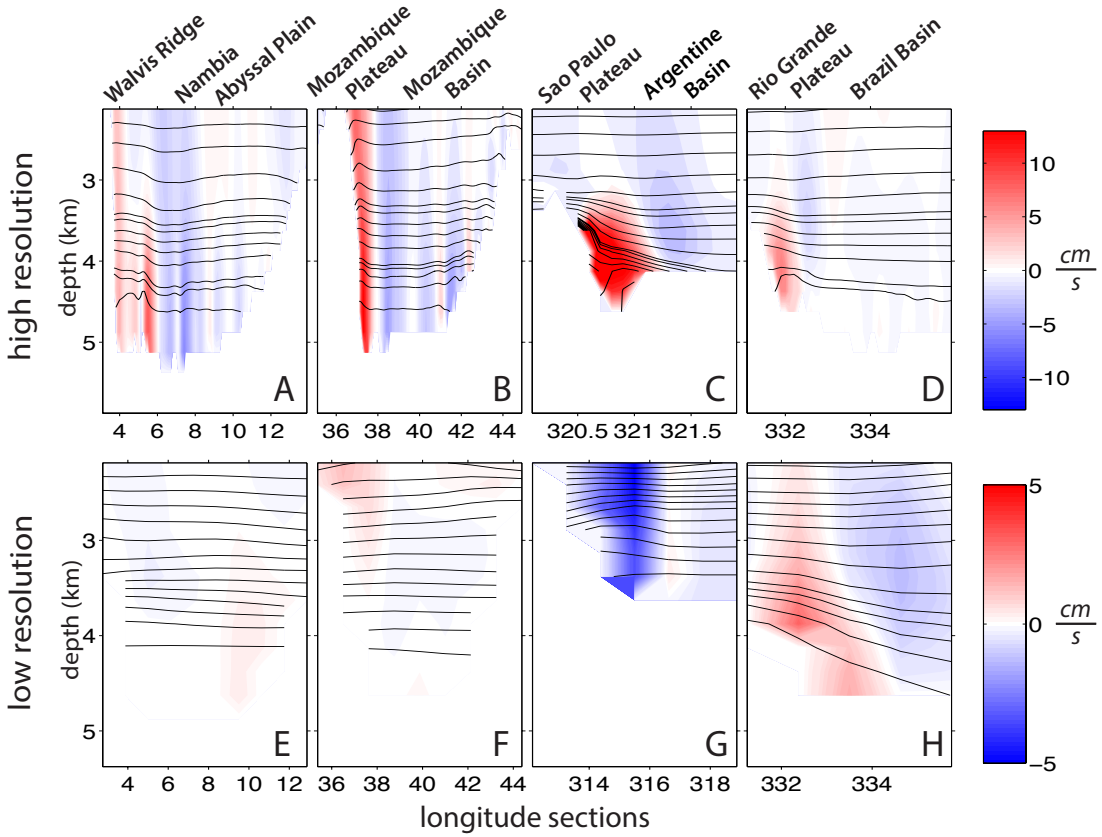

Figure 2.3.9: Zonal transects across key deep western boundary currents at 30 S as a function of longitude and depth (below 3000 m). The meridional velocity (color) is overlaid with isopycnals (black) in (a) through (d) HR and (e) through (f) LR. Positive (red) is northward. Isopycnal spacing varies with stratification, but is on average 0.01 kgm^{-3}. Bathymetric features are noted to orient the reader. Note the reduced color scale for LR.

isopycnal and depth-space overturning in Fig. 2.3.4. In HR, deep isopycnals slope steeply up towards the western continental boundaries or ridges, coincident with regions of strong meridional flow. The corresponding isopycnal slopes are notably flatter in LR, and the flow is much weaker. The reduced strength of these currents in LR, and associated weak abyssal overturning, follows from the elevated destruction of dense waters south of 30°S. However, Fig. 2.3.9 reveals that density gradients in HR can form on scales smaller than a single LR grid cell, indicating that correspondingly strong geostrophic currents are unresolvable in LR, even given a similar flux of dense water into the abyssal ocean. While the formation of boundary currents, and the mixing that erodes them, are coupled, further unraveling their interactions is beyond the scope of this article.

As a final diagnostic of the Southern Ocean circulation state and its dependence on resolution, we consider the twenty-year average integrated heat content tendency for a control volume bounded at 30Âř S, below each depth z^*, and spanning all longitudes. For HR:

$$-\frac{c_p\rho_0}{t_1-t_0}\int_{t_0}^{t_1}\int_{90S}^{30S}\oint\int_{-B(x,y)}^{z^*}\{\underbrace{(\frac{\partial\theta}{\partial t})}_{1}+\underbrace{\nabla\cdot(\bar{u}\bar{\theta})+\frac{\partial}{\partial z}(\bar{w}\bar{\theta})}_{2}+\underbrace{\nabla\cdot\bar{u'\theta'})+\frac{\partial}{\partial z}(\bar{w'\theta'}}_{3}$$
$$-\underbrace{\frac{\partial}{\partial z}(\kappa_{bg}\frac{\partial\bar{\theta}}{\partial z})}_{4}-\underbrace{\frac{\partial}{\partial z}(\kappa_{ML}\frac{\partial\bar{\theta}}{\partial z})}_{5}\}dxdydzdt \quad (2.7)$$

and for LR:

$$-\frac{c_p\rho_0}{t_1-t_0}\int_{t_0}^{t_1}\int_{90S}^{30S}\oint\int_{-B(x,y)}^{z^*}\{\underbrace{(\frac{\partial\theta}{\partial t})}_{1}+\underbrace{\nabla\cdot(\bar{u}\bar{\theta})+\frac{\partial}{\partial z}(\bar{w}\bar{\theta})}_{2}+\underbrace{\nabla\cdot\bar{u_b}\bar{\theta}+\frac{\partial}{\partial z}(\bar{w_b}\bar{\theta})}_{3}$$
$$-\underbrace{\frac{\partial}{\partial z}(\kappa_{bg}\frac{\partial\bar{\theta}}{\partial z})}_{4}-\underbrace{\frac{\partial}{\partial z}(\kappa_{ML}\frac{\partial\bar{\theta}}{\partial z})-\nabla\cdot\boldsymbol{K}redi\nabla\theta}_{5}\}dxdydzdt \quad (2.8)$$

Note that the sign convention is such that positive vertical fluxes across the upper bounding surface, z^*, are acting to increase the heat content of the control volume. Here $\theta=\theta(x,y,z,t)$ is potential temperature, $u=u(x,y,z,t)$ and $w=w(x,y,z,t)$ are the horizontal and vertical velocity, respectively, an overbar denotes a time-mean, the prime denotes a deviation from the time mean, the subscript "b" denotes a bolus field in LR, c_p is the specific heat capacity for seawater, and ρ_0 is a reference density. Plotted in Fig. 2.3.10 is the heat content tendency (labeled $\frac{dH}{dt}$) associated with the temperature trend (term 1). This tendency will depend on: heat transport by the mean flow (term 2); the transient eddy-induced flow (term 3); the background vertical diffusion, dependent on the background diffusivity, κ_{bg} (term 4); and a residual term that captures the remaining mixing processes, like KPP mixed-layer processes

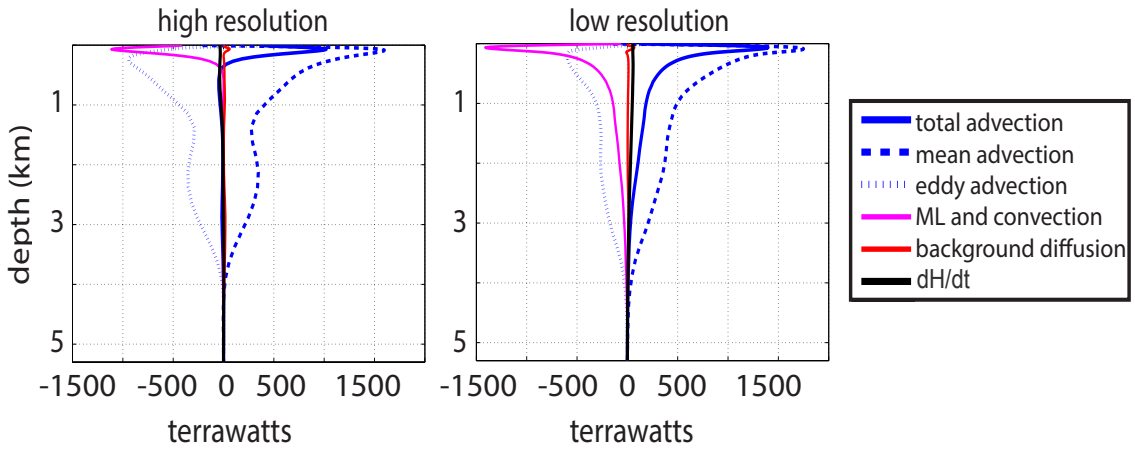

Figure 2.3.10: Relative contributions to the heat content tendency of the ocean volume below depth z*, south of 30 S in (left) HR and (right) LR. As defined in the legend at right, the total heat content will depend on total advective fluxes (solid blue); mean advective fluxes (dashed blue); eddy advective fluxes (short dashed blue); diffusive fluxes (red); mixed-layer, convective, and (in LR) Redi fluxes (magenta) and result in a very small temperature tendency (black solid). Fluxes are defined as positive downward.

and convection (term 5). In LR, this residual term also includes the parameterized along isopycnal diffusion (the Redi flux, dependent on the parameterized isopycnal diffusivity tensor, $\boldsymbol{K}_{redi}$). Thus, part of the impact of mesoscale eddies on the vertical heat budget is captured in this residual term in LR; the Redi fluxes couldn't be directly calculated because the time dependent diffusivity tensor was not saved in the monthly output files. While there is a small trend in heat content at either resolution, in the top 500 meters, advective warming nearly balances convective cooling. Below this depth, to first order at either resolution, eddy heat fluxes are sufficient to counter heat fluxes by the mean flow, emphasizing the importance of eddies in diffusing heat across strong temperature gradients. This breakdown of heat fluxes will be useful in the subsequent section to elucidate the physics responsible for deep ocean warming under greenhouse forcing.

2.4 Carbon Dioxide Doubling Response

We now show how resolution affects the response of the Southern Ocean in the 20 years of carbon dioxide stabilization after doubling. The Southern Hemisphere surface air temperatures increase at both resolutions: air temperatures in the high southern latitudes warm by up to 8 $^{\circ}C$ over some regions of the ocean and sea ice pack. Bryan et al. [2014] discuss how climate change depends on resolution more generally; here we focus on the deep Southern Ocean's response.

At both resolutions, the lower cell of the isopycnal MOC slows substantially in response to surface warming (Fig. 2.4.1), though this reduction is notably greater in HR. The response of the overturning, $\Delta\Psi_\sigma$, is dominated by a reduction in the circulation strength in the sub-polar range of the lower cell, with smaller changes across the abyssal range. The resolution dependence of the response to carbon dioxide doubling is primarily a feature of the mean isopycnal flow $\Delta\Psi^\sigma_M$; while the transient eddy-induced circulation response to carbon dioxide doubling, $\Delta\Psi^\sigma_E$, depends somewhat on resolution, it is comparatively small.

Surface warming and the associated changes in freshwater fluxes alter the surface water mass transformation, ΔF (see Fig. 2.4.2). There is a significant (positive) anomaly in ΔF across the outcrops of the lower cell. To understand the impact of these surface changes, relative to changes in interior transformation, we compare changes in the strength of processes contributing to the circulation response throughout the density range of the lower cell. Because the carbon dioxide forcing was only stabilized for 20 years, the response is transient and the isopycnal volume inflation is non-negligible. Thus, the response to carbon dioxide doubling apparent in the overturning, $\Delta\Psi_\sigma$, includes the contributions from changes in isopycnal volume, $\frac{\Delta V}{t}$, surface water mass transformation, ΔF, and implied interior mixing, ΔD_{mix} (see Fig. 2.4.3). In both LR and HR, the significant $\Delta\Psi_\sigma$ at $64^{\circ}S$ can be primarily

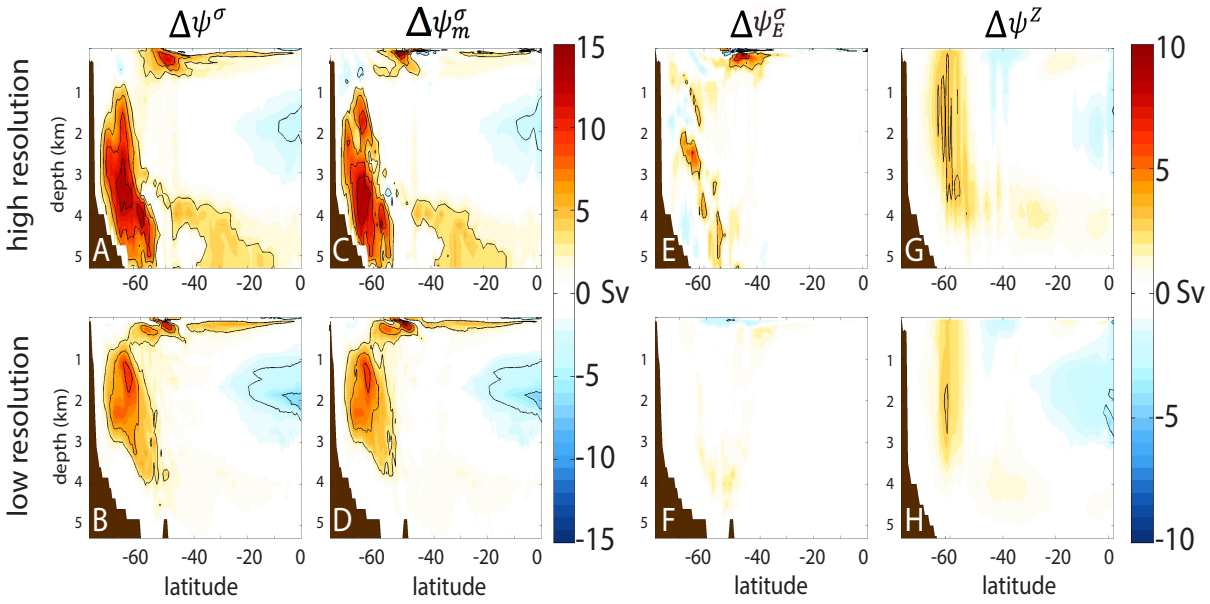

Figure 2.4.1: As in Fig. 2.3.4, but the anomaly in response to doubling carbon dioxide (i.e., perturbed 2 control). Contour intervals of 3 Sv are overlaid in black. Note reduced color scale for (e) through (h) the eddy-induced and depth-space circulation changes.

attributed to ΔF; this affirms the close connection between surface transformation and flow in the sub-polar range as diagnosed in the control climate. Further, ΔD_{mix} at $64°S$ is largely explained by the magnitude and pattern of ΔF. In other words, the reduction in shelf water mixing directly reflects the reduction in shelf water production. Further to the north, at $38°S$, there is little $\Delta\Psi_\sigma$ at either resolution. The large change in mixing-driven transformation between these latitudes (which is primarily a reduction in the effectiveness of mixing in the control simulations, i.e. of the same shape but of opposite sign) can again be explained as the result of a reduction in downwelling dense waters. Further north yet, at $30°S$, $\Delta\Psi_\sigma$ is increasingly small, implying a very small reduction in mixing between $38°S - 30°S$. Greater changes at these latitudes may occur over time, as the influence of high latitude processes spread northward; however, such changes aren't captured in our simulations. There is some redistribution of isopycnal volume from very dense to slightly less dense water classes, though it is small compared with ΔF.

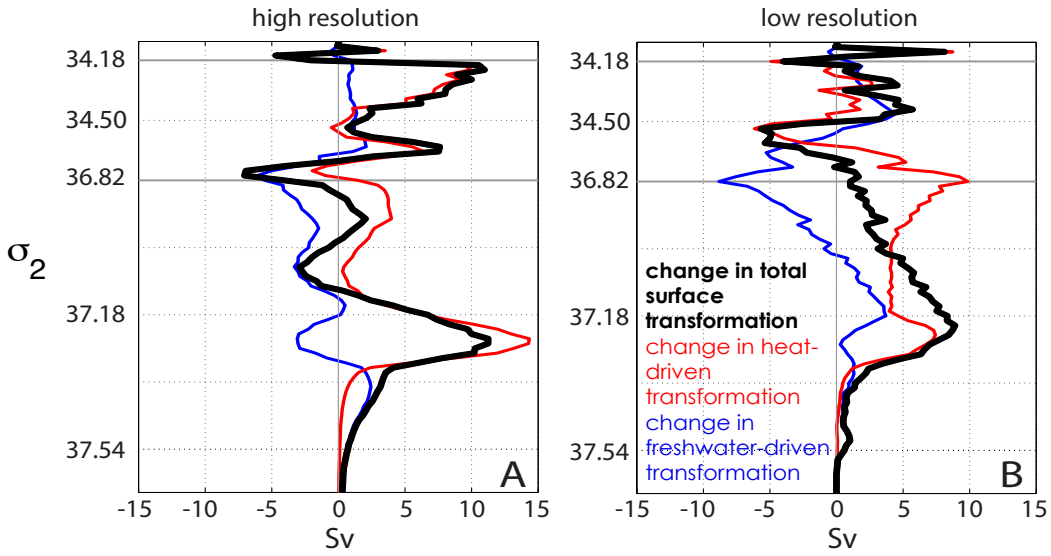

Figure 2.4.2: As in Fig. 2.3.5, but the anomaly in response to doubling carbon dioxide (i.e., perturbed − control).

In the control, Ψ^σ is sustained by both F and D_{mix}, though the influence of each varies with latitude. In contrast, these transient results suggest that the$\Delta\Psi^\sigma$ is almost entirely explained by a reduction in surface transformation, particularly so in the sub-polar range. Further, the resolution dependence of ΔF primarily explains the resolution dependence of $\Delta\Psi^\sigma$. Since the pattern of ΔF is both more peaked and confined to denser isopycnals in HR, $\Delta\Psi^\sigma$ in HR is larger and extends deeper in the water column than in LR. In HR, this peak is 15 Sv and is centered at an average depth of 3.8 km; in LR, the peak reduction is 12 Sv and is centered at an average depth of 1.7 km.

The surface transformation function response to carbon dioxide doubling is largely attributed to a reduction in surface heat fluxes. We interpret this as follows: in a warmer climate, there is a reduction in the air-sea temperature contrast in the coastal ocean, especially in winter-time, inducing a reduction in heat lost through the sea ice pack. The reduction in heat loss in response to carbon dioxide doubling is strongest in the winter months, and the (positive) anomaly in surface transformation occurs almost entirely in winter. Surface warming also drives a thinning of the ice pack irrespective of resolution. Sea ice volume is reduced by

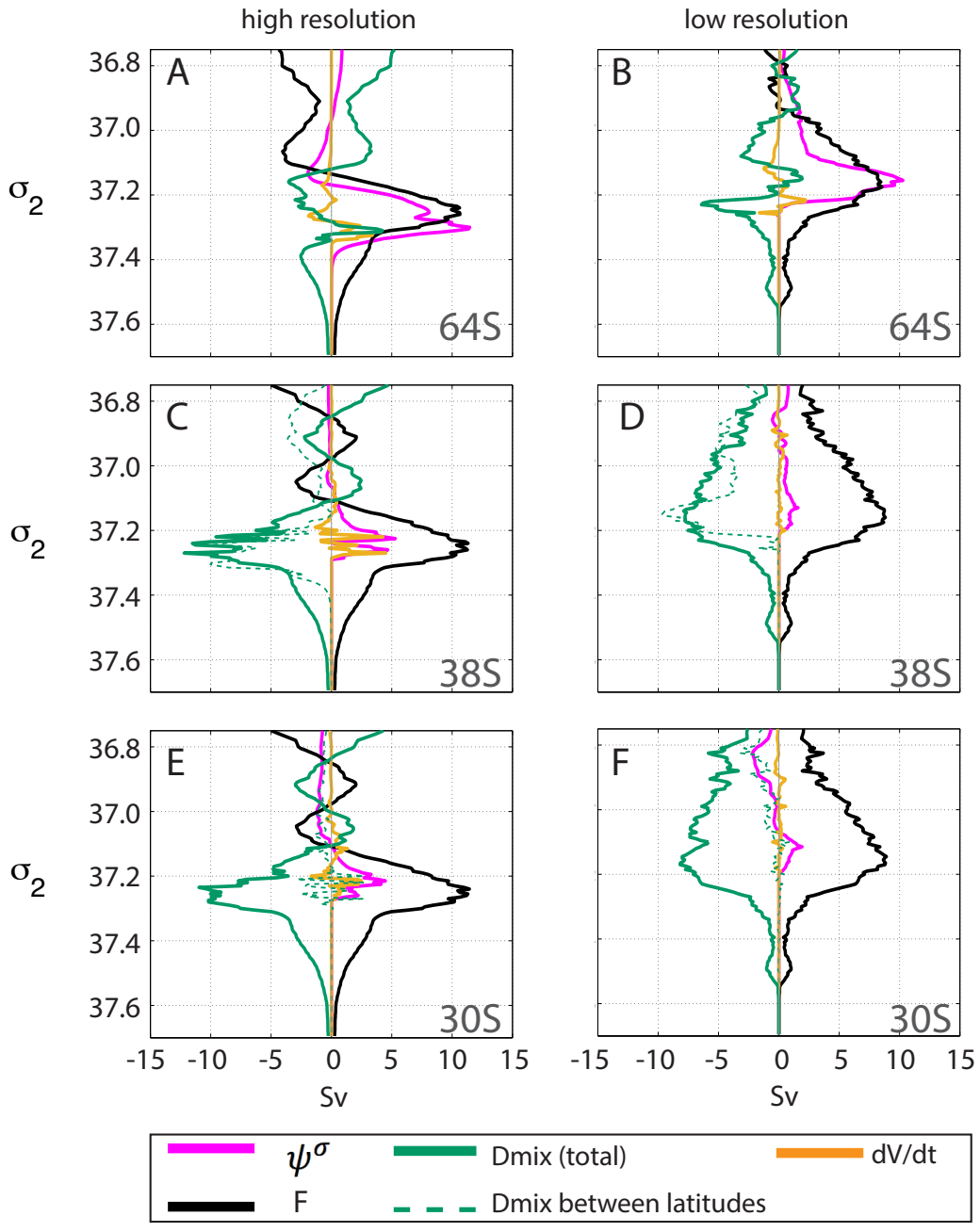

Figure 2.4.3: As in Fig. 2.3.6, but the anomaly in response to doubling carbon dioxide (i.e., perturbed − control). In addition, the anomalous response of the isopycnal volume inflation is shown in gold.

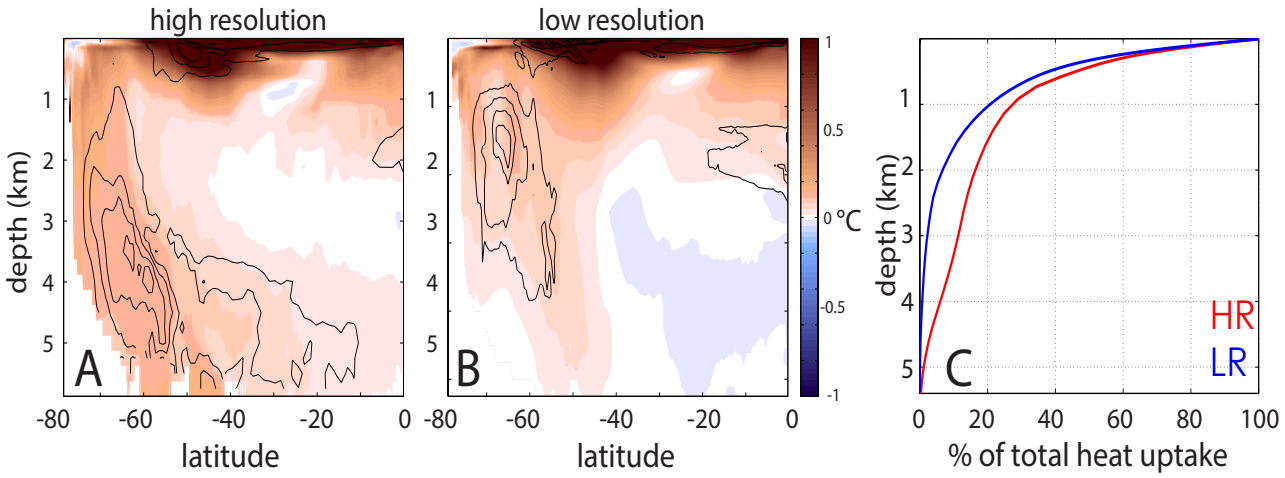

Figure 2.4.4: (a)âĂŞ(b) Zonally-averaged temperature change for the Southern Hemisphere in (a) HR and (b) LR, overlaid with contours of the anomalous isopycnal MOC streamfunction at 3, 6, 9, and 12 Sv; and (c) cumulative fraction of heat uptake south of the equator in HR (red) and LR (blue).

40 percent in LR and 26 percent in HR. While there is some decrease in ice extent at each resolution, this volume reduction is mainly caused by changes in ice thickness. This relatively greater thinning in LR is characteristic of thicker ice in the mean state (Bitz and Roe, 2004). Because thinner ice is less insulating, thinning provides a damping effect on what would otherwise be a larger reduction in heat loss in response to warming air temperatures. This damping effect is greater in LR because of the more substantial thinning in LR, revealing how sensitive the response to carbon dioxide doubling of the sea ice-atmosphere-ocean system can be to the mean state ice thickness. Lastly, larger changes in the meridional circulation in HR may reduce the rate of heat convergence into very dense waters this region. The shape of the anomaly in surface transformation is also impacted by a shift in the spatial distribution in surface densities. These combined changes drive the larger reduction in surface water mass transformation across a narrower range of denser waters in HR (note the differences in positive anomalies peaked around 37.25 in HR and 37.18 in LR). A shift in the density classes into which sea ice melts partially offsets the strong reduction in buoyancy loss from reduced heat loss in slightly lighter waters.

The circulation response to carbon dioxide doubling, and the sensitivity of each model to surface transformation changes, leads to a strikingly different distribution of ocean warming with resolution, particularly in the high latitude abyssal ocean. Fig. 2.4.4-b illustrates the zonal average temperature change with depth. In HR, warming extends along the path of dense water formation, from the coast into the abyssal ocean. In LR, warming is confined to the surface and mid depths, with nearly no warming of the abyssal ocean below 3500 m. These warming patterns lead to important differences in the total heat uptake with depth in the Southern Ocean (Fig. 2.4.4c). Changes in heat content are primarily explained by anomalous advective heat fluxes, as illustrated Fig. 2.4.5. In HR, the total advective warming into the ocean volume south of $30^{\circ}S$ is a result of anomalous positive vertical and horizontal eddy heat fluxes and anomalous vertical fluxes by the mean flow, which are partially compensated by anomalous negative horizontal fluxes by the mean flow (not shown). In LR, the total advective warming is primarily a result of anomalous vertical eddy fluxes, which are also partially compensated by anomalous negative horizontal fluxes by the mean flow. As can be seen in Fig. 2.4.4, the pattern of warming bears a close connection with circulation changes, which are in turn intrinsically related to the control state circulation. The relative magnitude of the control MOC strength (Ψ^{σ}) versus the magnitude of its reduction ($\Delta\Psi^{\sigma}$) is important in explaining why heat uptake differs across models (Banks and Gregory, 2006; Xie and Vallis, 2012; Rugenstein et al., 2013; Kostov et al., 2014). We attempt to address this by partitioning the total heat flux response to carbon dioxide doubling as:

$$\Delta(vT) = T\Delta v + v\Delta T + H.O.T. \tag{2.9}$$

where H.O.T. stands for higher order terms. Because we cannot calculate sub-monthly correlations between velocity and temperature, our calculations of the relative roles of eddy heat flux response are imperfect. With this caveat, we find that the total advective heat flux response due to changes in MOC strength, via ∇v, is responsible for 2-3 times (depending on the depth) more of the warming below 2000 meters than changes in the temperature field,∇T.

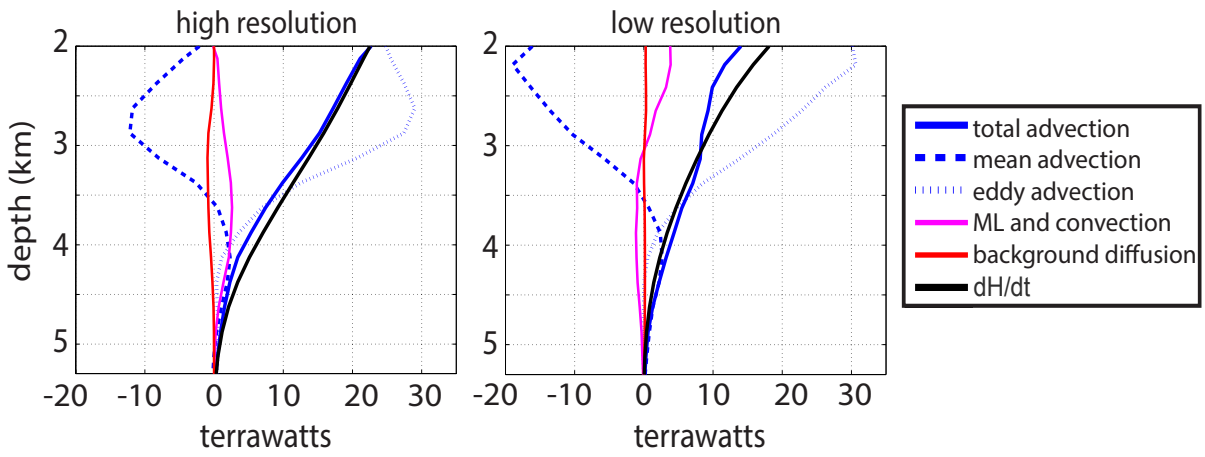

Figure 2.4.5: As in Fig. 2.3.10, but the anomaly in response to carbon dioxide doubling (i.e. perturbed - control).

Thus, a redistribution of ocean heat by the circulation response to doubling carbon dioxide is a key component of Southern Ocean warming.

2.5 Discussion and conclusions

These results support the notion that model resolution fundamentally alters simulated Southern Ocean dynamics. This possibility has been explored in numerous studies [e.g. Henning and Vallis, 2005; Hallberg and Gnandesikan, 2006; Farneti et al. 2010, Abernathey et al., 2011; Bryan et al, 2014; Farneti et al., 2014], which have justifiably focused on the first order effects of transient eddies on the residual circulation. In our experiments, the transient eddy-induced meridional circulation varies little with resolution, reinforcing findings by Gent and Danabasoglu [2011] and Gent [2016], who argued that employing an unconstrained spatially-varying GM coefficient greatly improves the agreement between the resolved and parameterized contribution of transient eddies to the circulation.

Here, we call attention to the influence of increased model resolution on the behavior of

other fundamental small-scale processes, in particular sea ice divergence and shear and the formation of small-scale ocean density gradients and flows. These processes are generally only resolved to the extent that grid spacing permits- without additional sub grid-scale parameterizations. The increased resolution of these processes has a major influence on the mean isopycnal flow of the lower cell in this model. To quantify the spatial distribution of processes sustaining this circulation, and contributing to circulation differences with resolution, we consider the evolution of water mass transformation (see, e.g., Walin, 1982) across latitudes of the Southern Ocean and focus on lower cell density classes. We conclude that downwelling near Antarctica is consistent with heat loss from isopycnal outcrops in the vicinity of leads in the sea ice pack, the simulation of which is greatly improved by increased resolution: these fine-scale, intermittent sea ice openings (polynyas and leads) are more frequent at higher resolution, enabling vast areas of thinner ice and more efficient surface heat loss over localized scales. Greater heat loss from very dense isopycnals at high resolution is sustained by a greater diapycnal convergence of heat into these density classes by the flow. The resolution dependence of transient eddy fluctuations across the shelf front (e.g. Stewart and Thompson, 2013) may play a role diapycnal heat fluxes. However, even our higher resolution experiment is too coarse to explicitly resolve their dominant scales at the shelf front.

As water flows northward from the shelf regions into the abyssal ocean, transformation from diapycnal mixing processes contributes increasingly to patterns of flow. Progressively greater interior transformation is expected as the volume of most density classes increases over the immediate domain northward from the continental shelves; correspondingly distinct patterns of interior transformation between resolutions emerge as different dynamics act on progressively larger volumes of water. Our higher resolution case forms more vigorous, small scale DWBCs, and experiences less diapycnal mixing of dense waters, sustaining a stronger abyssal circulation; vigorous mixing damps abyssal overturning strength dramatically at

lower resolution. These differences may be tied in part to a reduction in numerical mixing, though such mixing can persist in eddying models [Urakawa and Hasumi, 2014].

In the approximate steady state of our control simulation, processes regulating the transformation of seawater at the surface and in the interior together sustain the lower cell circulation. In contrast, we attribute *changes* in flow in response to a doubling of carbon dioxide predominantly to reductions in surface transformation. While the reduction in surface transformation leads to a dramatic reduction in overturning irrespective of resolution (14 Sv at high resolution, a reduction of $\sim 54\%$, and ~ 10 Sv at lower resolution, a reduction of $\sim 45\%$), these overturning changes are greater and deeper on average at high resolution because of a larger reduction in heat loss-induced transformation. There is a decrease in diapycnal mixing throughout the abyssal Southern Ocean with carbon dioxide doubling, though the magnitude of this decrease directly reflects the reduction in upstream dense water production at the surface. These results emphasize an important aspect in the dynamics of the lower cell circulation omitted from several theoretical and idealized studies [e.g., Ito and Marshall, 2008, Nikarushin and Vallis, 2011, 2012]. While these studies include a simplified form of buoyancy loss in the high latitudes, they don't include a theory for the sensitivity of the circulation to changes in surface fluxes. In the absence of any evolving surface buoyancy forcing, their results stress the lower cell's sensitivity to other processes: particularly, changes in southward eddy heat fluxes across the ACC, westerly wind strength, and abyssal mixing rates. These insights are crucial to understanding the system, but have limitations. Our results suggest that the lower cell circulation is most sensitive, at least in a "global warming" type of perturbation, to changes in surface heat loss with atmospheric warming, and that this heat loss is sensitive to surface processes. This is supported in the conceptual frameworks of Shakespeare and McC. Hogg (2012) and Stewart et al. (2014), and in the eddy-permitting model discussed by Kuhlbrodt et al. (2014). Further, the relationship between southward eddy heat fluxes and MOC strength becomes more convoluted

in a framework that includes evolving interactions with the atmosphere. In fact, southward eddy heat fluxes across the ACC are lower in our high-resolution control experiment (Bryan et al., 2014), while the lower cell is stronger. It is possible that the influence of abyssal mixing rates, as mediated by southward eddy heat fluxes, and westerly winds strength, are overemphasized, or misrepresented, in models that don't include realistically responsive surface fluxes.

The omission of evolving surface fluxes may alter mechanisms of heat uptake. Zhang and Vallis (2013) consider the impact of model resolution on ocean heat uptake in an idealized ocean-only model, which imposed surface heat fluxes and included neither sea ice nor the dependence of density on salinity. They attribute the greater abyssal heat uptake simulated in their higher resolution model to the greater advection of heat by the stronger mean state circulation, explained as a result of higher eddy heat fluxes across the ACC. In contrast, we find that circulation changes significantly redistribute the existing internal heat reservoir in our model in response to surface changes. This redistribution of heat is a larger component of abyssal Southern Ocean warming than the advection of anomalous heat taken up at the surface in these simulations, in agreement with the results of Xie and Vallis (2012).

Our results also suggest a possible shortcoming in the behavior of many standard resolution coupled models. Armour et al. (2016) studied Southern Ocean heat uptake across a range of standard resolution CMIP5 models, and found that the dominant mechanism for Southern Ocean heat uptake in these models was the northward advection, and ultimate subduction, of anomalous heat taken up at the Southern Ocean surface and resulting in warming in the upper 1500-2000 meters (Armour et al., 2016; Marshall et al., 2014). This mechanism of heat uptake is certainly active in our model, as evident by the significant mode water warming around $65°S - 35°$§(Fig. 2.4.4a-b). However, while the heat uptake of the Southern Ocean varies little with resolution ($2.5x10^{23}$ J at high resolution and $2.4x10^{23}$ J at low resolution),

more of this heat enters the lower cell in our simulations in our high-resolution experiment. This changes the distribution of heat with depth (Fig. 2.4.4c) as well as the circulation regime in which this anomalous heat resides. The models analyzed by Armour et al. (2016) produce unrealistically small volumes of, or spuriously formed, AABW (Heuzé et al., 2013). Our results raise the possibility that the response of standard resolution models to surface warming may be biased because of their inability to (realistically) simulate abyssal ocean warming, and instead these models warm too vigorously in the mode waters closer to the ocean surface. In other words, models with weaker lower cells versus those with stronger lower cells may have intrinsically different capacities to suppress surface warming over long timescales, as has been suggested for the AMOC (Winton et al., 2014). While temperature is not a passive tracer, the timescales at which anomalously warm interior waters might be expected to eventually alter SSTs likely differs for abyssal and mode waters because of their different residence times (Gebbie and Huybers, 2012, i.e.). Since radiative feedbacks are influenced by SST (Winton et al., 2010), a bias in the fate of heat taken up at the Southern Ocean surface could alter the evolution of transient climate change (Armour et al., 2013). We leave exploration of this possibility to future studies.

Chapter 3

Water Mass Transformation and Global Upwelling Pathways

3.1 Introduction

As discussed in Chapter 1, the formation of dense water must be compensated by interior transformation, which lighten dense interior waters, such that they can upwell through a steady density distribution. In this chapter, I apply the tools used in Chapter 2 not to probe the mechanisms by which dense water is formed, but instead to investigate the mechanisms by which dense water is upwelled. The question of how global deep waters are returned to the surface has galvanized the community for decades, and yet our understanding of this process is far from complete. Here, I propose a novel way of framing, and investigating, this historic question.

Chapter 2 introduced the concept of water mass transformation (WMT) as a tool with which the volume flux along isopycnals (the isopycnal circulation) can be related to an apparent flux of volume across isopycnals (the water mass transformation function) owing to interior mixing and surface fluxes. This WMT Framework was founded on the insights of Walin [1982], and has since been refined by numerous studies and used towards multiple ends. One common application of the framework asks variants of the question: how does surface transformation vary across different regions of the ocean? Such studies reveal that ocean-

atmosphere interactions depend dramatically on location (Speer et al., 1995; Howe and Czaja, 2009; Doney, 1998). In a second traditional approach, authors address the question: how do regional surface density fluxes versus internal ocean physics influence the regional isopycnal circulation? This approach can shed light on the influence of particular processes, such as light penetration (Iudicone et al., 2008), and non-linear mixing (Urakawa and Hasumi, 2012), or horizontal mixing, and seasonal deepening, of the mixed layer (Garrett, 1995; Marshall et al., 1999). A separate family of studies applies the principles of WMT to understand transport of heat and salinity through the global ocean (Ferrari and Ferreira, 2011; Zika et al., 2012; Nilsson et al., 2013; Xu et al., 2016). However, most frequently, the principles of WMT are employed to explore the dynamics of particular regions that are known to influence the large-scale ocean circulation. Such regions include dense-water formation regions at high latitudes (Speer and Tziperman, 1992; Newsom et al., 2016; Bryan et al., 2006; Langehaug et al., 2012), mode water formation regions (Cerovečki et al., 2013) and Southern Ocean upwelling regions (Abernathey et al., 2016; Lumpkin and Speer, 2007). These locations are widely studied precisely because their unique conditions allow for dramatic heat and freshwater exchange with the atmosphere. Yet, the existence of dense-water formation regions in a steady-state ocean inherently requires "companion" regions that experience an opposing exchange of heat or freshwater with the atmosphere. Yet, no study has attempted to use the principles of the WMT Framework to identify the internal ocean processes that couple these interconnected regions.

Here, I propose to do so. Specifically, I will address the question: what internal ocean processes, over the scale of the full ocean, are responsible for the upwelling of dense water masses? Essentially, what mechanisms close the Global Overturning Circulation (GOC)? I tackle this question from a theoretical perspective that applies principles of the WMT Framework to a closed, steady-state GOC. I am specifically interested in understanding how adiabatic and diffusive processes contribute to interior upwelling. This problem is best ad-

dressed within an isopycnal-diapycnal coordinate system. Adopting this perspective will aid in clarifying the distinct roles of adiabatic, diffusive, and surface processes in the global ocean.

3.2 WMT in a Closed Circulation System

3.2.1 Defining the problem

In this section I define a framework to address the relationship between surface density flux and mechanisms of ocean upwelling. Specifically, I probe the relationship between diapycnal (or diffusive) and along-isopycnal (or adiabatic) transports in the context of a closed circulation system in which downwelling away from the surface and upwelling to the surface are in balance. To do so, we introduce a framework to ensure a circulation is closed within the domain examined. The requirements of our framework are: 1) the system is in steady state, so there is no tendency in volume or density; 2) there are no internal sources or sinks of volume or density; 3) there is no thermodynamic interaction with seawater volume outside the domain, which is enforced by requiring that there is no transport of any kind across its internal ocean boundaries (any transport, across density classes, or integrated across them, would lead to an exchange of density, as will be shown below).

Here, I will develop a set of equations that will describe the transport of volume through a closed circulation, based on a derivation of the WMT following Iodicone et al., [2008B] and Urakawa and Hasumi [2012], among others. To ensure that adiabatic and diffusive processes can be identified throughout the domain, I adopt an orthogonal coordinate system. This is most straightforward if we define our coordinates relative to isopycnal distribution in an idealized basin domain bounded by isopycnals σ_{max} and σ_{max} (with $\sigma_{min} < \sigma_{max}$, and σ represents potential density), and the surface or bottom bathymetry that they intersect. We make the simplification that there are no zonal variations in isopycnal slope and or flow, and

thus can simplify the problem into two dimensions. To do so, we define coordinates as a directions $\hat{s}$, parallel to isopycnals everywhere, and $\hat{r}$, perpendicular to isopycnals everywhere. Distances within the domain are measured by vectors r and s in this coordinate system, where the minimum and maximum values of r (r_1 and r_2) coincide with σ_{max} and σ_{min}, respectively. The dimension s spans the length of isopycnals, from where they outcrop or intersect the ocean bottom. We call the southern extent of isopycnals s_{SH} and the northern extent s_{NH}. Fig. 3.2.1 illustrates these coordinates in their native space; projections of this into spatial coordinates, for given circulation systems, will be illustrated in Section 3.3, Fig 3.3.1.

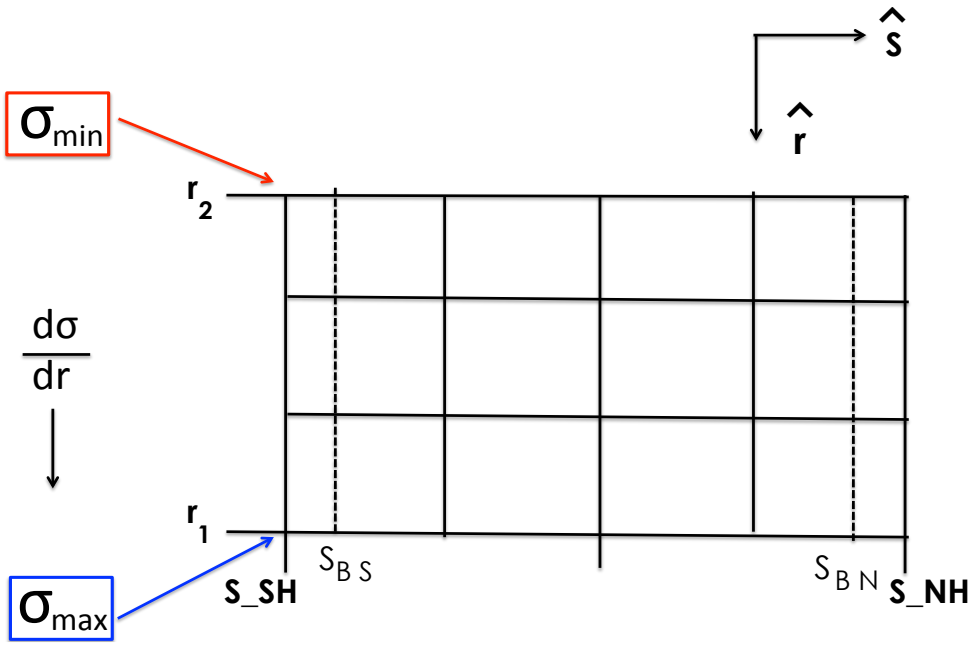

Figure 3.2.1: A schematic of the $r - s$ coordinate system. Note that the maximum density in the domain, σ_{max}, is located at r_1, the minimum density in the domain, σ_{min} is located at r_2. The minimum s value, s_{SH}, defines the location of the "Southern Hemisphere" surface outcrop or ocean bottom, while s_{NH} defines the location of the "Northern Hemisphere" outcrop, or the ocean bottom. The locations of two surface boundary layers, s_{B_S} and s_{B_N} will be important to the derivation below.

The flow velocity in this domain has no zonal component (as we assume no variations with longitude within the domain) and can be written as $\vec{v} = v_s\hat{s} + w_\sigma\hat{r}$. The total volume trans-

port across isopycnal surface σ towards lower density classes, and between s_{SH} and s is given by $\Omega(r, s)$, where

$$\Omega(r, s) = \int_{s_{SH}}^{s} w_\sigma(r, s) ds. \tag{3.1}$$

In this coordinate system, Ω is associated purely with the rate of water mass transformation, meaning the redistribution of volume between density classes from non-advective processes such as eddy stirring, diffusion, mixing, and air-sea flux. The total volume transport below an isopycnal surface at r, and across s, is given by $\Psi(r, s)$, where

$$\Psi(r, s) = \int_{r_1}^{r} v_s(r, s) dr. \tag{3.2}$$

Essentially, Ψ is the circulation that arrives from the distribution of adiabatic, along-isopycnal flow throughout the domain. In a steady-state, incompressible ocean, these transports balance, and thus

$$\Omega = \Psi. \tag{3.3}$$

In this study we are particularly interested in how diffusive and adiabatic processes redistribute *density* between surface regions. To address this, we note that a volume transport through an ocean with spatially varying σ must also convey mass to maintain a steady state; indeed, Ψ and Ω act together to redistribute density from regions where it is gained at the surface towards regions of the surface where it is lost. The volume transport across and along a field of isopycnals is thus related to the "density transport," M, which, because of

the orientation of our coordinate system, is most clearly associated with stream function Ω. This follows because a volume flux between different density classes cannot occur without a change in the density of any parcel being transported, and thus a convergence of density transport. We define M as:

$$\Omega = -\frac{\partial M}{\partial \sigma}, \tag{3.4}$$

relating a convergence in net density transport to diapycnal volume flux (which will be explicitly illustrated below). This convergence will alter isopycnal volume, which in steady state must be balanced by an equivalent volume transport *along* isopycnals. In other words, by continuity and Eq. 3.3,

$$\Psi = -\frac{\partial M}{\partial \sigma}, \tag{3.5}$$

such that the density transport associated with the diapycnal transformation is balanced by that associated with the isopycnal circulation (i.e. Marshall et al., 1999, Eq. 2.5). Here, M is an analogue to the Heat and Salinity Functions (Ferrari and Ferreira, 2011; Zika et al., 2012; Xu et al., 2016), but differs in that it quantifies a net density transport exactly along and across isopycnals, and thus will quantify the density transport enabled by adiabatic, and diffusive processes throughout the domain (these transports cannot be precisely separated everywhere in studies using non-orthogonal coordinate systems).

Now, I will justify why Ω can be explicitly linked to interior diffusive processes and surface density flux , and in doing so, discover what sets the pattern of density transport through the ocean at any location. First, note that because of our coordinate system, the tendency in potential density experienced by a moving parcel (equivalently, the material derivative)

can be related directly to the cross-isopycnal velocity w_σ

$$\frac{D\sigma}{Dt} = w_\sigma \frac{d\sigma}{dr}. \tag{3.6}$$

Thus, at a particular location, Ω is given by,

$$\Omega(r,s) = \int_{s_{SH}}^{s} w_\sigma ds = \frac{\partial}{\partial \sigma} \int_{s_{SH}}^{s} \int_{r_1}^{r} \frac{D\sigma}{Dt} dr ds, \tag{3.7}$$

Secondly, note that a tendency in potential density, and thus a diapycnal velocity in a given location, can arise from air-sea forcing (which I separate into component f) or by interior ocean mixing, eddy-stirring near the surface, and diffusion (component d) [e.g. Urakawa and Hasumi, 2013, Groeskamp et al., 2016, Abernathey et al., 2016 Marshall et al., 1999], or

$$\frac{D\sigma}{Dt} = f + d. \tag{3.8}$$

I will use these distinct components of the material derivative to break the total water mass transformation, Ω, into the component associated with surface density flux, F (or the surface transformation), and the component associated with any other interior ocean process that leads to diapycnal volume flux, D (as was done in Chapter 2). Before explicitly defining these components from Eq. 3.8 and relating them to the circulation, Ψ, I clarify several important features of this framework. First, note that while the structure of f is associated purely with density flux acting exactly at the surface boundary, this framework (which uses volume conservation to equate a discrete value of cross-isopycnal volume flux at the surface to an equivalent volume flux along isopycnals towards or away from the surface) rests upon the notion that F is defined over some finite distance between the ocean surface and an

interior point — I call this the "surface boundary layer," which must be finite but can be arbitrarily small. Essentially, because the velocity normal to the ocean surface must be zero at the surface, I cannot meaningfully relate the rate of surface transformation to Ψ except over some distance away from the surface where along-isopycnal velocity can be non-zero. The boundary layer, as defined here, may be much smaller than the mixed layer in regions where significant horizontal mixing occurs near the surface (for instance, in the equatorial regions, where Ψ may vary greatly from F within the mixed layer) [e.g. Garrett and Tandon, 1997, Marshall et al., 1999, Groeskamp et al., 2016]. Thus, Ω at any point will be governed by: F, the constant diapycnal volume redistribution *required* by surface forcing, and D, the diapycnal volume redistribution induced by interior ocean mixing, eddy-stirring, and diffusive processes. By our definition, $d = 0$ within the surface boundary layer; the thickness of this boundary layer, and thus the distance away from the ocean surface at which mixing and diffusion begin to affect the circulation, will depend greatly on local ocean physics.

A second feature of the framework which must be kept in mind when defining the total water-mass transformation Ω at any point within the domain is that while F is (by construction) defined to be one value at every r over an discrete boundary layer, D is an *integrated* quantity that expresses the total diapycnal volume flux across a given isopycnal between the surface outcrop and a given s. Thus, the definition of Ω, relative to each component, depends on where I choose to begin this integration. For this study, I define $D = 0$ at s_{SH} (the "southern hemisphere" surface outcrop) and integrate towards s_{NH} (which corresponds to the "northern hemisphere" surface outcrop in a circulation within which isopycnals outcrop twice, or the location of the ocean bottom in a circulation system in which all isopycnals outcrop only once). With that in mind, I define a general relationship between Ω, F, and D, throughout the domain:

$$\Omega(r, s_{BS}) = F_{SH}(r) \quad \text{at } s = s_{BS}, \tag{3.9}$$

$$\Omega(r, s) = F_{SH}(r) + D(r, s) \quad \text{for all } s_{BS} < s < s_{BN} \quad \text{and} \tag{3.10}$$

$$\Omega(r, s_{BN}) = F_{SH}(r) + D(r, s_{BN}) + F_{NH}(r) \quad \text{at } s = s_{NH} \tag{3.11}$$

where

$$D(r, s) = \frac{\partial}{\partial \sigma} \int_{s_{SH}}^{s} \int_{r_1}^{r} d \; drds. \tag{3.12}$$

and by construction, $D = 0$ within the "southern" surface boundary layer (defined between s_{SH} and s_{BS}). Further, D gains no *additional* magnitude between s_{BN} and s_{NH} (the width of the northern surface boundary layer). Within each surface boundary layer, the only contribution to Ω is from surface transformation, F, explicitly defined as:

$$F_{SH}(r) = \frac{\partial}{\partial \sigma} \int_{s_{SH}}^{s_{BS}} \int_{r_1}^{r} f drds; \tag{3.13}$$

$$F_{NH}(r) = \frac{\partial}{\partial \sigma} \int_{s_{BN}}^{s_{NH}} \int_{r_1}^{r} f drds. \tag{3.14}$$

Using this decomposition of Ω, I step through the domain to ascertain the structure of Ψ at particular s values (to the extent that is possible within this framework):

$$\Psi(r, s_{SH}) = 0 \quad \text{(in a non-divergent ocean)} \tag{3.15}$$

$$\Psi(r, s_{BS}) = F_{SH}(r) \tag{3.16}$$

$$\Psi(r, s) = F_{SH}(r) + D(r, s) \quad \text{for any } s_{BS} < s < s_{BN}, \text{ and} \tag{3.17}$$

$$\Psi(r, s_{BN}) = F_{SH}(r) + D(r, s_{BN}) + F_{NH}(r) \tag{3.18}$$

$$\Psi(r, s_{NH}) = 0 \quad \text{(again, in a non-divergent ocean).} \tag{3.19}$$

Eq. 3.19 requires that

$$D(r, s_{NH}) = -[F_{SH}(r) + F_{NH}(r)] \tag{3.20}$$

$$\text{such that} \quad \Psi(r, s_{BN}) = -F_{NH}(r). \tag{3.21}$$

The negative sign in Eq. 3.21 arises because the relationship between along-isopycnal and across-isopycnal volume flux depends upon the direction in which each volume component is defined to be positive. For example, the equivalent positive value of Ψ, at a given s, will fill a volume sitting to its "south" and empty a volume sitting to its north. Given the sign conventions chosen, and since I integrate water-mass transformation northward from s_{SH}, Ψ will be opposed by surface transformation in the "northern" hemisphere.

We can gain further insight into this system if we consider the behavior of Ω at the boundaries of the domain. To do so, note that a change in density experienced by a moving parcel, $\frac{D\sigma}{Dt}$ results from a Eulerian convergence or divergence of surface density flux (λ, where $\nabla \cdot \lambda = \frac{D\sigma}{Dt}$) either acting into the ocean surface or across isopycnal surfaces in the ocean's interior [e.g. Marshall et al., 1999, Groeskamp et al., 2016]. Using the divergence theorem and Eq. 3.14,

I explicitly define F from surface density fluxes, as

$$F(r)_{SH} = \frac{\partial}{\partial \sigma} \int_{r_1}^{r} \lambda(r, s_{SH}) dr \quad \text{and} \tag{3.22}$$

$$F(r)_{NH} = \frac{\partial}{\partial \sigma} \int_{r_1}^{r} \lambda(r, s_{NH}) dr \quad \text{and} \tag{3.23}$$

where $\lambda(r, s_{SH})$ and $\lambda(r, s_{NH})$ are the patterns of surface density flux on the southern and northern surfaces, respectively. I use this definition to relate surface transformation and interior transformation over the full domain (noting that these components must sum to zero when integrated over the domain to conserve volume):

$$0 = \Omega(r_2, s_{NH}) \tag{3.24}$$

$$= \frac{\partial}{\partial \sigma} \int_{s_{SH}}^{s_{NH}} \int_{r_1}^{r_2} \frac{D\sigma}{Dt} dr ds \tag{3.25}$$

$$= \frac{\partial}{\partial \sigma} \int_{r_1}^{r_2} \lambda(r, s_{SH}) dr + \frac{\partial}{\partial \sigma} \int_{r_1}^{r_2} \lambda(r, s_{NH}) dr + \frac{\partial}{\partial \sigma} \int_{s_{SH}}^{s_{NH}} \lambda(r_1, s) ds + \frac{\partial}{\partial \sigma} \int_{s_{SH}}^{s_{NH}} \lambda(r_1, s) ds \tag{3.26}$$

$$= F_{SH}(r_2) + F_{NH}(r_2), \tag{3.27}$$

which follows because $\lambda(r_1, s) = \lambda(r_2, s) = 0$ for all s, by the requirement that there be neither internal sources of density, nor thermodynamic interaction with any volume outside the domain. Thus, in a steady state,

$$F_{SH}(r_2) = -F_{NH}(r_2), \quad \text{and equivalently,} \tag{3.28}$$

$$\int_{\sigma_{min}}^{\sigma_{max}} F_{SH} d\sigma = -\int_{\sigma_{min}}^{\sigma_{max}} F_{NH} d\sigma. \tag{3.29}$$

Eq. 3.29 states both that volume must be conserved within the domain, and that the total

surface density flux into all surface outcrops bounding the domain must be zero in steady state.

For this study, I want to use these components of volume transport to ascertain how density is transported between ocean surface regions, M. I can now express M, in terms of each component of the volume balance:

$$M(r,s) = -\int_{\sigma} F_{SH}(r)d\sigma - \int_{\sigma} D(r,s)d\sigma = -\int_{\sigma} \Psi(r,s)d\sigma \quad \text{for all } s < s_{B_N} \tag{3.30}$$

Recall, M in this study is similar to the Heat function of Salinity Function (e.g. Ferrari and Ferreira, 2011). Now that I have defined M explicitly, it is useful to revisit how it differs from these previously defined functions. Here, M expresses the transport, at any point of a volume-integrated density flux. Physically, this equates to a transport in mass away from the average mass of a parcel of seawater, capturing the combined effects of how heat and freshwater transport influences the gravitational force acting on a seawater parcel in a given region in a Boussinesq ocean. In the interior ocean, this mass transport will balance the surface density flux integrated across the surface of distinct regions (which effectively adds a perturbation in mass to the ocean). A quantity of particular interest is the *total* mass transport moved by the system between ocean surfaces (meaning when integrated across the full density range at a given s) described by

$$M_{tot} = M\Big|_{\sigma_{max}}^{\sigma_{min}}. \tag{3.31}$$

M_{tot} is of particular significance, within this coordinate system, because it is constant at every s in the domain. Note that this quantity is only constant in an isopycnal-diapycnal

coordinate system. This can be shown by considering the behavior of M_{tot} over some small distance, Δs, away from the ocean surface. Because there can be no density flux acting perpendicular to isopycnals in the ocean interior, (i.e. $\nabla \cdot \lambda = \frac{d\lambda}{ds}$ at any point away from the ocean surface),

$$\frac{\Delta M_{tot}}{\Delta s} = \int_{\sigma_{max}}^{\sigma_{min}} \lambda(r_2, s)\Delta s - \int_{\sigma_{max}}^{\sigma_{min}} \lambda(r_1, s)\Delta s = 0.$$

This follows because, as noted above, $\lambda(r_1, s) = \lambda(r_2, s) = 0$ for all s, physically stating that the total density content cannot be altered within the domain at any s away from the surface. Thus a non-zero M_{tot} indicates a surface density flux imbalance on different sides of the same isopycnal, an imbalance which must be transported from one surface outcrop to another. Meaning, any non-zero value of M_{tot} is an indication of some net, adiabatic surface-to-surface density transport, as required by some net imbalance between surface outcrops, and can quantified as:

$$M_{tot} = -\int_{\sigma_{max}}^{\sigma^{min}} F_{SH}(s)d\sigma = -\int_{\sigma_{max}}^{\sigma^{min}} \Psi(r, s)d\sigma = \int_{\sigma_{max}}^{\sigma^{min}} F_{NH}(s).d\sigma \tag{3.32}$$

This essentially states that the density transport (when summed across all density classes) at any point s in the domain (i.e. between "hemispheric" outcrops) is exactly set by the magnitude of the surface density flux incurred on either surface, in a direction that conveys the amount gained at one surface towards the surface over which it is lost at a constant rate for all s. However, if every density class in the domain outcrops only once, Eq. 3.32 becomes

$$\boldsymbol{M_{tot}} = -\int_{\sigma_{max}}^{\sigma^{min}} F_{SH}d\sigma = -\int_{\sigma_{max}}^{\sigma^{min}} \Psi(r, s)d\sigma = 0. \tag{3.33}$$

in steady state. In this case, while F_{SH} can be non-zero on a given isopycnal (or, locally over some surface region), there can be no total surface imbalance over the entire surface, nor any interior density transport in $\hat{s}$ over the full domain, in steady state.

Eqs. 3.32 and 3.33 clarify the distinct roles of Ψ and D, in the transport of *density* between regions of the ocean surface. We can now understand the isopycnal circulation, Ψ, as the interior mechanism that conveys imbalances in surface density flux between outcrop regions at opposite ends of the *same* isopycnal; indeed, such persistent surface forcing *requires* interior adiabatic transport. Conversely, diapycnal transport, D (or the effective diapycnal redistribution from eddy stirring, mixing and diffusion) is the interior mechanism that serves to redistribute imbalances in surface density flux between outcrops of *different* density classes. These distinctions are depicted schematically in Fig.3.2.2.

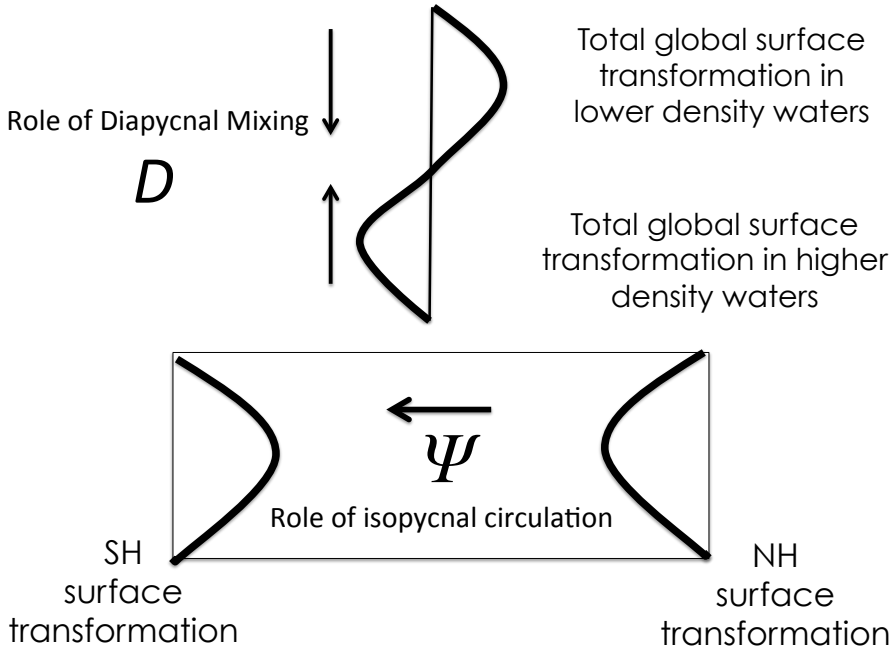

Figure 3.2.2: A schematic representation of the roles of the isopycnal and diapycnal volume transport, Ψ and D, in redistributing surface transformation on a global scale.

By definition, Ψ and D play distinct roles in the system, but the total amount of den-

sity flux these components transport, together at any point in the domain, will be set by the distribution of surface density flux (integrated from σ_{max} to σ_{min}). An important point to make, for the coming chapters, is that there can be rich spatial structure in the relative strength of diapycnal or isopycnal transport across each density class in the interior, so long as this structure adheres to the constraints on the system at every point. The distribution of surface density flux, as well as the relationships between components throughout the domain, as derived throughout this section, will govern the circulation everywhere in our domain. Here I summarize them:

Governing Equations of volume and density transport for any closed circulation in a steady state ocean

$$D(\sigma, s_{SH}) = 0; \tag{3.34}$$

$$D(\sigma,_{NH}) = -(F_{SH} + F_{NH}) \tag{3.35}$$

$$\Psi(\sigma, s_{B_S}) = F_{SH}(\sigma) \tag{3.36}$$

$$\Psi(\sigma, s) = F_{SH}(\sigma) + D(\sigma, s) \quad \text{for all } s < s_{B_N} \tag{3.37}$$

$$\Psi(\sigma, s_{B_N}) = -F_{NH}(\sigma) \tag{3.38}$$

$$M(\sigma, s) = -\int_{\sigma} \Psi(\sigma, s) d\sigma = -\int_{\sigma} (F_{SH}(\sigma) - D(\sigma, s)) d\sigma \quad \text{for all } s < s_{B_N} \tag{3.39}$$

$$M_{tot} = \int_{\sigma_{max}}^{\sigma_{min}} \Psi d\sigma = -\int_{\sigma_{max}}^{\sigma_{min}} F_{SH} d\sigma = -\int_{\sigma_{max}}^{\sigma_{min}} F_{NH} d\sigma \tag{3.40}$$

Several examples of the relationships summarized here are schematically depicted in Fig. 3.2.3. I will now demonstrate the of utility these governing equations to explore the dynamics of several simplified circulation systems.

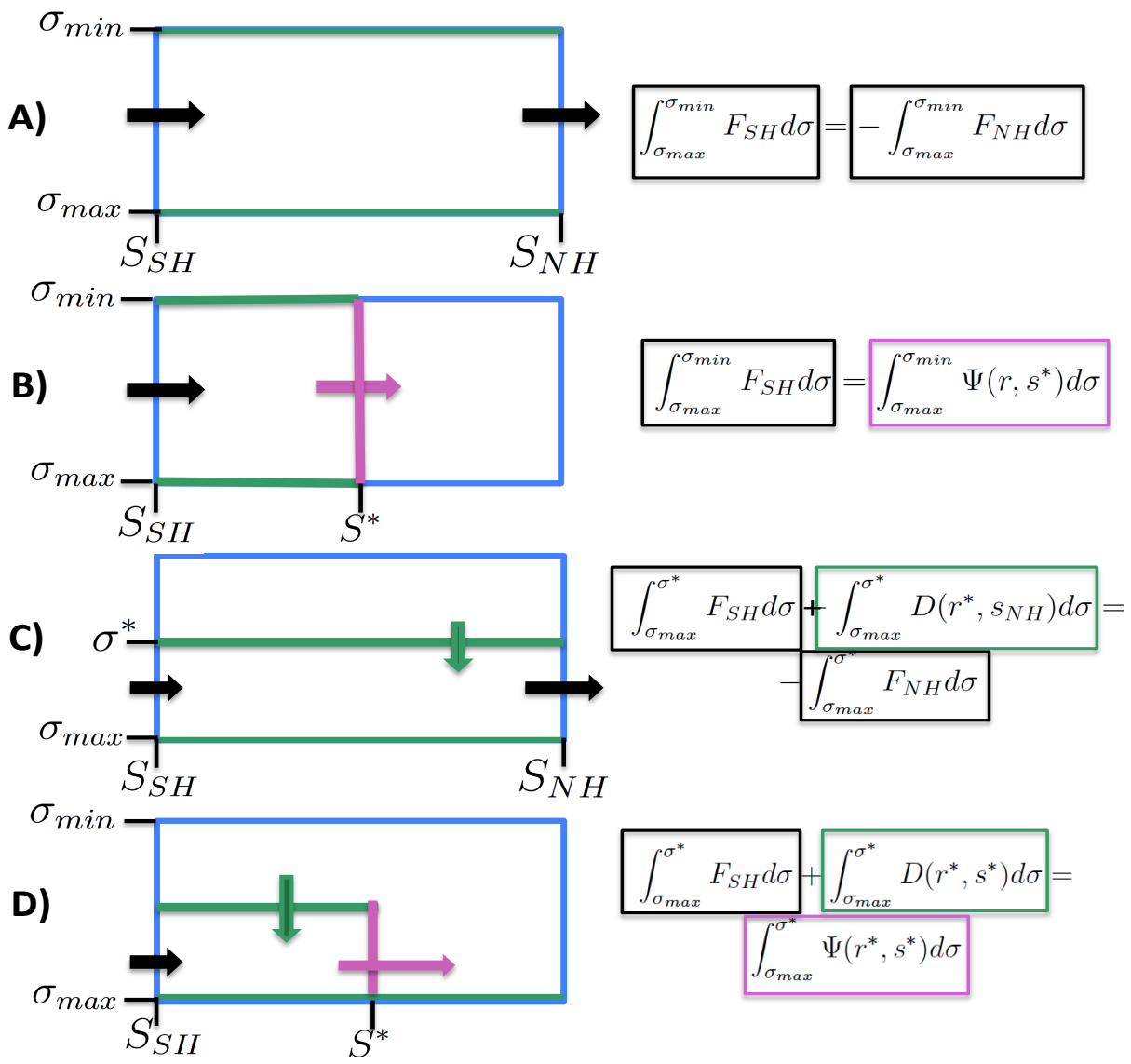

Figure 3.2.3: A schematic representation of net density transport across and along a field of isopycnals at different points in the domain. Colors refer contributions to net density transport from F (black), D (green), and Ψ (magenta). A) Net density gain into s_{SH} is balanced by net loss at s_{NH}; B) Net density gain into s_{SH} is balanced by all adiabatic flow for $\sigma > \sigma_{min}$ at s^*; C) Net density gain into s_{SH} below σ^* is balanced by net interior diapycnal volume flux across σ^* and net density loss at s_{NH}; D) Net density gain into into s_{SH} below σ^* s balanced by net interior diapycnal volume flux across σ^* between s_{SH} and s^*, and by adiabatic flow along all $\sigma > \sigma^*$ at s^*.

3.3 Probing Idealized Systems

3.3.1 Simple analytic models for closed circulations

The simple theory developed in Section 3.2.1 will govern the density transport at a given point in space in a complete steady state circulation. To demonstrate the utility of this

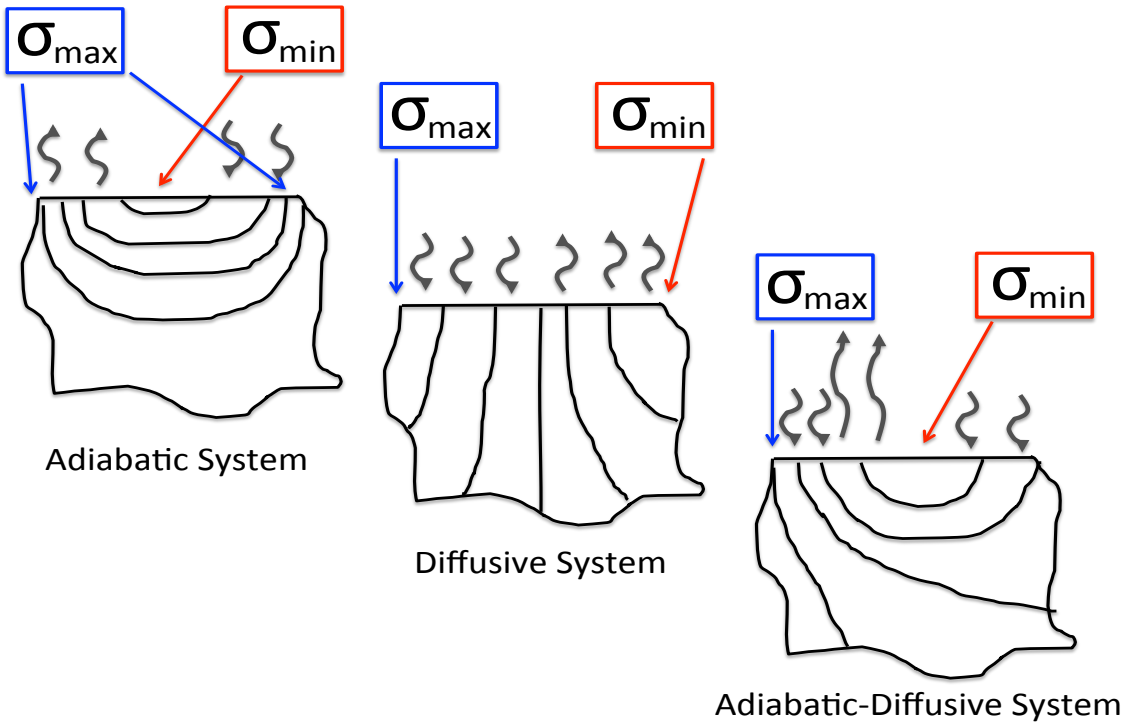

Figure 3.3.1: The $r - s$ coordinate system, projected into $y - z$ space (assuming no zonal variations). Each schematic represents the physical distribution of isopycnals for each idealized system discussed in Section 3.3. A) The adiabatic system; B) the diffusive system; and C) The adiabatic-diffusive system. Arrows at the ocean surface represent the direction of density flux, positive into the ocean (corresponding to dense water formation). NOTE- will add sigma and r and s labels, lettering,

theory, I will apply it to several idealized ocean circulations, each of which is maintained by differing interior mechanisms and regional surface transformation distributions. To most clearly illustrate how much can be determine about a given system when considering these thermodynamic relationships alone, I do not use any fields from climate or ocean models that simulate actual physical processes. Thus, for circulations that include diapycnal mixing (the "Purely Diffusive" and "Adiabatic Diffusive" systems described below), I prescribe simple interior mixing patterns.

System 1) Pure adiabatic closure

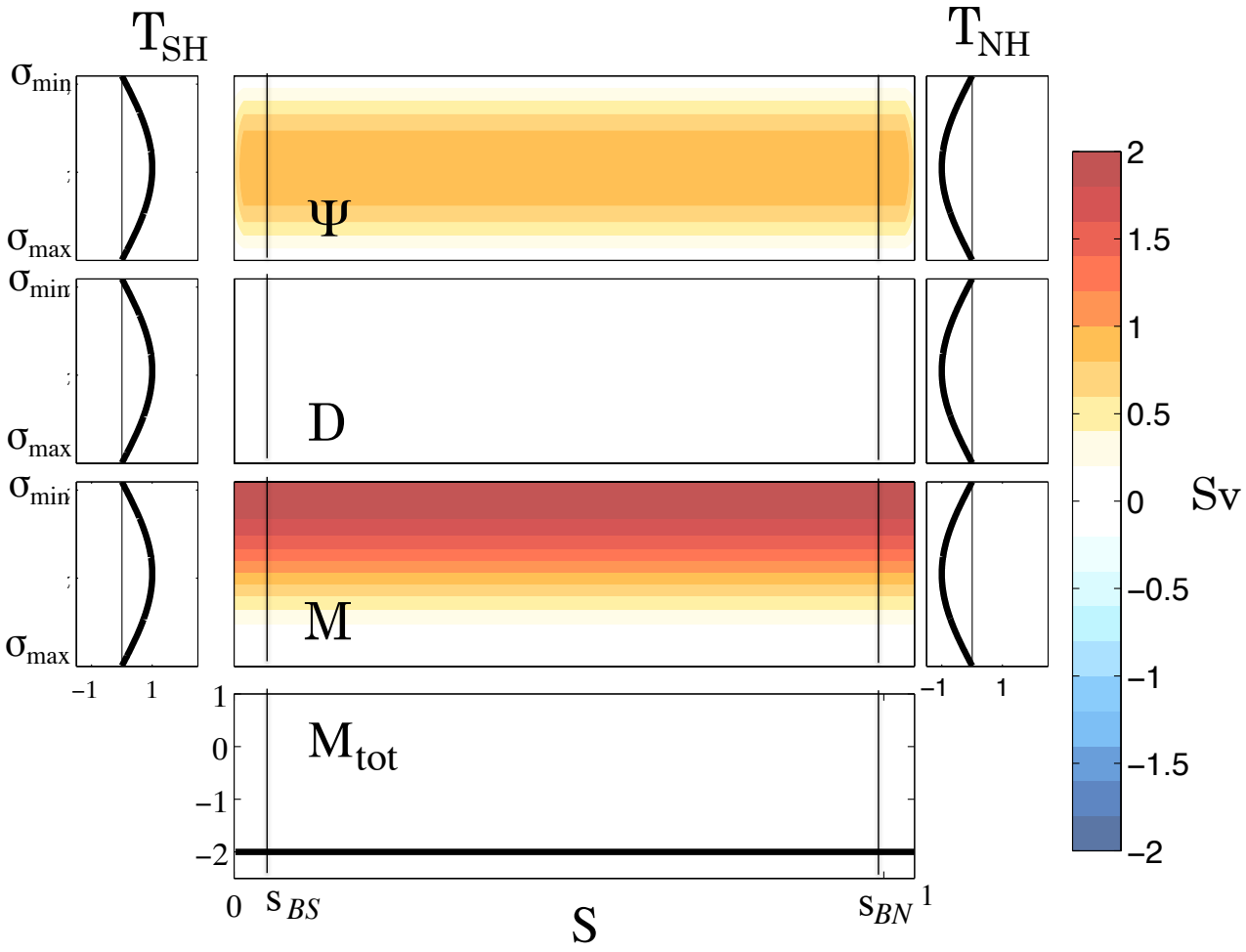

Figure 3.3.2: Components of volume and density transport in an idealized purely adiabatic circulation. Side panels: distribution of surface transformation, F, across the surface boundary regions of the Southern and Northern surface outcrops, respectively. Central panels: first panel) distribution of the isopycnal circulation, Ψ, at every point within the domain, between surface boundary regions; within each boundary regions, Ψ will go to zero at each surface; second panel) distribution of mixing driven transformation, D; third panel) distribution of cumulative density transport, M, at every point; fourth) the value of M_{tot} at every s value throughout the domain.

First I consider a system with no interior mixing whatsoever. A circulation of this type is often referred to as an "adiabatic circulation" [e.g. Wolfe and Cessi, 2011, 2013]. In an adiabatic circulation, all isopycnals *must* outcrop twice at the surface (any surface density flux experienced on one outcrop cannot be balanced by any cross-isopycnal flow) meaning all volume and σ redistribution must be sustained by an imbalance in surface transformation between outcrops, as quantified by our system of governing equations. This system will have

a non-zero M_{tot}. Note that we use the term "purely adiabatic" even though non-zero surface transformation drives cross-isopycnal circulation in the surface mixed layer.

To compare how F, D, Ψ and M interact in a purely adiabatic system, let's suppose there is positive surface transformation in the "Southern Hemisphere" when integrated from σ_{max} to σ_{min}, of the form

$$F_{SH} = \sin(\frac{\sigma_{max} - \sigma}{\sigma_{max} - \sigma_{min}}\pi) \tag{3.41}$$

where θ depends linearly on σ. Using our general system of equations and applying the specifications of this adiabatic circulation, we arrive at:

Governing equations for a purely adiabatic system

$$1) \quad \theta = \frac{\sigma_{max} - \sigma}{\sigma_{max} - \sigma_{min}}\pi \tag{3.42}$$

$$2) \quad 0 \leq \theta \leq \pi \tag{3.43}$$

$$3) \quad F_{SH} = \sin(\theta) \tag{3.44}$$

$$4) \quad F_{NH} = -\sin(\theta) \tag{3.45}$$

$$5) \quad D(\theta, s) = 0 \tag{3.46}$$

$$6) \quad \Psi(\theta, s) = F_{SH} + D = -F_{NH} = \sin(\theta) \tag{3.47}$$

$$7) \quad M(\theta, s) = -\int_0^\theta \Psi d\theta - 1 = [\cos(\theta) - \cos(0)] - 1 \tag{3.48}$$

$$8) \quad M_{tot} = -2 \tag{3.49}$$

Fig. 3.3.2 illustrates how this surface forcing field relates the circulation Ψ and the associated net density transport, M. In the absence of mixing, no mechanism can redistribute density

across isopycnals, and thus all fields are constant in s throughout the domain. Because the system experiences a gain in density at its northern surface and loss from its southern surface, a density transport is conveyed southward between surfaces to counter the surface forcing. This transport in isolation would continually make waters denser in the Southern Hemisphere ($-\hat{s}$) and lighter the Northern Hemisphere ($+\hat{s}$). While clearly idealized, many studies have noted that a component cell of the GOC could be quasi-adiabatic, as enabled by wind-driven upwelling in the Southern Ocean (Wolfe and Cessi, 2011, 2015; Radko et al., 2008; Radko and Kamenkovich, 2011).

System 2) Purely diffusive closure

The opposite endmember to an purely adiabatic circulation is a circulation in which all regional differences in surface transformation, F, are balanced by diapycnal mixing (Fig. 3.3.3). While I call such circulations "purely diffusive", note that there can be some along-isopycnal volume transport so long as there is no net transport of density between surface outcrops (i.e. $M_{tot} = 0$). For this reason, isopycnals can only outcrop once at the surface in a purely diffusive system, and the total surface transformation must be zero when integrated across all density classes. Surface transformation is entirely balanced by interior ocean mixing and, unlike in a purely adiabatic system, the spatial structure of the circulation, $\Psi(r, s)$, will depend sensitively on the distribution of this mixing. Thus, I must prescribe a mixing pattern that adheres to the requirements of our closed circulation. Here, I illustrate the behavior of the system in response to intensified mixing along the densest waters in the system (focused at σ_{max}), in a system forced by sinusoidal surface transformation. The resultant structures of Ψ, D, and M in this purely diffusive system are given below.

Governing equations for an idealized diffusive system

$$1) \quad \theta = \frac{(\sigma_{max} - \sigma)}{(\sigma_{max} - \sigma_{min})} 2\pi \tag{3.50}$$

$$2) \quad 0 \leq \theta \leq 2\pi \tag{3.51}$$

$$3) \quad F_{SH} = -\sin(\theta) \tag{3.52}$$

$$4) \quad F_{NH} = 0 \tag{3.53}$$

$$5) \quad D(\theta, s) = \sin(\frac{\theta}{s}) \quad \text{for } \theta \leq 2\pi s \tag{3.54}$$

$$D(\theta, s) = 0 \quad \text{for } \theta > 2\pi s \tag{3.55}$$

$$6) \quad \Psi(\theta, s) = F_{SH} + D = F_{SH} = \sin(\theta) + \frac{s}{2\pi}\sin(\theta - s) \tag{3.56}$$

$$7) \quad M(\theta, s) = -\int_0^\theta \Psi d\theta + 1 \tag{3.57}$$

$$8) \quad M_{tot} = \cos(2\pi) - \cos(0) = 0 \tag{3.58}$$

For this example, I've chosen a specific, idealized mixing pattern. In reality, the distribution of D will vary greatly depending on internal ocean physics. For instance, D might erode F significantly within the mixed layer if there is significant horizontal mixing, or seasonal fluctuations in mixed layer depth [e.g. Garrett and Tregue **]; further, the distribution of bathymetry will influence where mixing actually occurs in the abyssal ocean. However, this example illustrates several important features universal to any purely diffusive system. First of all, for a given F, D will be the same at the boundaries in all diffusive systems, regardless of internal ocean physics. Additionally, as noted above, $M_{tot} = \int_0^{2\pi} \Psi d\sigma = 0$, which physically means that there can be no density transport along isopycnals when integrating flow over the full range of density classes (which would lead to a density tendency at the end of the domain at the ocean bottom). This has two important implications for the structure of the circulation, Ψ: first of all, Ψ must slow to zero at the ocean bottom. Secondly, Ψ cannot be characterized by a single circulation cell. Specifically, so that there is no net density transport in $\hat{s}$ at any s, one cell rotating across a density gradient in one direction (which will result

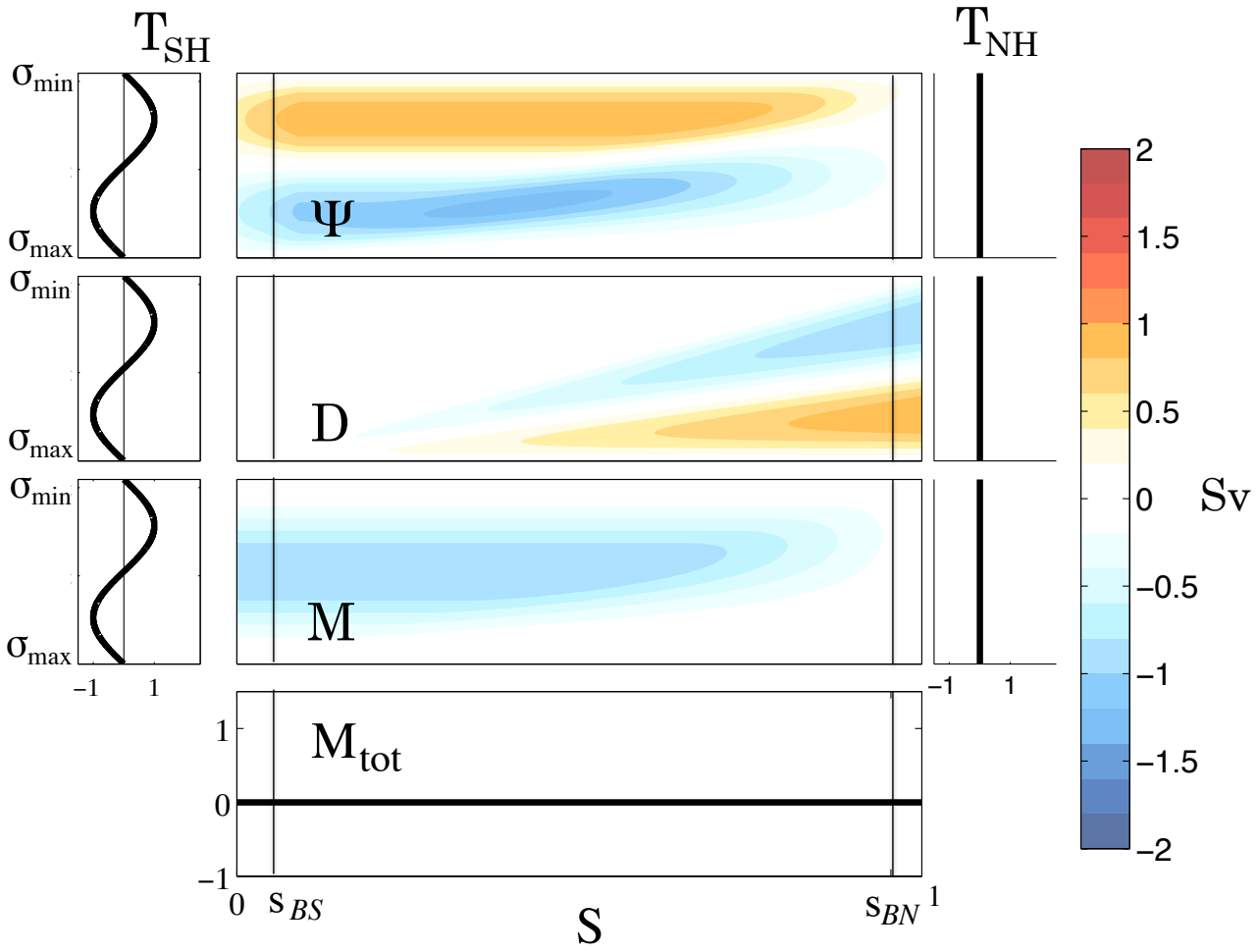

Figure 3.3.3: As in Fig. 3.3.2, but for a purely diffusive system.

in a net density transport in $\hat{s}$) must be balanced by a counter-rotating cell which results in the equivalent density transport in $-\hat{s}$ (so long as the density gradient is monotonic, as will be the case for the majority of the ocean). The strength of each cell can vary in concert with variations in stratification (as can be seen in Fig. 3.3.3), but, their combined circulation is constrained everywhere.

The structure of M reveals the fundamental coupling between circulation cells in this purely diffusive system. Note that across the density class where the clockwise and counterclockwise cells diverge in Fig. 3.3.3 (at which $\Psi(r, s) = 0$), $|M|$ is at its peak. This maximum value captures the total transport of density between counter-rotating cells, essential for main-

taining the system wide constraint that $M_{tot} = 0$, and physically illustrating that diapycnal mixing lightens dense waters, and makes light waters more dense. This is arguably the the most important feature demonstrated in this system: while each cell may appear to be a distinct circulation, the two cells in this system, and any circulation cells in a system in which diffusive interior transformation balances surface transformation, are deeply coupled from a thermodynamic perspective. This has important implications for the overturning circulation in the real global ocean, as will be discussed in the following example- a mixed adiabatic-diffusive circulation.

System 3: Adiabatic-diffusive closure: a simplified zonally-averaged MOC

-As a final application of the closed circulation transformation framework, I consider a circulation which is maintained by both diffusive and adiabatic processes. I use this simplified system to highlight aspects of the real GOC, as we expect there to be both diffusive, and adiabatic, processes at work in the real ocean [e.g. Ferrari, 2014] In this type of system, different surface outcrops will experience differing patterns of forcing, meaning there can be a net imbalance in surface density flux across differing density classes and between different surface outcrops. To mimic the deep pole-to-pole cells of zonally-summed GOC (the "Upper" and "Lower" Cells), I consider a system that experiences a positive density flux into the densest waters outcropping in each hemisphere (and drives negative surface transformation). This negative transformation mimics dense water formation in each hemisphere, and is balanced by the positive transformation (density loss) of lighter waters at the "southern" surface. I choose a surface forcing pattern which captures these features, and is meant to illustrate the dynamics of a system in which all dense water formation is balanced by buoyancy gain into upwelling waters in the Southern Ocean. Again prescribing the bottom-intensified mixing distribution, D, as used in the previous circulation system, I now quantify the relationships between F, Ψ, D, and M throughout the domain.

Governing equations for an idealized adiabatic-diffusive, "MOC" system

$$1) \quad \theta = \frac{(\sigma_{max} - \sigma)}{(\sigma_{max} - \sigma_{min})} 2\pi \tag{3.59}$$

$$2) \quad 0 \leq \theta \leq 2\pi \tag{3.60}$$

$$3) \quad F_{SH} = -\sin(\theta) \quad (0 \leq \theta \leq \pi); \quad F_{SH} = -2\sin(\theta) \quad (\pi \leq \theta \leq 2\pi) \tag{3.61}$$

$$4) \quad F_{NH} = 0 \quad (0 \leq \theta \leq \pi); \quad F_{NH} = \sin(\theta) \quad (\pi \leq \theta \leq 2\pi); \tag{3.62}$$

$$5) \quad D(\theta, s) = \sin(\frac{\theta}{s}) \quad \text{for } \theta \leq 2\pi s \tag{3.63}$$

$$D(\theta, s) = 0 \quad \text{for } \theta > 2\pi s \tag{3.64}$$

$$6) \quad \Psi(\theta, s) = -\sin\theta + \frac{s}{2\pi}\sin(\theta - s) \quad (0 \leq \theta \leq \pi); \tag{3.65}$$

$$\Psi(\theta, s) = -2\sin\theta + \frac{s}{2\pi}\sin(\theta - s) \quad (\pi \leq \theta \leq 2\pi) \tag{3.66}$$

$$7) \quad M(\theta, s) = -\int_0^\theta \Psi d\theta + 1 \tag{3.67}$$

$$8) \quad M_{tot} = -2 \tag{3.68}$$

The components of this system are illustrated in Fig. 3.3.4. Given that the system is highly idealized, it is encouraging that the emergent circulation has several physically relevant features. First of all, note the formation of a counterclockwise (negative) "Lower Cell" emanating from boundary layer the southern surface, the strength of which is reduced to zero by the end of the domain. This circulation is compensated by a clockwise "Upper Cell" that is weakest at the northern surface boundary layer, and stronger at its southern boundary layer. The total magnitude of the "Upper Cell" is greater than that of the "Lower Cell," because it contains an adiabatic, surface-to-surface component, and a diffusive component that counters the along-isopycnal net density transport of the "Lower Cell." Meaning, the "Upper Cell" must both convey an inter-hemispheric net density imbalance, and redistribute a diapycnal net density imbalance, at the rate determined by pattern of surface transforma-

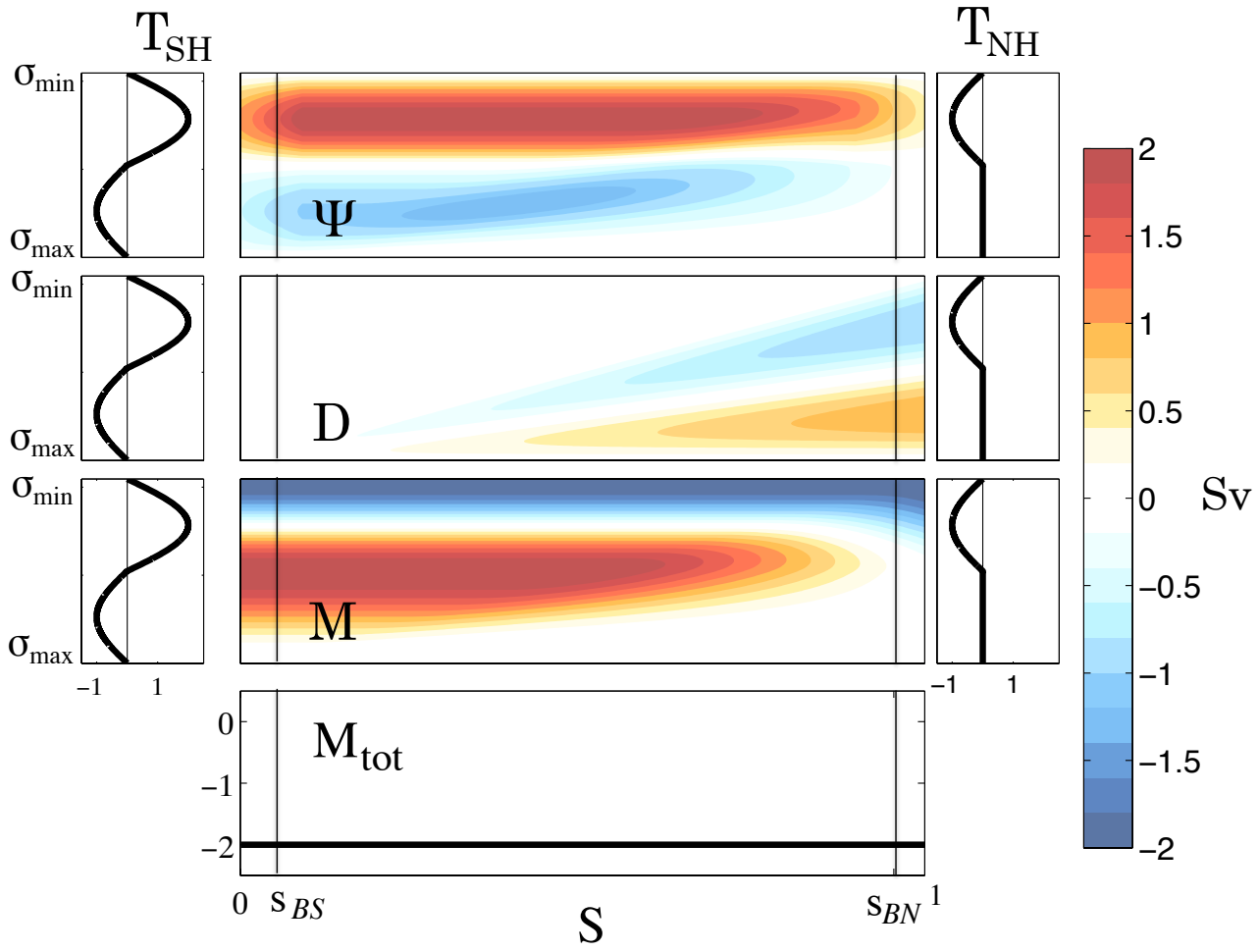

Figure 3.3.4: As in Fig. 3.3.2, but for a purely diffusive system.

tion. This simplified example illustrates a key feature of the real GOC: the "Lower Cell" is only one half of the overturning associated with the formation, and diffusive internal destruction, of AABW in the ocean (represented here by the dense water sourced at the "southern" surface). A stronger "Upper Cell" circulation, relative to its "Lower Cell" counterpart is fundamentally required so long as the later is diffusively sustained in the interior. The elevated strength of the "Upper Cell" (at its maximum), versus the "Lower Cell" (at its minimum), is a feature that is simulated in climate models (see for instance, Fig. 4.3.2 in Chapter 4). Here, while greatly simplified, we have mimicked these features by simply imposing a surface transformation distribution, mixing pattern, and constraining each component by the relationships derived in Section 3.2.1.

The structure of M provides a quantification of the inherent coupling between these cells. Because there is a net positive perturbation in mass (a density flux, integrated over the entire surface) acting into the "northern" surface ocean, and a net negative perturbation in mass out of the "southern" surface, the system must convey a perturbation in mass between hemispheres. This is the physical interpretation of $M_{tot} \neq 0$. Essentially, together, the "Upper" and "Lower" Cells act to both transport this mass perturbation between hemispheres, and that between density classes required by the difference in surface forcing across density classes. This redistribution is captured in the structure of M throughout the domain. Like in the purely diffusive system, the interior structure of M reveals this deep thermodynamic coupling between the "Upper" and "Lower" Cells. Again, while each cell might appear to be a closed circulation, $|M|$ peaks across density class at which these cells diverge. This is important to keep in mind when considering the dynamics of the GOC in different climate states, for instance, the LGM, during which it has been suggested that the Upper and Lower Cells were nearly uncoupled [e.g Ferrairi et al., 2014].

3.3.2 Insights into a real ocean system

System 3 hints at a compensating relationship between the overturning rates of the Upper and Lower Cells in the global ocean. Here I clarify how the pattern of surface transformation constrains their relative strengths, as exemplified in the simple system above. In System 3 above, M_{tot} is constant, a feature of the system which is sustained, or equivalently, required, by the imbalance in the total surface transformation between hemispheres. M_{tot} can be expressed as the sum of a component of density transport in $\hat{s}$ in the Lower Cell (below the isopycnal at which the direction of circulation reverses, or σ_d) and a component of transport in the Upper Cell (above σ_d), or

$$M_{tot} = \int_{\sigma_{max}}^{\sigma_{min}} \Psi(r,s) d\sigma \tag{3.69}$$

$$= \Psi_{LC}(r,s) d\sigma + \int_{\sigma_d}^{\sigma_{min}} \Psi_{UC}(r,s) d\sigma \tag{3.70}$$

$$= \int_{\sigma_{max}}^{\sigma_{min}} F_{SH} d\sigma = -\int_{\sigma_{max}}^{\sigma_{min}} F_{NH} d\sigma, \tag{3.71}$$

where subscripts "UC," "LC," denote the Upper and Lower Cell. Essentially, a given M_{tot} can be sustained by many combinations of density structure (stratification), and Upper Cell and Lower Cell strengths and structures. However, the *total* effect of these cells in moving density imbalances through the ocean by transporting seawater across isopycnals and between surface outcrops, is constrained by the magnitude of M_{tot}. For instance, for a given M_{tot}, a strengthening of the Upper Cell could be compensated by a strengthening of the Lower Cell, or a reduction in the stratification across which the Upper cell circulates (a shift in σ_d). Of course, adjustments in any component of the system would likely lead to adjustments in the others. However, acknowledging the required compensation between each overturning cell, identifiable from the rate of surface transformation on a global scale, gives us a new way to understand the relative strength of the Upper and Lower Cell during different climate states. No such compensating relationship, constraining the relative strength of the Upper and Lower cells deriving from constraints in the momentum budget, exists, to my knowledge. Further, in practice, it is difficult to comprehensively measure overturning and mixing rates throughout the global ocean. It is arguably easier to calculate M_{tot}, which can be done from surface measurements alone, by comparing the total density flux integrated over the ocean surface in the Northern Hemisphere to that integrated over the ocean surface in the Southern Hemisphere. The thermodynamic compensation exposed in this closed circulation theory developed in this chapter, used with a global measurement of M_{tot} can give us a new way to understand the dynamics of the system, in theory, and constrain the interior circulation, in practice.

3.4 Discussion and Conclusions

The aim of this chapter was to investigate upwelling processes, within a closed, full circulation system, from a theoretical perspective. By examining the components of the WMT Framework in an isopycnal-diapycnal coordinate system, and imposing a set of boundary conditions that define a steady-state, full circulation system, I identified a system of simple, though fundamental, relationships among the components of volume flux through the ocean, given by the surface transformation, the diffusively-driven transformation ($\Omega = F + D$), and the adiabatic isopycnal circulation (Ψ). Further, I quantified the cumulative density transport associated with each component of volume transport, which together redistribute regional differences in surface transformation. These balances may shed new light on the mechanisms that perpetuate the real GOC.

From the thermodynamic perspective adopted in this analysis, the roles of the adiabatic and diffusive components of the ocean circulation emerge clearly. Specifically, it was shown that the isopycnal circulation, Ψ is the mechanism by which differences in surface density forcing *on a given isopycnal* are moved through the ocean. Essential, the integral across all density classes of Ψ captures the component of the system that balances surface transformation without requiring any mixing or diffusion. The interior water mass transformation component, D, is the mechanism by which global differences in density flux *across isopycnals* are redistributed through the ocean, balancing surface transformation without requiring an isopycnal to outcrop twice at the ocean surface. While neither term can add new sources of density to the ocean, along-isopycnal advection will transport density between regions of the ocean surface, while the diapycnal transport term will redistribute existing density between isopycnals. Because the density transport associated with Ψ and D occurs in orthogonal directions, we can identify the role of mixing and along-isopycnal volume transport at every point in the ocean's interior; note, however, this is only the case when considering

the problem in coordinates aligned with isopycnals. In any other coordinate system, the component of density transport due to diapycnal, versus along-isopycnal, transport cannot be decomposed.

Framed this way, my interpretation of the respective roles of the isopycnal circulation, Ψ, and interior-mixing driven transformation, D, may not be surprising nor seem particularly new. Indeed, the idea that internal mixing can destroy any differences in surface forcing that increase the global density range has long been appreciated (McDougall and Garrett, 1992; Howe and Czaja, 2009). Further, the possibility for adiabatic flow to be maintained between isopycnals outcropping in the Northern Atlantic, and Southern Oceans, has been widely noted (e.g. Wolfe and Cessi, 2011, 2015; Radko et al., 2008; Radko and Kamenkovich, 2011). However, this analysis adds the ability to exploit these fundamental, and in fact definitive, interpretations of Ψ and D to constrain the circulation characteristics within a domain, given the spatial pattern of surface density fluxes relative to the distribution of isopycnal outcrops (information which, together, sets the surface transformation rate, e.g. Eqs. 2.4 and 3.14).

I demonstrated how these relationships give rise to distinct circulation patterns by constructing analytic representations of highly idealized ocean systems. While crude, these systems share some interesting features with the "real" ocean (in a zonally-averaged sense); this motivates applying these theoretical relationships to a more complex system. Additionally, by noting that each individual circulation "cell" may have both adiabatic and diffusive components, given the pattern of surface transformation, we arrive at a predictive relationship between the relative strength of circulation cells in the zonal average.

This study, while theoretical, shows that the global-scale ocean circulation is deeply tied to the spatial distribution of surface transformation. Yet, there is a surprising dearth of

study regarding how the pattern of surface density flux and surface transformation interacts with the overturning circulation on a comprehensive global scale. As mentioned in Chapter 1, most theoretical and modeling studies, across multiple scales of complexity, have probed the relationship between of interior dynamics and changes in surface flux patterns over the Southern Ocean and North Atlantic in particular (Togweiller; Morrison et al., 2011; Wolfe and Cessi, 2011, 2015; Nikurashin and Vallis, 2011, 2012). Even those studies that acknowledge the importance of low-latitude upwelling (e.g. Jochum and Eden, 2015; Thompson and Stewart) do not address where the surface-buoyancy fluxes, sustaining this upwelling, are sourced. Indeed, the role of lower-latitude surface fluxes in the GOC remains largely unexplored. However, I will argue these fluxes will contribute significantly to the relative distributions of adiabatic and diffusive processes in the ocean.

Chapter 4 is intended to amend this gap. In it, I will relate the pattern of the GOC to the pattern of surface transformation, in a fully-coupled global climate model.

Chapter 4

Surface Transformation and the Global Overturning Circulation

4.1 Introduction

The previous chapter was a theoretical and conceptual exploration of volume and density transport in the global ocean. The major conclusion of that study was that the dynamics of any equilibrated circulation system are closely tied to its thermodynamic coupling with the atmosphere. With that in mind, the purpose of this chapter is to apply the principles established in Chapter 3 to explore the coupling of surface density fluxes and the Global Ocean Circulation (GOC, e.g. Talley [2013]). In particular, I will investigate how atmospheric heat and freshwater fluxes (which transform waters into lighter or denser water classes, in different regions, a process know as "surface transformation") influence the three-dimensional structure of the GOC and the distribution of adiabatic and diffusive internal processes.

This study is motivated by an expectation that surface transformation patterns will differ significantly in different regions of the ocean. This expectation follows from a long-standing appreciation for the distinct characteristics of the Atlantic, Pacific, and Southern Oceans. Most notably, the Atlantic Ocean is far more saline than the Pacific, and the climatic impacts of this asymmetry have been studied for decades [e.g., Weyl, 1968]. Many explanations for why this asymmetry persists have been proposed, each linked to the areal distribution

and topography of the continents that separate the ocean basins. The mechanisms proposed to explain this asymmetry can be grouped into: the net atmospheric export of freshwater from the Atlantic to the Pacific (Warren, 1983; Emile-Geay, 2003; Sinha et al., 2012; Czaja, 2009); inflow into the Atlantic from the evaporative Mediterranean Sea [Reid, 1997]; and contributions from the warm and salty waters penetrating into the Atlantic around the Cape of Great Hope- the "Agulhas Leakage" [e.g. Gordon, 1996, (Nilsson et al., 2013) .

The high salinity of Atlantic surface waters is universally noted as an important precursor to the formation of NADW; similarly, the relative freshness of the Pacific helps to explain why no dense water forms in the North Pacific (Warren, 1983). The emphasis of how this salinity contrast impacts the global climate is often placed upon the distinct features of the Atlantic, relative to other ocean basins. From this perspective, flow from other ocean basins into the Atlantic has been cast as a means of replenishing the volume lost from the Atlantic because of the formation and export of NADW. Two major features connecting ocean basins and sustaining the export of NADW have been identified: transport across the Indonesian Through-Flow [e.g. Gordon, 1996, 2001] and the transport of Antarctic Intermediate Water [AAIW] out of the Southern Ocean [Rintoul et al., 1991]; each has been established as an essential component that maintains the Atlantic Meridional Overturning Circulation (AMOC) as it has come to be known.

Despite the well-established asymmetries in basin-wide water-mass properties, many studies take a zonal-mean perspective when studying the dynamics of the overturning circulation (e.g. Marshall and Radko, 2003). The total GOC streamfunction (calculated from the velocity summed zonally across all basins) suggests that meridional transport occurs in two distinct cells, each associated with the formation of a separate dense water mass— the "Upper" and "Lower" Cells. However, as referenced in Chapter 1, recent work expounds the limitations of this two-dimensional description of the overturning. Talley [2013] summarized

the work of many observational studies into a cohesive description of the GOC. Talley argued, based on regional heat budgets and water mass distributions, that the return of NADW to the North Atlantic surface must be preceded by its diabatic transformation in the deep Indian and Pacific Oceans. This abyssal transformation process replenishes dense waters with the majority of heat lost at high latitudes during dense water formation— Talley noted that ≈ 0.7 PW is lost during the formation of AABW and NADW, while only ≈ 0.1 PW is gained at the surface of the Southern Ocean (where buoyancy gain can be primarily attributed to surface freshening, e.g. Abernathey et al., 2016). The rest (≈ 0.6 PW) is gained from diapycnal mixing driven water-mass transformation in the Indo-Pacific. This implies that 0.6 PW of heat must be sourced somewhere at the ocean's surface and be conveyed into the deep Indo-Pacific Oceans. However, neither Talley nor any subsequent study has identified the surface processes that sustain this diffusive Indo-Pacific upwelling.

Talley noted important basin-scale excursions from the zonal-mean, "two-celled" overturning paradigm. Talley argued that this global transit occurs as follows: a large fraction of the Atlantic-sourced deep waters that surface in the Southern Ocean tend to lose heat upon upwelling and then are transformed to AABW, sinking to the abyss and spreading northwards into all basins. Volumetrically, the transport of AABW is greatest into the Pacific and Indian basins, where diapycnal mixing converts this abyssal water mass into Indian and Pacific Deep Waters (IDW and PDW), which are ultimately exported back into the Southern Ocean. The Southern Ocean serves as a great mediator of these flows, enabling vigorous lateral transports, water-mass transformations, and enabling the wind-driven upwelling of the deep water-masses emanating from the Atlantic, Pacific, and Indian Ocean. Ultimately, IDW and PDW upwell and are transformed into lighter water classes, where they become known as intermediate waters. Most of this intermediate water mass, AAIW, penetrates northward in all basins, moving furthest into the Atlantic Basin [e.g. Rintoul, 1991]. Another portion of intermediate water transits the Indonesian Through-flow [e.g. Gordon, 1992]. Together these

two sources of intermediate water go on to replenish surface flows into the North Atlantic and sustain the formation of NADW.

Talley's study highlighted the realization that the complexity and spatial richness of the GOC. Here, I investigate whether the theories developed in the simple systems of Chapter 3 can shed new light into these complex dynamics. Specifically, Talley's description of the overturning circulation requires the participation of both adiabatic and diffusive elements of the circulation, each associated with distinct regions of the ocean. The partition between these thermodynamically distinct components of the circulation should be tied to the spatial pattern of surface transformation, according to results from Chapter 3. Talley's description thus raises the possibility that other regions of the ocean surface, beyond the Southern Ocean and North Atlantic, are be essential in setting the structure of the overturning circulation. Here, I shall investigate this possibility in detail. The chapter is organized as follows: first I discussing the model and experiment used. Secondly, I orient the reader to the large-scale patterns of surface processes and circulation in the zonal mean. I then discuss the distinct contributions the Atlantic, Indo-Pacific, and Southern Oceans add to these zonally-averaged fields. I close with a discussion of these regional features in the context of the global scale circulation.

4.2 Model, Experiments, and Methods

4.2.1 Model

For this study I use the Community Climate System Model version 4 (CCSM 4), an update of the lower resolution version of the model described in Chapter 2 (CCSM 3.5) that is configured with identical grid geometry in the ocean and sea ice and employing the same mixing parameterizations, as described in detail by Danabasoglu et al. (2012). As noted in Chapter 2, the circulation may be biased by shortcomings in these parameterizations

[e.g. Bryan, 1987; Griffes et al., 2000]. One important alteration to the model used in this study is the addition of an "overflow parameterization" which was implemented to amend issues in deep- water production and associated biases in water mass properties. However, as discussed by Danabasoglu [2012], this feature did not reduce existing biases in the abyssal ocean. Lastly, resolution-based biases in AABW formation, as documented in detail for the low resolution model used in Chapter 2, likely persist in this version.

4.2.2 Experiment and Methods

All analysis in this study uses a 1850s pre-industrial control integration [e.g. Danabasoglu, 2012]. I examined model behavior during years 1270-1299 of the simulation. As in Chapter 2, the isopycnal circulation and water-mass transformation components F and D were calculated in potential density anomaly σ_2, as referenced to 2000 dbar. For simplicity, I henceforth refer to this potential density anomaly as simply σ. As discussed in Chapter 2, use of potential density will not account for non-linearities in the effect of pressure on the equation of state. This possibility should be kept in mind, and will be discussed below.

In Chapter 3, I emphasized the benefits gained by considering overturning dynamics in an isopycnal-diapycnal coordinate system. In practice, calculating the components of water-mass transformation in this coordinate system would be extremely complex and would be beyond the scope of this study. However, I can exploit the general meridional density distribution to approximate an orthogonal (isopycnal-diapycnal) coordinate system in certain regions of the ocean- specifically, at the ocean surface and at the equator. Because isopycnals tend to be flat across the equator, I make the assumption that isopycnals are aligned with depth coordinates, meaning $\hat{r} \approx \hat{z}$ in this region. In contrast, we expect that isopycnal slopes tend towards vertical over some small distance near the surface, supporting the approximation that $\hat{r} \approx \hat{y}$. One might note that these assumptions are inherently part of the standard definition of the isopycnal-meridional overturning, e.g. Eq. 2.1 in Chapter 2, as well as the

traditional definition of surface transformation, e.g. Eq. 2.4. Thus, for this study, I will compute the isopycnal-meridional circulation, and assume that it provides a good estimate of the true isopycnal-diapycnal circulation at the equator; the equatorial circulation will be compared to patterns in surface transformation, and each will be calculated using Eq's 2.1 and 2.4. Note that our examination of the cross-equatorial flows is additionally informative because, in the absence of any continents (or, on an "aquaplanet") and if eccentricity = 0, the climate system would be symmetric about the Equator. Any deviations from this symmetry will lend insight into how the climate system overcomes geometrical constraints to maintain a global energy balance.

4.3 Intra-hemispheric and Intra-basin scale relationships

4.3.1 Global Properties

While I anticipate important differences in oceanic processes and surface transformation rates between ocean regions, I first describe the global average behavior of the system against which regional behavior can be compared. For this study, I examine the relationship between surface transformation and interior circulation. This direct relationship between these fields is made possible because they are both functions of density class. However, their direct dependence on density class, as opposed to latitude, can obscure the physical meaning of "surface transformation". Since our goal is to understand the physics of the real ocean system, it behooves us to revisit this meaning of this field from a physically intuitive perspective.

Consider a water parcel of a given density at the ocean surface. Any surface flux experienced by the parcel, such as heat loss or evaporation, will change its density. Yet, in steady state, the spatial distribution of isopycnals must remain steady in time. This implies that if a

parcel becomes denser, it must flow towards a denser isopycnal to maintain a steady density distribution. The surface-transformation function, F, quantifies this effect; it measures the amount of volume that is constantly redistributed between isopycnals at the surface, given the spatial pattern of surface flux relative to the amount of area each density class occupies at the ocean surface. This is reflected in Eq. 2.4.

The magnitude of F thus depends on two fields: the rate of surface density flux into each density class, $\lambda(\sigma)$, and the area of the ocean surface that each density class occupies, $A(\sigma)$. Fig. 4.3.1C-D illustrates these fields as a function of density class; their spatial counterparts (meaning, the average density flux into the ocean as a function of latitude and the total ocean width with latitude) are provided in Fig. 4.3.1A-B to show the geographical distribution of each variable. Several things are important to keep in mind when interpreting all figures in this chapter that are plotted as a function of density. In the Southern Hemisphere, fields are plotted as a function of decreasing density. This convention reverses at the equator, to orient the reader to the general meridional distribution of each field. On average, surface waters are light at low latitudes, where the ocean is warmed and freshened by the atmosphere. Waters near the poles tend to be dense, because of heat loss and sea-ice formation. The actual spatial distribution of surface density is complex; however, in a zonal mean sense, surface density increases monotonically (though not linearly) with increasing latitude. Indeed, the differences between Fig.4.3.1A-B and Fig. 4.3.1C-D convey the complex relationship between latitude and density. Note that on an "aquaplanet," each field would be symmetric about the Equator, and thus any hemispheric differences arise from the structure of the continents and ocean basins.

Each of these zonally-averaged fields collapses a rich zonal structure, as will be discussed in more detail in subsequent sections. For this section, we simply note that on a global scale, density is lost at low latitudes and densities and is gained at high latitudes and den-

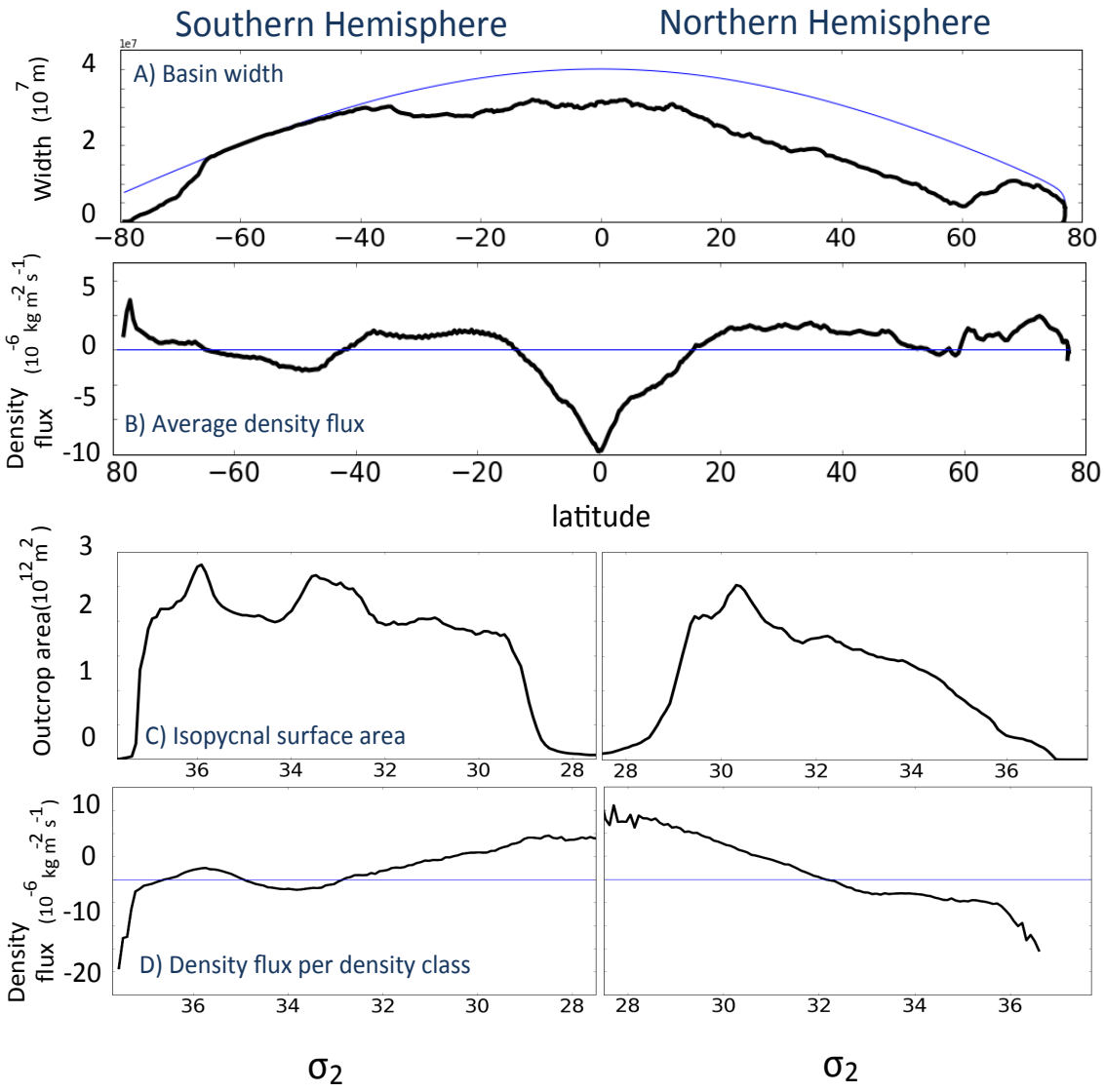

Figure 4.3.1: Surface geometry and density flux in latitude, and density space. A) Total ocean width with latitude; B) Average density flux with latitude; C) Total isopycnal outcrop area in the Southern (left) and Northern (right) Hemispheres; D) $-1\times$ the average density flux per density class in the Southern (left) and Northern (right) Hemispheres; note, these fields are plotted with this sign convention to enable direct visual comparison with F in Fig. 4.3.2.

sities. There are important distinctions between processes occurring at mid-latitude and intermediate density waters between hemispheres. Lastly, the distribution of ocean surface area varies greatly with latitude and density class between each hemisphere. This is an important feature, and will be discussed in subsequent sections.

Now, I examine the distribution of the surface transformation function and its correspondence to the global isopycnal overturning stream function. The relationship between surface transformation and circulation is complex, as discussed in the previous chapters. In the absence of any mixing, negative surface transformation will drive a counter-clockwise circulation pattern (corresponding to a negative Ψ) in the Southern Hemisphere, and a clockwise circulation in the Northern Hemisphere (a positive Ψ). Differences between the sign and magnitude of F and Ψ quantifies the effects of mixing (and diffusive processes) on the circulation, as noted in Chapter 2, and discussed more theoretically in Chapter 3.

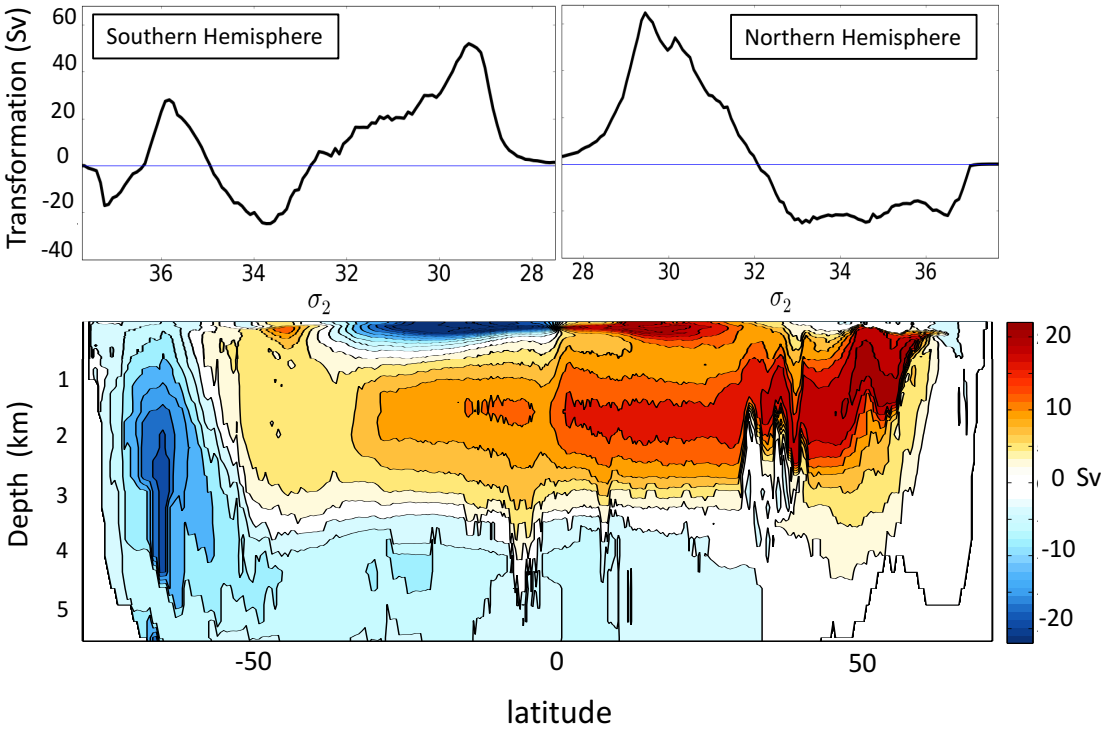

Figure 4.3.2: The all-basin distribution of surface transformation, F, with density class in the Southern Hemisphere (top row, left) and in the Northern Hemisphere (top row, right) and its general correspondence to the isopycnal overturning circulation Ψ (bottom row). Warm colors denote clockwise circulation, cool colors denote counterclockwise circulation.

Fig. 4.3.2 roughly depicts the correspondence between the surface transformation, F, and the isopycnal overturning circulation, Ψ projected onto zonal-mean isopycnal depths. For this analysis, we maintain sign convention used in Chapter 3, and integrate the components of water mass transformation northward from the South Pole. Negative F values are associated with volume transport towards denser waters, and thus are driven by a *positive* density flux into the ocean (due to heat loss, evaporation, or sea ice formation); positive F values imply volume flux towards lighter waters as a result of a negative density flux (due to a gain in heat or freshwater). A negative slope in F indicates that there is a greater volume of water from lighter waters than the flux towards denser waters; this convergence in surface transformation, $\frac{\partial F}{\partial \sigma}$ in our terminology (and simply "F" in the nomenclature of Speer and Tziperman (1992)) is called "formation" and quantifies the component of downward along-isopycnal volume flux from surface forcing. In sum, the surface transformation function, F, and its associated water mass formation, $\frac{\partial F}{\partial \sigma}$, can provide valuable insight into how global water masses are formed at the ocean surface.

The surface transformation in each hemisphere shares several features. On average, the densest waters in each hemisphere experience negative surface transformation, corresponding to the high latitude losses of heat and freshwater. In these regions, the direction of the overturning circulation tends to correspond to the sign of the surface transformation, revealing that surface transformation plays and important role in setting the local overturning structure (as discussed in Chapter 2). Low density waters in each hemisphere experience vigorous peaks in positive surface transformation, associated with the immense solar heating and precipitation that acts into expansive isopycnal surface outcrops at low latitudes. Here, the direct correspondence between the sign of surface transformation and the direction of the circulation below the surface is eroded, exposing the fundamental influence of diffusive interior processes in the shallow low latitude overturning circulation.

These similarities might be expected, given the relative warmth of the equatorial climate, versus that at high latitudes. However, there is one essential difference between the hemispheric pattern of surface transformation, which also appears in the surface density flux fields (Fig. 4.3.1D). In the Southern Hemisphere, surface waters at approximately $35 \leq \sigma \leq 36.5$ experience a peak in positive surface transformation. These density classes outcrop (roughly) across the latitudes of the Drake Passage, where wind-driven upwelling draws deep waters from the interior ocean to the surface along isopycnals. Buoyancy gains at the ocean surface enable the equatorward flow of upwelled waters, across the strong meridional surface density gradient (e.g. Marshall and Radko, 2003; Abernathey et al., 2016). Conversely, in the Northern Hemisphere, these density classes outcrop in the North Atlantic, where high rates of heat loss enable the formation of NADW. The possibility that waters across this density range travel from one surface to the other, experiencing little to no mixing (so, considered to move adiabatically), has been widely discussed (Wolfe and Cessi, 2011, 2015; Radko et al., 2008; Radko and Kamenkovich, 2011), and is important to note for this study.

We now consider the problem broken down by major ocean basin, to investigate how key aspects of in water mass transformation and overturning are obscured in this all-basin perspective.

4.3.2 Basin-wide Properties

Temperature, salinity, and the overturning streamfunction

This study asks if the GOC pattern, as described by Talley [2013], is associated (and consistent with) major variations in regional surface transformation. To address this question, however, we must first assess if the modeled circulation bears any resemblance to this three-dimensional GOC paradigm. For ease, "basin-scale" will henceforth correspond to the zonal average behavior within in the Atlantic, or Indo-Pacific Oceans; "intra-basin" will signify

differences between these regions. My particular focus will be regarding differences between the Indo-Pacific, and Atlantic Oceans, as mediated by the Southern Ocean.

Let us first examine the basin-scale water mass properties (salinity and temperature) in the Indo-Pacific and Atlantic basins, as water masses emanating in and out of the the Southern Ocean tend to have distinct signatures in these properties. Fig. 4.3.3 reveals that, as expected, the water mass properties of the Indo-Pacific and Atlantic basins have dramatic differences. Indeed, the Atlantic is far more saline on average than the Pacific, while the Pacific tends to be colder through the majority of its intermediate and deep waters. A cold, fresh tongue of AABW extends northward from the abyssal Southern Ocean into each basin, though its influence on the abyssal properties of the Indo-Pacific is greater. At deep and intermediate depths, a relatively warm and salty tongue of Circumpolar Deep Water is evident upwelling out of the Atlantic. Finally, a fresh and relatively cold tongue of near-surface and intermediate waters (AAIW) flows northward from the Southern Ocean surface and extends into both basins; however, its signature reaches further northward in the Atlantic basin.

These distinct water mass properties are encouraging evidence of intra-basin differences in the large-scale circulation. To understand how these properties relate to the circulation, we examine the isopycnal-meridional stream function calculated for each basin northward of the Southern tip of Africa (Figs. 4.3.4 and 4.3.5). To interpret these figures, note that so long as density increases monotonically with depth (which is generally true), a clockwise circulation will transport a density anomaly towards the north; conversely, a counterclockwise circulation will transport density southward. Significant differences in circulation are immediately evident between basins: in the Atlantic (Fig. 4.3.4), there is vigorous clockwise overturning, associated with the formation of NADW in the northern latitudes and export at depth, and import of intermediate waters from the Southern Ocean flowing northward in the upper ocean. The abyssal circulation carrying AABW northward from the high southern

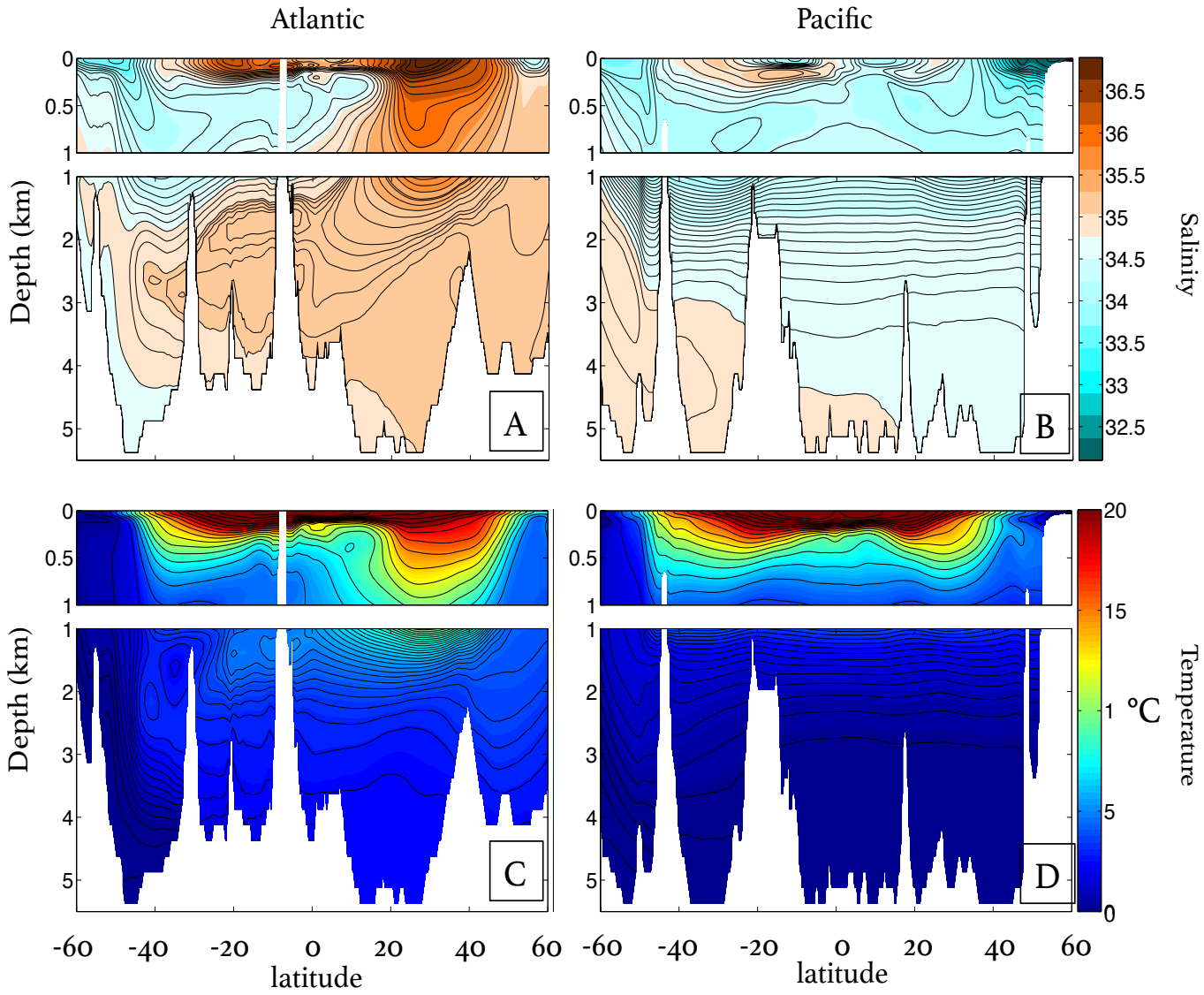

Figure 4.3.3: Top row: zonally-averaged salinity in the Atlantic (left) and Pacific (right) basins; bottom row, the same, but for temperature.

latitudes is very weak by the time it reaches the equator. Conversely, in the Indo-Pacifc basin (Fig. 4.3.5), no deep water is formed, and therefore no large-scale "Upper Cell" dominates. Instead, the vigorous but shallow equatorial cells (note the differing color scales in Fig. 4.3.4 and Fig. 4.3.5) overlie a counter-clockwise circulation characterized by an import of AABW in the abyss (at rates greater than into the Atlantic), its conversion into deep and intermediate waters, and its export back out of the Indo-Pacific basins below ≈1000m. There is a secondary, weak maximum in this counter-clockwise circulation at ≈1500 m in a

cell that spans the equator and is associated with import of AAIW at ≈1500, its transformation, and subsequent export back into the Southern Ocean at ≈1000m. This broad-scale counterclockwise circulation system in the region below $1000m$ weakly couples the abyssal and intermediate ocean. While the flow is weak, the stratification in the upper ocean is not, such that this circulation is associated with significant diapycnal transport. Note that overturning in the Southern Ocean is captured in Fig 4.3.2, south of $30°S$.

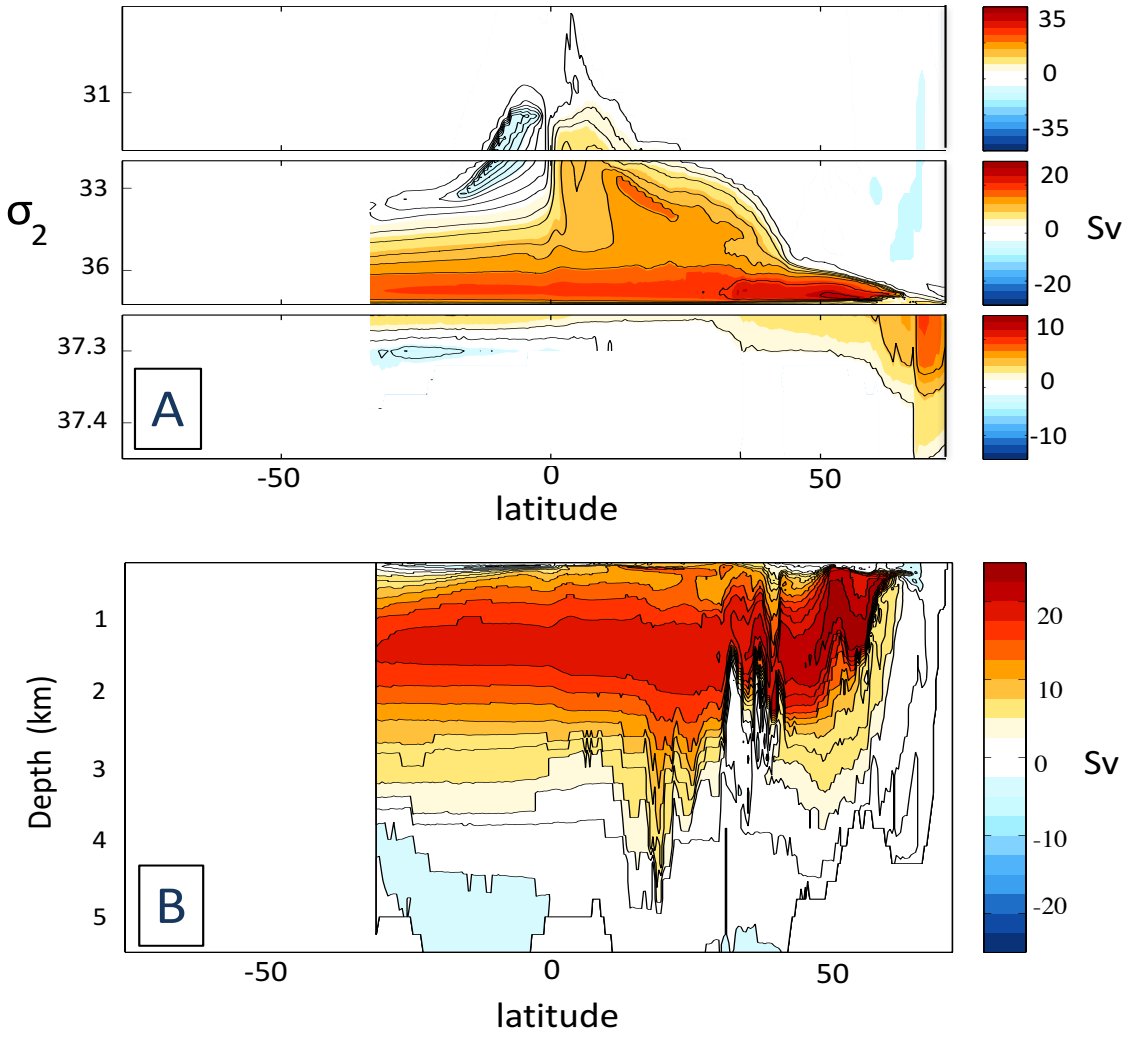

Figure 4.3.4: Isopycnal Overturning in the Atlantic Basin (north of 30S). A) the isopycnal stream function (Sv); B) the isopycnal stream function projected projected onto zonal and time mean isopycnal depths for visualization.

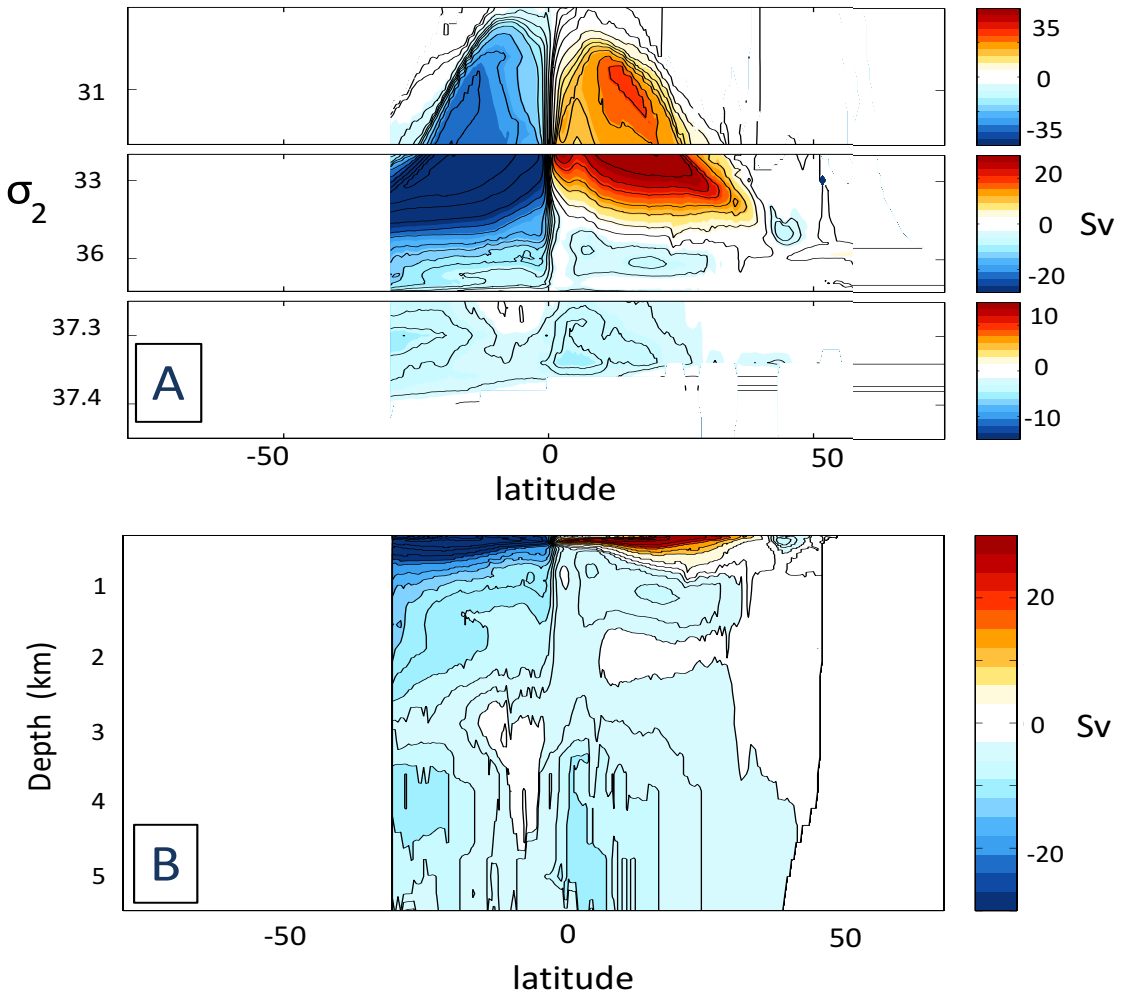

Figure 4.3.5: Same as Fig. 4.3.4, but for the Indian-Pacific Basins

Basin-scale surface transformation

Clearly, the circulation patterns in each basin contribute distinctly to the GOC stream function. Do these significant intra-basin differences in circulation correspond to differences in surface water mass transformation? Fig. 4.3.6 compares the surface transformation between basins. The surface transformation is a function of the surface outcrop distribution, and the distribution of surface density flux, as illustrated in Fig. 4.3.7C-E, which are related to the spatial distribution of ocean surface area, and surface denstiy flux, illustrated in 4.3.7A-B.

It is immediately clear that the patterns characterizing the global-scale surface transfor-

mation, Fig.4.3.2, arise from distinct basin-scale structures. There are striking differences in the surface transformation experienced at low densities (which outcrop at low latitudes) between the Atlantic and Indo-Pacific. The significant peak in low density surface transformation in the global sum is primarily explained by processes occurring in the Indo-Pacific in both hemispheres, spanning density classes of approximately $\sigma < 32$ in the Northern Hemisphere, and $\sigma < 33$ in the Southern Hemisphere. This feature was noted by Speer and Tziperman [1995] in their calculation of global surface transformation rates from the COADS observational data set; our estimate broadly agrees with their calculations, with rates of low-density transformation peaking at ≈ 60 Sv in our model, as compared to their roughly 70 Sv. This peak is primarily explained by high rates of heat uptake into the ocean (Fig. 4.3.6, bottom panel), though freshwater gain contributes significantly at very low densities (approximately $\sigma \leq 30$). Conversely, the magnitude of positive, low density transformation is far smaller in the Atlantic in both hemispheres, resulting from significantly lower rates of heat-driven transformation and because this heat gain is collocated with regions of net evaporation. The relatively modest magnitude of low density Atlantic transformation (≈ 12 Sv) is corroborated by Speer and Tzipermann [1995], who estimate an even lower rate from observations, of ≈ 4 Sv.

Notable intra-basin differences are also evident in higher density waters. In the Northern Hemisphere, the majority of the negative transformation of waters at approximately $\sigma \geq 34$ in the all-basin total occurs in the North Atlantic. Here, vigorous heat-loss drives negative transformation over a large density range (approximately $33 \leq \sigma \leq 37.2$). This heat loss goes relatively unabated by high latitude freshwater gains, which provide only a modest contribution of positive transformation. In contrast, the heat loss induced transformation in the northern Indo-Pacific occurs at intermediate densities (approximately $32.5 \leq \sigma \leq 35.8$)and is countered more effectively by freshwater fluxes.

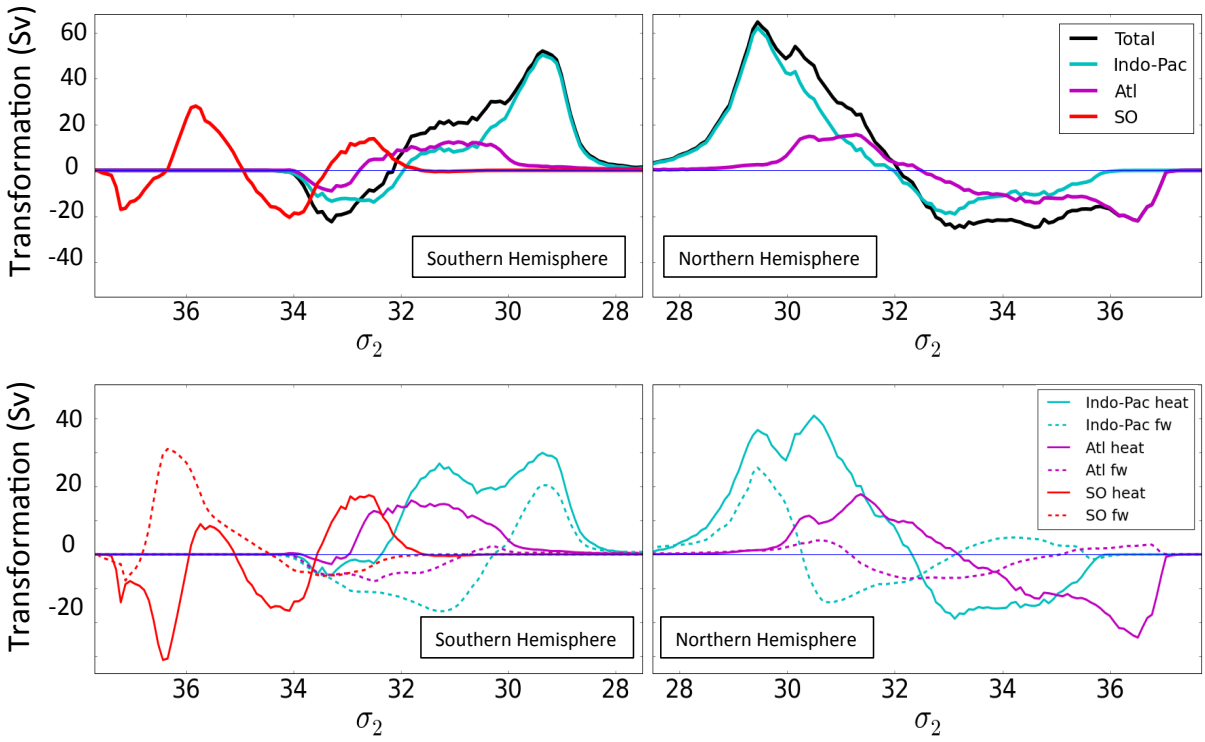

Figure 4.3.6: Top row: total surface transformation in the Indo-Pacific (teal), Atlantic (magenta), and Southern Oceans (red) compared to the all-basin total (black) in the Southern Hemisphere (right) and Northern Hemisphere (left); bottom row: the heat- (solid) and freshwater- (dashed) driven surface transformation components in each hemisphere and basin. F is plotted as a function of increasing density north of the equator and as a function of increasing density south of the equator, to generally correspond to the meridional surface density gradient.

The higher density classes in the Southern Hemisphere outcrop in the Southern Ocean, where unique regional conditions enable a band of positive transformation at relatively high latitudes and across densities of approximately $35 \leq \sigma \leq 36.5$, as evident in the all-basin global total. As noted, this singular Southern Ocean feature has important implications for the global circulation, as will be considered in more detail in Chapter 5. This positive transformation feature is primarily explained by freshwater gains [e.g. Abernathey et al., 2016], especially at higher densities in this range; heat gains also contribute in slightly lighter waters.

As noted above, surface transformation depends on the area of isopycnal surface outcrops

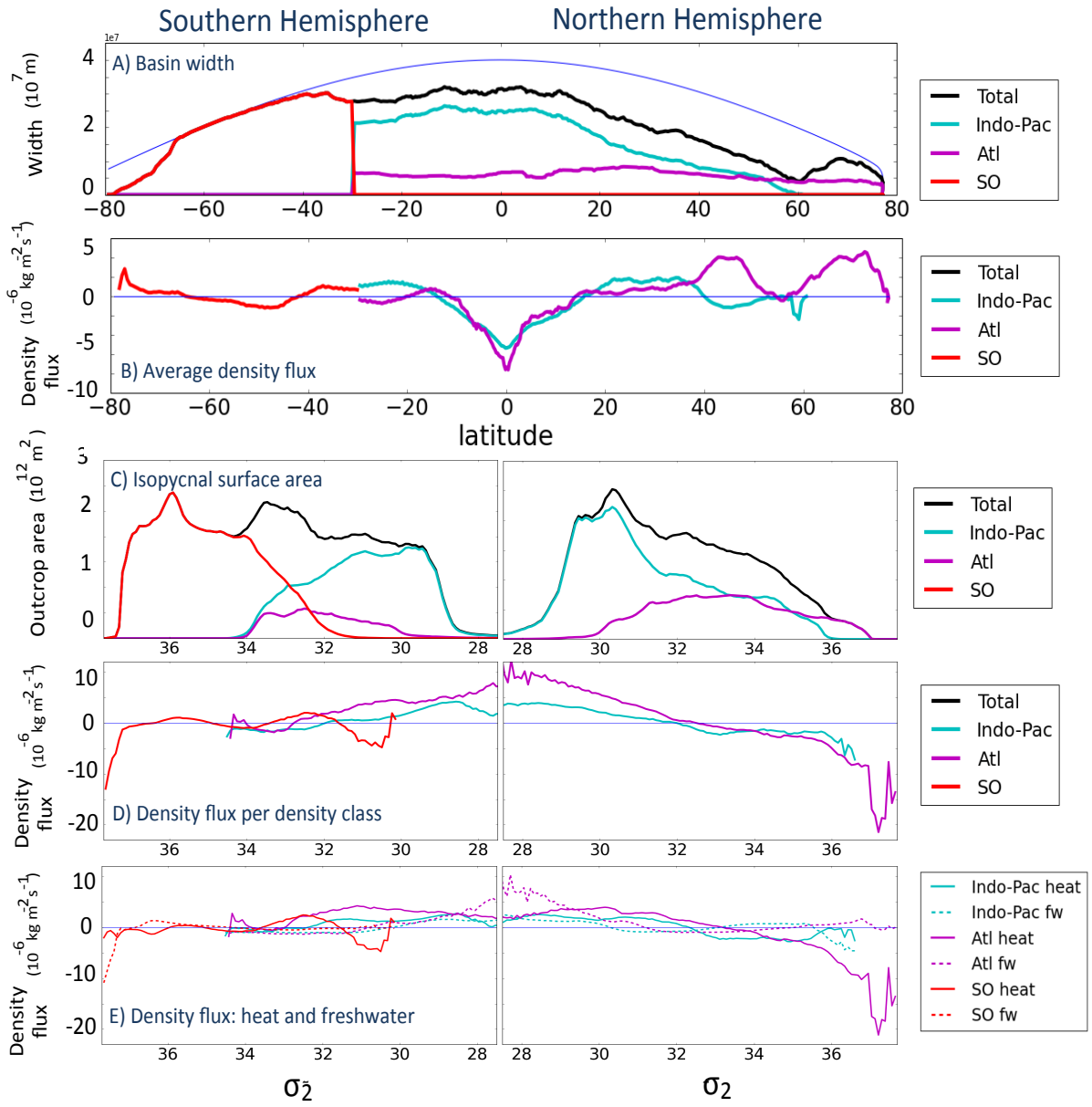

Figure 4.3.7: Surface geometry and density flux in the Southern Ocean (red), Indo-Pacific (teal) and Atlantic (magenta) Basins. A) Total ocean width with latitude in each basin; B) average density flux with latitude in each basin; C) Total isopycnal outcrop area in each basin in the Southern (left) and Northern (right) Hemispheres; D) Average density flux per density class, in each basin in the Southern (left) and Northern (right) Hemispheres; E) Average density flux from heat flux (solid) and freshwater flux (dashed) per density class, in each basin in the Southern (left) and Northern (right) Hemispheres.

and the surface density flux (Fig. 4.3.7C-E). The distribution of outcrop area varies widely between basins and hemispheres. The northern Indo-Pacific occupies far more surface area at low densities (and latitudes) than at high densities (and latitudes). In the Atlantic, which

physically occupies relatively little area at low latitudes and significantly more at high northern latitudes, no water lighter than $\sigma \approx 30$ outcrops, though for densities $\sigma \gtrsim 30$, outcrop area is relatively constant. All waters denser than $\sigma \approx 36$ in the Northern Hemisphere outcrop in the Atlantic. Conversely, the significant peak in positive low density surface transformation in the Indo-Pacific is primarily explained by the vast area over which these low density waters outcrop, coincident with regions of negative density fluxes, in this basin. Indeed, across the majority of the density range shown here, the outcrop area appears to have a dominant role in setting the transformation distribution, and intra-basin differences therein. However, note that positive lobe of surface transformation in the Southern Ocean relies on a unique interaction between these two fields. Waters at these densities occupy vast surface area because of the lack of landmasses across these latitudes of the Southern Ocean. However, the sign of surface transformation can only be altered by the density flux, and thus the nature of ocean-atmosphere coupling in the region. The density classes associated with the lobe of positive Southern Ocean transformation (approximately $35 \leq \sigma \leq 37.2$) experience a loss of density in the Southern Ocean, in stark, and important contrast with the density gained by these density classes at the North Atlantic surface.

Lastly, to relate the patterns in surface transformation, and its components, to the distribution of distinct water masses and the organization of interior flow, I compare F to its formation rate, $\frac{dF}{d\sigma}$ [Speer and Tziperman, 1992], which quantifies the component of downwelling (positive formation) and upwelling (negative formation, or "destruction") at each density class driven by surface fluxes; the total along-isopycnal flow will be additionally influenced by mixing rates near the surface. For this study, I only note several important features in the formation function. In the northern Indo-Pacific basins, there is a large peak in positive formation of low density waters (approximately $\sigma \leq 29.5$), driven by both heat and freshwater flux; waters at approximately $29.5 \leq \sigma \leq 33$ are "destroyed." This pattern likely corresponds to a the lateral cycling of surface waters through, and out of, the sub-

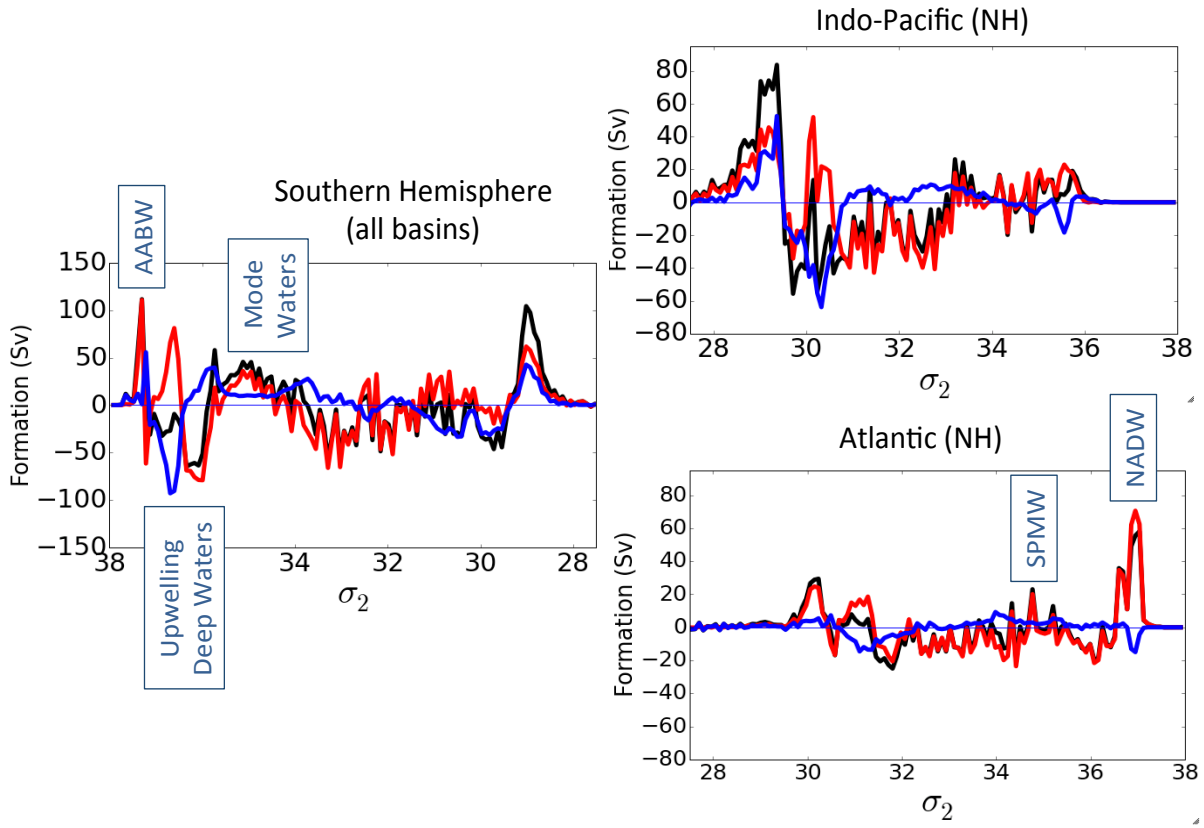

Figure 4.3.8: Water mass formation in the Southern Hemisphere (left), Northern Hemisphere Indo-Pacific (top right) and Northern Hemisphere Atlantic (bottom right). The total formation (black) is the sum of formation from heat flux (red) and freshwater flux (blue).

tropical gyre (which appears as the shallow, clockwise overturning cell in Fig. 4.3.5B. The most notable feature in the Northern Atlantic is the vigorous formation of dense waters, corresponding to the formation of NADW; a secondary peak weakly denotes the formation of Subpolar Mode Water (SPMW). In the Southern Hemisphere, the formation occurring in all basins has been consolidated, for simplicity. At lower densities, there is a dipole-like pattern similar to that of the Northern Hemisphere Indo-Pacific, and also likely attributable to the subtropical gyre circulation. At higher densities (all within the Southern Ocean), there are three important features to note. At very high densities ($\sigma \geq 37.5$), vigorous heat loss drives AABW formation, a process that was explored in great detail in Chapter 2. At slightly lower densities, waters are upwelled, and destroyed by freshening and warming, in turn. At progressively lower densities, note the formation of mode and AAIW waters, driven

by heat loss, with some contributions from evaporation. These features are consistent with the Southern Ocean system as documented by numerous studies (Cerovečki et al., 2013; Abernathey et al., 2016; Newsom et al., 2016; Talley, 2013).

4.4 Discussion and Conclusions

4.4.1 Summary of Results

In this study, I have comprehensively documented the distribution of surface transformation across the major ocean basins of the global ocean. When their regional contributions are combined, the global distribution of surface transformation as a function of density class conforms to a pattern that might be anticipated based on the distribution of insolation, and the tight coupling between air-sea temperature contrasts. Meaning the atmosphere warms low density (and low latitude) waters, constantly making them lighter, and cools high density (and high latitude) waters, constantly making them more dense. These effects are modulated by the hydrological cycle, which broadly freshens low and intermediate/high density waters, at the expense of intermediate density waters, which are made more dense from evaporation. The magnitude of freshwater transformation is generally lower than that driven by heat fluxes. However, because the distribution of surface freshwater flux does not directly depend on the salinity of the ocean surface, the distribution of this component, relative to density class, varies among basins, with important effects on the circulation.

This global picture is partitioned in complex ways between the major ocean basins. While there are similarities between the surface transformation occurring in each basin, their striking differences matter most for this discussion, which I will summarize. The Atlantic basin stands apart for its relatively low contribution of positive surface transformation in both hemispheres and for its disproportionate contribution of negative surface transformation in the Northern Hemisphere, associated with NADW formation. The Indo-Pacific stands out

as the dominant global source of positive surface transformation; this positive transformation is attributable to enormous gains of heat at low to intermediate surface densities, gains which are compounded by a significant freshening at very low density; indeed, the Indo-Pacific contributes the great majority of low latitude freshwater transformation. Thus far, these intra-basin differences correspond to highly distinct distributions of isopycnal surface area, which outcrop under density flux patterns that are broadly similar. The Southern Ocean, meaning all waters that outcrop south of $30°S$, stands apart in one particularly important feature: a lobe of positive surface transformation across higher density classes (those shared with the North Atlantic ($35 \leq \sigma \leq 36.8$). This transformation is primarily driven by freshening, with non-negligible contributions from heat flux. This positive lobe is made possible (from a transformation-based perspective) by the interaction of two factors: the expansive surface area occupied by these density classes (corresponding to the swath of zonally-unbounded ocean surface between approximately $30°S$ and $68°S$) and, importantly, a negative density flux, highlighting that key differences in ocean-atmosphere coupling between the Southern Ocean, and North Atlantic. Specifically, the same density classes that experience vigorous heat loss in the North Atlantic experience strong freshwater fluxes and moderate heat gains in the Southern Ocean. The possibility that this asymmetry in surface forcing across this density range could adiabatically sustain the AMOC has been proposed by many studies (e.g. Wolfe and Cessi, 2011, 2015; Radko et al., 2008; Radko and Kamenkovich, 2011; Howe and Czaja, 2009). At very high density classes, indeed the highest densities in the open global ocean, the Southern Ocean also enables a significant component of negative surface transformation, primarily driven by heat loss, though brine rejection also plays a role in extremely dense waters (as documented in detail in Chapter 2). While the positive lobe of surface transformation ($35 \leq \sigma \leq 36.8$) indicates that the Southern Ocean supports an adiabatic component of upwelling in the ocean system, this negative lobe, producing waters that don't outcrop elsewhere at the surface ($\sigma \approx 37$), indicates that the region is also diffusively coupled to other parts of the global ocean.

These features can be cast in terms of our results in Chapter 3. In that chapter, I recognized that diffusive transport, and the mixing that enables it, is the interior ocean mechanism that redistributing imbalances in surface transformation that persist across density classes (see Fig. 3.2.2). In the simulated global system examined in this chapter, the Indo-Pacific accounts for the majority of positive, heat driven transformation into low density classes; we can therefore conclude that these basins provide buoyancy that ultimately sources the majority of diffusive dense water upwelling in the global ocean. Conversely, I showed that the isopycnal circulation (Ψ) in the interior is redistributes differences in surface transformation between two opposing outcrops of the same density class; indeed, no diffusive processes can balance these differences on a global scale when in steady-state. Based on those findings, I argue that the opposing Southern Ocean-North Atlantic surface transformation feature not only reveals the potential for adiabatic transport in the system, but requires it. Many studies have noted the potential for adiabatic surface-to-surface transport, though these studies propose this as a mechanism to close a distinct Upper Cell, confined to the Atlantic— the AMOC. Here, I emphasize that the transformation patterns require *net* volume transport between isopycnal outcrops, meaning that there can be diapycnal transport across these classes, so long as the total diapycnal transport in and out of this density range is zero. This distinction, a step away from the classic interpretation of this adiabatic feature that is suggested from the air-sea flux, is important to make and will be discussed further in Chapter 5.

Finally, I quantify the net density flux into and out of each region, at the surface and in the interior, via Eq. 3.30. The net density flux into the surface of the Indo-Pacific north of the Equator is $-6.5x10^7 \ \frac{kg}{s}$. The isopycnal circulation imports $\approx 3.8x10^7 \frac{kg}{s}$ into the basin. This relationship (while clearly not in a perfect balance) was anticipated, due to the dominant counterclockwise regional circulation. However, these calculations indicate

that a significant amount of diffusive volume redistribution (or water mass transformation) occurs in the Northern Hemisphere of the Indo-Pacific; this transformation thus must be sustained by surface density fluxes into the ocean north of the equator. This indicates some mechanism of coupling between the equatorial and abyssal circulations in this region. My technique, as it stands, cannot reveal what processes enable this coupling, a question that will be addressed in future work. Further, the difference in the magnitude of total surface density loss and interior density transport into the Pacific highlights limitations in our analysis that will be addressed in future studies. Specifically, if the system were in steady state, and our assumption that the equation of state were valid, these density transports should balance. The imbalance calculated for this simulated circulation could derive from several important sources. First of all, it is unlikely that the simulated system is in a true steady state, especially in the abyssal ocean. To identify the role this plays in the density budget, I will calculate an isopycnal volume inflation term (as was done in Chapter 2), in future work. Additionally, a linear equation of state assumption likely discounts important contributions in the ocean density budget. The imbalance between surface transformation and isopycnal transport could be evidence that significant cabbeling occurs in the North Pacific in this model, as is anticipated, particularly in the Kurishio [Yun and Talley, 2003, Urakawa et al., 2013, (Thomas and Shakespeare, 2015) This interior density contribution is balanced on a global scale by an opposing net buoyancy flux into the ocean surface, which arises because heat flux has a greater impact on seawater density at higher temperatures than at lower temperatures. This net surface buoyancy gain is often expressed as a volume flux, and is estimated to be within the range $0.07 - 0.1$ Sv (Schanze and Schmitt, 2013); our model simulates a surface imbalance of approximately 0.14 Sv. Lastly, pressure has important effects on the seawater density, a complication that can be overcome by calculating neutral density instead of potential density; this technique will be adopted in my future work. When the volume tendency and pressure effects are accounted for, this framework will provide a useful way of identifying the total regional densification due to cabbeling, within a given

basin against which to compare observational estimates. When interpreting these quantities, however, it is important to note that cabelling rates, and indeed the regional circulation, will depend on how mixing is simulated in the model. For instance, it is conceivable that the model biases explored in Chapter 2 have led to a spuriously weak abyssal circulation in the Indo-Pacific, and thus that I have underestimated the associated Indo-Pacific diapycnal upwelling.

The relationship between surface transformation and interior circulation in the Atlantic, north of the Equator, also supports a clear relationship between net surface density flux and the direction of density transport across the Equator. The net surface density flux in this region is $2.3 \times 10^7\ kg\ s^{-1}$; that being transported across the Equator by along-isopycnal flow occurring at different rates across differing density classes (calculated as $\int_{\sigma_{max}}^{\sigma_{min}} \Psi d\sigma$) is $6.0 \times 10^7\ kg\ s^{-1}$. Like in the North Pacific, we anticipate significant rates of cabelling in the North Atlantic (particularly within the Gulf Stream, as seen previously by Thomas and Shakespeare (2015)). Given the limitations of our technique, the imbalance between surface and interior transport estimates suggest that cabelling is significant component of the system in this region.

Finally, the net surface density flux into Southern Ocean is notably small relative to other basins: $5.7x10^{-6}\ \frac{kg}{s}$. Meaning, while certain regions of the Southern Ocean surface experience strong positive and negative net density flux, their combined contribution at the surface is quite small. Instead, these heterogeneous fluxes act to redistribute density across density classes, though they provide little additional density to the global ocean. This minimal surface forcing occurs even while mass is moved into and out of the Southern Ocean, as illustrated in Fig. 4.4.1, which shows northward mass perturbation transport at ever latitude in each basin. Note that the circulation acts to transport a mass flux southward out of the Atlantic into the Southern Ocean, and northward out of the Southern Ocean into the

Indo-Pacific.

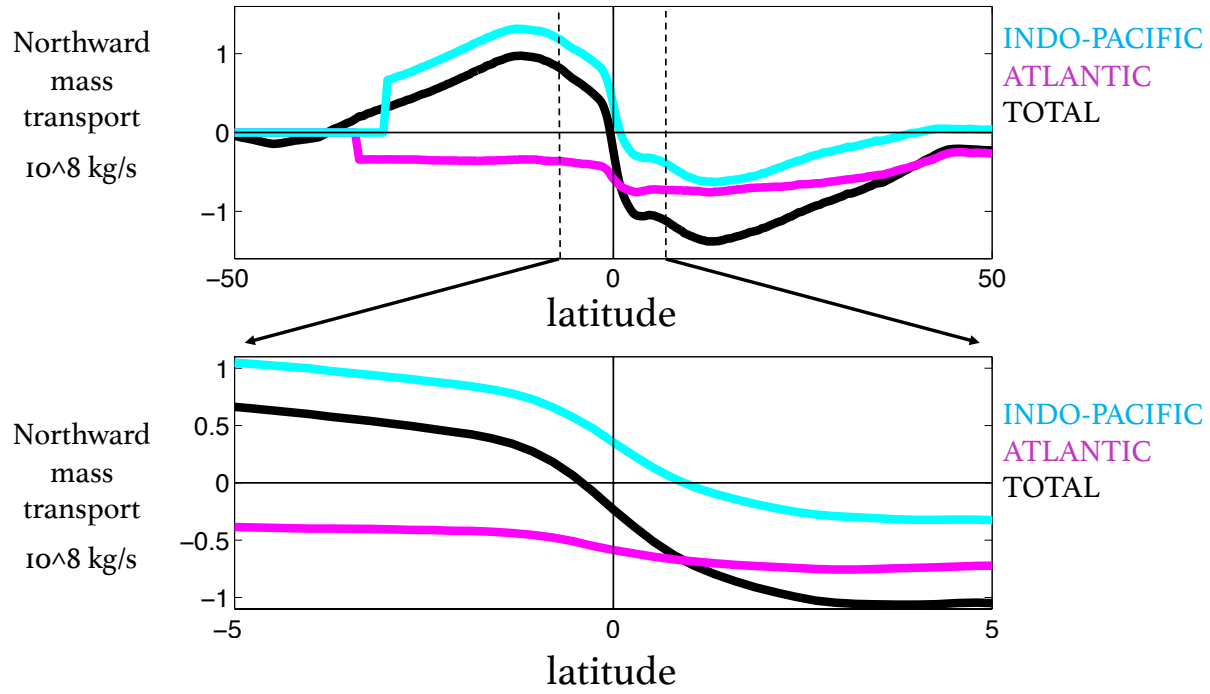

Figure 4.4.1: Top: northward mass transport (which arises from the meridional volume transport of seawater at differing density classes) with latitude in the Indo-Pacific (teal) and Atlantic (magenta) Ocean basins. Bottom: the northward mass transport between $5°S$ and $5°N$, expanded to emphasize the direction of cross-equatorial transport in each basin.

An aspect of the GOC, yet to be identified in the literature, emerges when comparing interior mass transport (Fig. 4.4.1) to basin-scale rates of surface transformation (Fig. 4.3.6A). This basin-scale comparison clearly demonstrates, even given its limitations, that the GOC redistributes mass out of the Northern Hemisphere Atlantic Ocean, through the Southern Ocean, and into the Northern Hemisphere Indo-Pacific Oceans. This mass transport is sustained by regional differences in surface density fluxes, which perturb the average ocean mass when integrated over the ocean surface in each basin. The basin-scale balance between interior transport and surface forcing is not perfect and is complicated by non-linearities in the equation of state, which enable interior processes to increase seawater density within the water column. The influence of these non-linearities will be explored in future work, includ-

ing the possibility that they introduce a positive feedback into the system that reinforces a requirement that mass be fluxed into the Indo-Pacific (where the ocean gains the majority of excess surface buoyancy). Finally, even while the most dramatic zonal asymmetries in surface density forcing occur north of 30° S, these comparisons reveal the vital role of the Southern Ocean in permitting circulation and mass transport between each northern basin while contributing little to the net surface density flux. In future work, I will explore how variations in the zonal structure of the Southern Ocean enable the regional circulation to mediate mass exchanges throughout the global ocean system.

Chapter 5

Towards a New Conceptual Model for the Ocean's Global Overturning Circulation

5.1 Summary of Work

Dense waters formed in the high latitudes must be lightened and returned to the ocean surface in what has come to be known as an "overturning circulation". Our understanding of this circulation, and how it is maintained in the ocean's interior, has evolved over the decades it has been studied. In particular, many theories have been developed to explain the meridional dynamics of this circulation, which give rise to its rich meridional structure, namely the existence of two dominant, global-scale overturning cells. Yet, recent work has proposed that the emphasis place on the meridional structure of overturning, and thus the zonal-average perspective taken by most dynamical studies of this circulation, has obscured fundamental aspects of its structure. [Talley, 2013]. Talley argued that ocean overturning occurs in a continuous, three-dimensional loop transiting all major ocean basins; this continuous circulation, or a "Global Overturning Circulation" (GOC) only *appears* to be comprised of two distinct cells when zonally-averaged across all basins.

In light of this recent insight, my thesis has been a comprehensive investigation into several important components of this GOC that are not emphasized in a zonally-averaged perspec-

tive on meridional dynamics. My work has used a thermodynamically-based framework that relates the physical transport of water through the ocean to the changes in density it must undergo along the way— the Water Mass Transformation (WMT) Framework [Walin, 1982].

In my first study, I explored how the Antarctic Bottom Water (AABW), one of the two major classes of dense waters in the global ocean, forms at high southern latitudes. The formation of AABW is often under-emphasized in studies probing the dynamics of the overturning circulation, which have historically focused on Upper Cell dynamics. My results highlight the crucial role of heat loss in AABW formation; while brine, rejected when sea ice forms, is important near the Antarctic coast, heat loss is the primary contributor to AABW formation, in the models considered, because it occurs over much broader scales around the coastal ocean. This conclusion was based on an analysis of the rate of surface water mass transformation, which quantifies the component of the total isopycnal circulation that is sustained, thermodynamically, by surface density fluxes. My results, based on this method, are consistent with a review of observational studies by (Nicholls et al., 2009). The processes that mediate this surface heat loss have fundamental effects on the circulation. In particular, I found that transient openings in the Antarctic sea-ice pack (leads) enable heat to evacuate the ocean surface, and thus concluded that the simulation of Antarctic sea ice greatly impacts how dense water is formed, and how effectively it is moved into the ocean's interior, in climate models. This study advocates for a nuanced consideration of AABW formation and its role in the large-scale climate system.

One major implication of the formation and export into the deep ocean of AABW and North Atlantic Deep Water (NADW), is that compensating processes, occurring elsewhere in the ocean, must lighten these dense waters so that they can upwell to the surface again. Fluxes into the ocean surface, away from regions of dense-water formation, must provide enough buoyancy to sustain this upwelling. To probe the relationships between downwelling, up-

welling, and surface heat and freshwater fluxes (which together, give rise to a surface density flux), I constructed a theoretical framework to explore the closed overturning circulation in a closed domain (one with no flow across its boundaries). This study highlights the fundamental, and indeed, definitive, roles of "diffusive" or "adiabatic" transport in the ocean. The most important conclusion of this study was the requirement, within the theoretical framework derived, that the global-scale partition between adiabatic and diffusive volume transport (circulation) depends entirely on the distribution of surface transformation across and between the outcrops of density surfaces. This surface transformation distribution, in turn, depends on the surface density fluxes integrated over the outcrop area of each density class.

The relationships derived in Chapter 3 have important implications for the real global ocean system. To explore how my theoretical findings related to a realistic representation of the system, my final study was an exploration of the surface transformation and the interior circulation in a fully coupled global climate model. I demonstrated that there are dramatic differences in both the isopycnal overturning circulations, and surface transformation distributions, in the Indo-Pacific, Atlantic, and Southern Oceans. To the best of my knowledge, this is the first study to document the relationship between surface transformation and the overturning circulation on a comprehensive global scale. The complex, regional relationships between the surface and interior ocean processes are consistent with my theoretical predictions. Further, key regional differences in the coupling between the circulation and the surface transformation lends insight into the larges-scale organization of the ocean system.

To close this chapter, I would like to consider the nature of the "whole" global system, through the intra-basin relationships documented in Chapter 4. Specifically, as an exercise, I ask question: what fundamentally sets the three-dimensional pattern of the GOC in our current climate state?

5.2 Unifying Results and Reflections on the Influence of Basin Geometry

5.2.1 Thought Experiment: the Impact of Basin Geometry on the Structure of Global Overturning

The question of why the overturning circulation has its global structure can be framed, from a water-mass-transformation perspective, as: is the large-scale structure of the interior ocean circulation set by the distribution of surface heat and freshwater fluxes, or are these surface fluxes set by the circulation? Here, I advance a hypothesis that even in this complex and coupled system, basin-scale surface transformation rates (a function of surface heat and freshwater fluxes) are enforced by the geometry of the earth's continents, preconditioning the GOC to be organized in the structure observed.

As discussed in Chapter 4, multiple aspects of Earth's continental geometry or topography have been theorized to cause major differences between the properties of the Pacific and Atlantic Oceans. Arguably the most straightforward influence the distribution of landmasses can exert on the ocean is the confinement of each ocean basin to a distinct location on the planet. Without invoking any differences in atmospheric circulations, or topography, I consider how the total surface transformation in each basin is affected by basin width. This exercise is inspired by the vast differences in the width of ocean basin as a function of latitude, as demonstrated in Chapter 4; this information provided again Fig. 5.2.1, which illustrates the fractional contribution of each basin to the total ocean width.

As noted in Chapter 4 (Fig. 4.3.1 A), the differences between basin width are striking: the Indo-Pacific basin accounts for the majority of earth's low latitude ocean surface area,

and, the Atlantic basin occupies much less low-latitude area and occupies the majority of the ocean surface north of 60N.

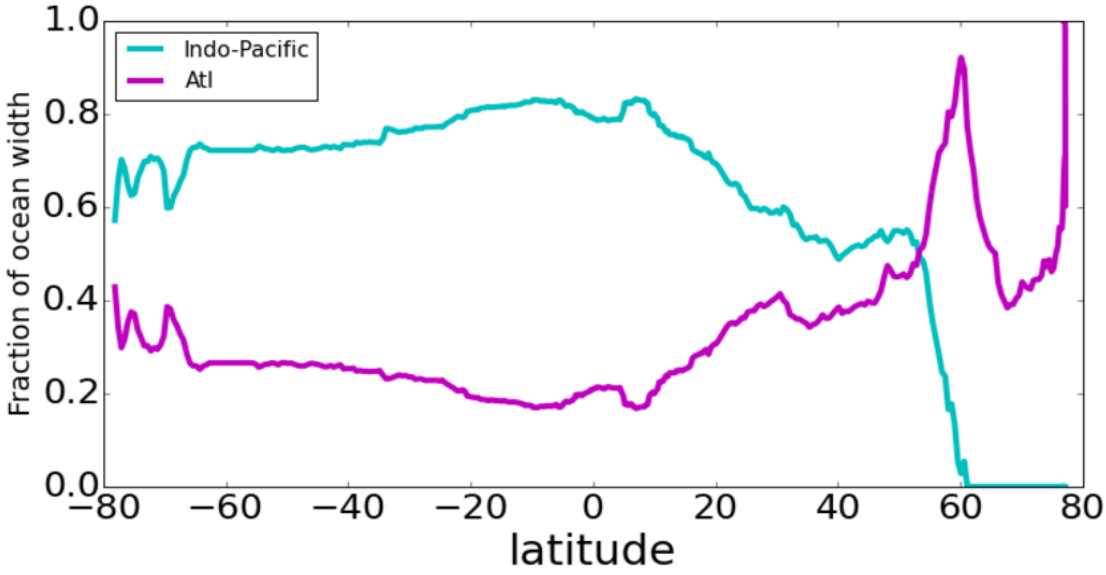

Figure 5.2.1: Fraction of the total ocean width contributed by the Indo-Pacific Basin (teal) and Atlantic Basin (magenta) at every latitude.

Here, I consider the influence these geometrical differences might have on the system in the following thought experiment: I first consider how a planet *without* the influence of continents — an ocean covered "aquaplanet" — might equilibrate (thermodynamically) in steady state. This is done by solving for the meridional distribution of surface density flux exchanged between the ocean and atmosphere that would enable a steady-state. While there are many features in the coupled ocean-atmosphere system that may affect the meridional structure of this density flux, I consider only two fundamental features: Earth's spherical geometry and the large-scale distribution of insolation from the current climate. My specific intention is to isolate the effects of these external and persistent features on the climate system, which I henceforth refer to as "external constraints." I then consider how these external constraints might influence ocean-atmosphere coupling and ocean circulation on a planet with more realistic basin geometry.

To construct a simple, insolation-based density flux distribution as a function of latitude ($\lambda_{Aq}(\theta)$), I note several important aspects of the theoretical system. Generally, I expect the ocean to warm at low latitudes and cool at high latitudes. Specifically on an aquaplanet, I expect processes in each hemisphere to be symmetric about the equator (there is no mechanism to disrupt this symmetry), the surface density flux in each hemisphere to be zero (in steady-state), and the surface transformation function to have an identical distribution in each hemisphere. Further, because there are neither zonal variations in flow nor in surface density flux, Eqs. 3.14 and 3.30 can be written

$$0 = \int_{\sigma_{max}}^{\sigma_{min}} F d\sigma = \int_A \lambda_{Aq}(\theta) dA \tag{5.1}$$

in steady state. On a planet of radius R_E, spanned by latitude, θ, and longitude, ϕ, Eq. 5.1 can be written:

$$0 = R_e^2 \int_0^{2\pi} \int_0^{\frac{\pi}{2}} \lambda(\theta)_{Aq} \cos\theta d\theta d\phi \tag{5.2}$$

Due to the insolation gradient, I suppose that the ocean surface poleward of some latitude θ^*, experiences a positive density flux, countered by a negative density flux into the ocean surface equatorward of θ^*, or:

$$R_e^2 \int_0^{2\pi} \int_0^{\theta^*} \lambda(\theta)_{Aq} \cos\theta d\theta d\phi = -R_e^2 \int_0^{2\pi} \int_{\theta^*}^{\frac{\pi}{2}} \lambda(\theta)_{Aq} \cos\theta d\theta d\phi, \tag{5.3}$$

To maintain simplicity, I make the approximation that the density flux varies linearly with latitude. While I expect a real system to be more complex, this simplification helps to clarify

the effects of our external constraints. The density flux into the ocean is greatest at each pole ($\theta = \pm\frac{\pi}{2}$) and decreases towards its most negative value at the equator ($\theta = 0$) at rate C, crossing from a positive to negative value at θ^* ($\lambda(\theta^*) = 0$):

$$\lambda_{Aq}(\theta) = C(|\theta| - \theta^*) \tag{5.4}$$

Considering the Northern Hemisphere, and substituting from Eq. 5.2, allows us to solve for θ^*.

$$2\pi {R_e}^2 C \int_0^{\frac{\pi}{2}} (\theta - \theta^*) \cos\theta d\theta = 0 \tag{5.5}$$

$$2\pi {R_e}^2 C[(\theta - \theta^*)\sin\theta + \cos\theta]\Big|_0^{\frac{\pi}{2}} = 0 \tag{5.6}$$

$$2\pi {R_e}^2 C(\frac{\pi}{2} - \theta^* - 1) = 0, \tag{5.7}$$

giving

$$\theta^* = \frac{\pi}{2} - 1 \approx 33^\circ \quad \text{N or S} \tag{5.8}$$

hence,

$$\lambda_{Aq}(\theta) = C(|\theta| + 1 - \frac{\pi}{2}). \tag{5.9}$$

This density flux distribution and geometry are represented in Fig. 5.2.2.

I have now constructed a simple density flux pattern that is influenced solely by the insolation gradient and Earth's spherical geometry. I now explore how the dramatic variations in ocean basin width of the "real" Earth (i.e. Fig. 5.2.1) might be influenced by our external constraints. I do so by calculating the how much surface transformation would occur in a

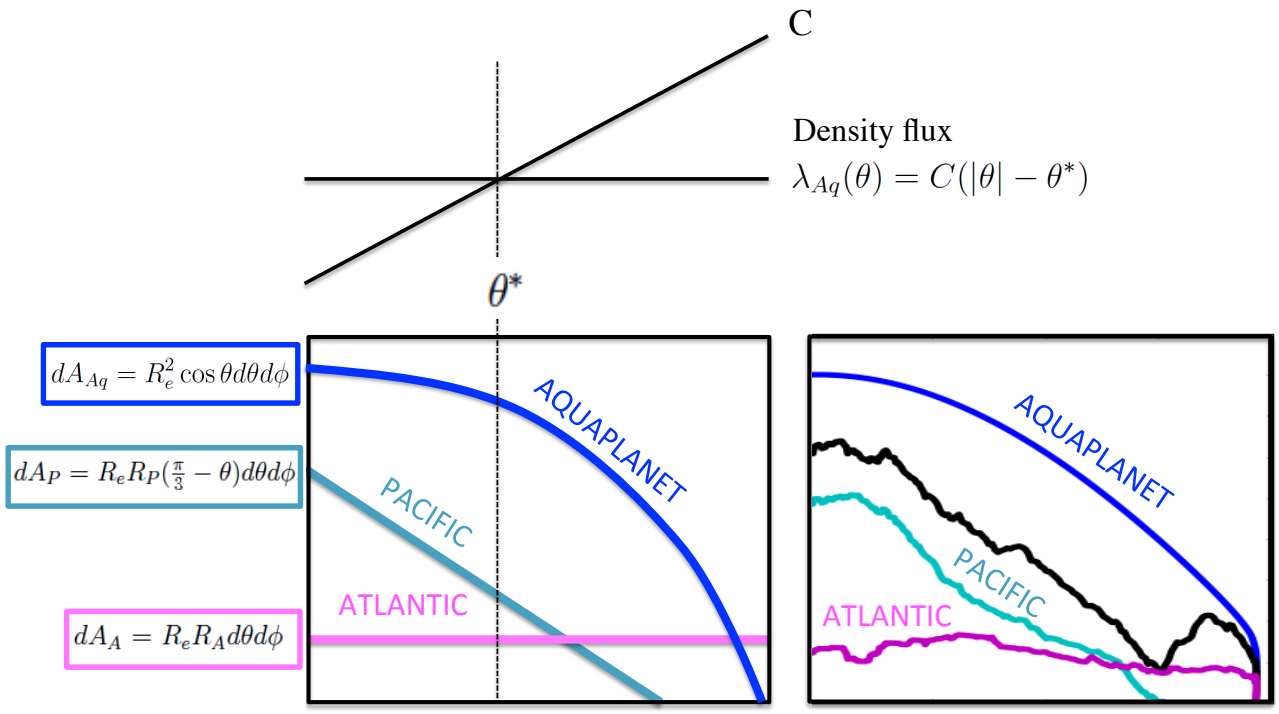

Figure 5.2.2: Schematic depicting the idealized linear density flux (λ_{Aq}) acting into the Northern Hemisphere ocean basins, as approximated meridional surface area distributions of the Atlantic (dA_A, magenta) and Indo-Pacific (dA_P, teal) basins. Basin width with latitude of each approximation (middle schematic) is compared to the actual distribution of basin width at each latitude (at right)

given basin, were it forced by the "insolation-based" density flux distribution λ_{Aq}. In doing so, I am ignoring any feedbacks between the regional ocean circulation and the surface density flux, and thus isolating the influence of our external constraints. Do note that even in the complex "real" system, the average density flux is relatively similar between ocean basins across most of their shared latitudes (Fig. 4.3.7).

The difference in ocean width between the Atlantic and Pacific is far greater in the Northern Hemisphere. For this exercise, I consider this hemisphere alone, both for simplicity, but also because I expect the dramatic geometrical distinctions in this region to most profoundly influence the rate at which seawater is transformed in basin, especially because regions north of the Equator are far from the Southern Ocean, where all ocean basins merge. From Eq.

5.9, the approximate total density flux into each basin of area A_{basin} north of the Equator,

$$\int_\sigma F_{basin} d\sigma = \int_{A_{basin}} \lambda_{Aq}(\theta) dA_{basin}. \tag{5.10}$$

where F_{basin} is the surface transformation in a given basin. The width of the Atlantic is relatively constant with latitude, while the width of the Indo-Pacific decreases (roughly) linearly from the Equator towards $\approx 60°N$. I approximate the area element in the Atlantic, $dA_A = R_e R_A d\theta d\phi$, where R_A is the width of the Atlantic basin at the Equator, so the approximate total density flux:

$$\int_\sigma F_A d\sigma = \int_A \lambda(\theta) dA_A = R_e R_A C \int_0^{2\pi} \int_0^{\frac{\pi}{2}} (\theta + 1 - \frac{\pi}{2}) d\theta d\phi \tag{5.11}$$

$$= 2\pi R_e R_A C \theta [\frac{\theta}{2} + (1 - \frac{\pi}{2})]\Big|_0^{\frac{\pi}{2}} \tag{5.12}$$

giving,

$$\text{Northern Hemisphere Atlantic total density flux} \approx 0.34(2\pi R_e R_A C)\ kg\ s^{-1}. \tag{5.13}$$

If I approximate an area element in the Pacific as $dA_P = R_e R_P (\frac{\pi}{3} - \theta) d\theta d\phi$, where R_P is the equatorial width of the Pacific basin, then

$$\int_\sigma F_P d\sigma = \int_A \lambda(\theta) dA_P = R_e R_P C \int_0^{2\pi} \int_0^{\frac{\pi}{3}} (\theta + 1 - \frac{\pi}{2})(\frac{\pi}{3} - \theta) \theta d\theta d\phi\ kg\ s^{-1}. \tag{5.14}$$

giving

$$\text{Northern Hemisphere Pacific total density flux} = -0.12(2\pi R_e R_P C) \tag{5.15}$$

In the absence of circulation between basins, the Atlantic in this system would become progressively denser, as the Pacific became increasingly less dense. Clearly, some mechanism is required to compensate this constant surface forcing, were this system to equilibrate. For instance, regions of the ocean surface south of the Equator could experience an opposing surface density flux sufficient to balance surface fluxes north of the Equator within each basin. However, this local compensation is not observed in the simulated or real ocean system. In the absence of these compensating surface fluxes, a circulation which conveyed mass flux *between* northern basins could compensate for the intra-basin differences in surface forcing (note that if the average width of the Indo-Pacific were ≈ 3 times that of the Atlantic, surface forcing in each basin would balance on a global scale). Essentially, this idealized system could equilibrate if the circulation conveyed mass from the Atlantic to the Indo-Pacific, a feature shared with the complex system analyzed in Chapter 4 (Fig. 4.4.1).

5.2.2 Relationship to the Global Overturning Circulation

Large-scale structure

This thought experiment regards a far simpler system than the real ocean. In maintaining this simplicity, however, I have supported the possibility that where ocean basins are located, relative to the insolation gradient in the current climate state, alone could precondition the system for a structure which transports mass throughout the global ocean in the direction described in Chapter 4. Specifically I argue that, due to the enormous outcrop area of the equatorial Indo-Pacific, this basin is preconditioned to be a source of buoyancy to the global ocean (meaning that in total, surface fluxes acting into this basin will constantly decrease

the ocean's density). Conversely, I argue the North Atlantic is preconditioned to be a sink of buoyancy (meaning that fluxes acting into this basin will constantly increase the ocean's density). In this case, the ocean circulation may be preconditioned for a structure that can transport mass between these northern basins, a transport which occurs in the comprehensive, fully-coupled climate model examined in Chapter 4. Of course, this preconditioning will compete with myriad other processes which complicate the system. For instance, any zonal variations in surface density flux or interactions with the hydrological cycle will have profound effects on the system. Contributions from the hydrological cycle may be somewhat constrained towards broad-scale zonal symmetric: regions of moisture convergence (and thus precipitation) and moisture divergence (and thus evaporation) seem to be broadly confined to the equatorial and mid latitudes and subtropics, respectively, regardless of continental distribution (see e.g. Enderton and Marshall, 2009; Frierson et al., 2013). However, zonal differences in ocean-atmosphere coupling due to the real dynamic coupling between the ocean and atmospheric circulations could dramatically influence the structure of the GOC, a possibility that may be important in other climate states.

Adiabatic and diffusive processes and the vital role of the Southern Ocean

The thought experiment explored here, together with the results of Chapter 4, proposes that the Southern Ocean is a essential mediator between the Atlantic and Indo-Pacific basins. This notion is consistent with many previous studies that emphasize the vital role of the Southern Ocean in the climate system; here vigorous wind-driven upwelling can occur because of the region's unique geometry (e.g. Toggweiler and Samuels, 1995; Marshall and Speer, 2012). Of particular relevance to this work, it has been proposed that this wind-driven upwelling could support adiabatic, or quasi-adiabatic flow directly between the Southern and North Atlantic Oceans, sustained thermodynamically by opposing surface density fluxes acting into the isopycnals that outcrop in both the Southern and North Atlantic (Wolfe and Cessi, 2011, 2015; Radko et al., 2008; Radko and Kamenkovich, 2011). In Chapter 4, this

thermodynamic surface feature appears in the basin-scale surface transformation patterns; across approximately $35 \leq \sigma \leq 36.8$, a range I will refer to as "adiabatic density classes" for ease, the surface transformation has an opposing sign in each hemisphere. These differences can only persist (in steady-state) if there is a volume transport between surface outcrops along these "adiabatic density classes," an inference based on the results of Chapter 3 and consistent with the studies cited above. This transport has been refereed to as an "adiabatic" component of the global circulation, however, its dynamics have only been deeply explored in idealized models consisting of a "Southern Ocean" re-entrant channel, appended to *one* northern basin (Wolfe and Cessi, 2011, 2015; Radko et al., 2008; Radko and Kamenkovich, 2011). Such models, when forced with opposing surface density fluxes in each hemisphere, indeed simulate intra-hemispheric adiabatic flow directly between high latitude regions. These studies then interpret this model behavior as evidence for adiabatic flow directly from the surface of the North Atlantic to the surface of the Southern Ocean in the real global ocean. A schematic of this interpretation from Wolfe and Cessi [2015] is illustrated in Fig. 5.2.3.

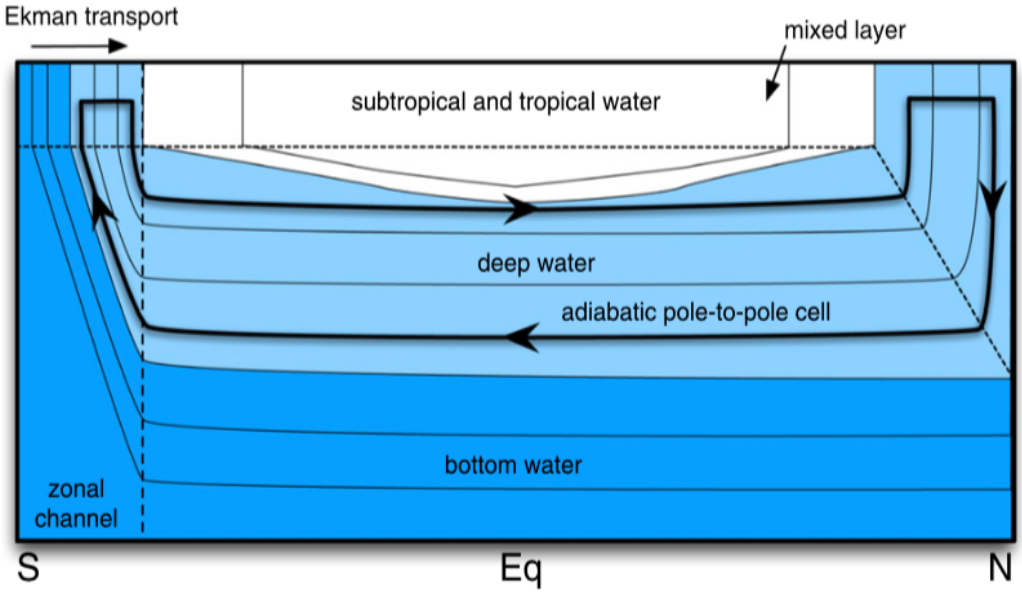

Figure 5.2.3: Schematic from Wolfe and Cessi [2013]. Thin black lines depict average isopycnal height, solid black lines show the circulation of their "adiabatic pole-to-pole circulation" in a idealized model, comprised of a zonally-reentrant southern channel, and a single northern basin.

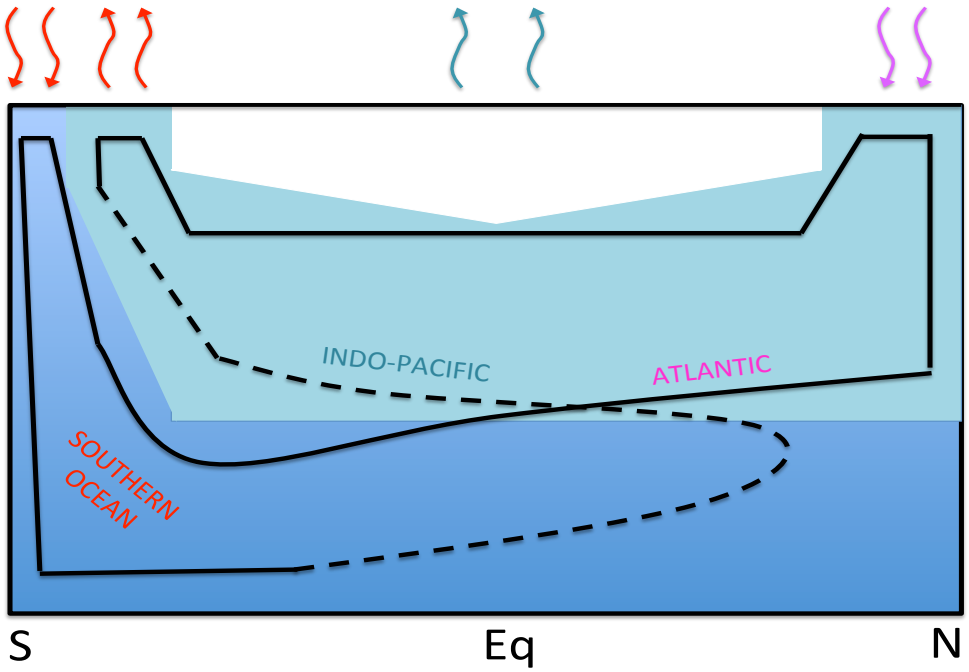

Figure 5.2.4: Updated schematic of an "adiabatic pole-to-pole" circulation (as compared to Fig. 5.2.3) when considering two northern basins. Black lines represent the circulation in depth and latitude. Solid black lines denote circulation in the Atlantic, and Atlantic sector of the Southern Ocean; dashed black lines denote circulation through the Indo-Pacific and Indo-Pacific sector of the Southern Ocean. Surface fluxes acting into the Atlantic (magenta), Indo-Pacific (teal) and Southern Ocean (red) are denoted as arrows into the surface, and balance on a global scale through both adiabatic, and diffusive coupling.

Yet, these interpretations ignore several important features of the real ocean system. The first: there are multiple ocean basins north of the Southern Ocean. The second, NADW actually becomes denser before it outcrops at the Southern Ocean surface [e.g. Zika et al., 2013], which means that much of its volume is transported diapycnally out of these "adiabatic" density classes. Lastly: these interpretations ignore the significant negative surface transformation of water masses *denser* than those in this "adiabatic" range; essentially, they ignore the formation of AABW, a water mass so dense that it does not outcrop elsewhere in the global ocean. In reality, the coexistence of upwelling towards *and* downwelling from the

Southern Ocean surface requires that the region be both adiabatically *and* diffusively coupled to the northward ocean basins. When considering the complex global system more comprehensively than the studies cited above, acknowledging the existence of multiple ocean basins north of the Southern Ocean and the formation of AABW, the role of "adiabatic" transport in the global ocean can be interpreted quite differently. I argue that, while the pattern of surface transformation in the Southern Ocean requires some *net* along-isopycnal volume transport between isopycnal outcrops within the "adiabatic" density classes, this transport could be achieved in two distinct ways. In one case, there could be an along-isopycnal volume transport between surfaces in an ocean with no mixing (and thus no diapycnal volume transport). In a second case, one which would sustain an equivalent surface transformation pattern as the first, there could be *net* volume transport between outcrops along a density class into which any diapycnal volume transport *cancels* over the global scale. In this way, the unique pattern of surface transformation across these "adiabatic" density classes could arise from the export (towards denser classes) of NADW and the import (back out of these denser classes) of IDW and PDW. This alternate description of some "adiabatic" component to the GOC requires that a density class exist that is consistently denser than NADW, IDP and PDW. This alternate interpretation allows for some net volume transport between the North Atlantic to the Southern Ocean surfaces; however, this transport is accomplished along a convoluted pathway involving all three ocean basins. In this alternate description, the system *requires* the formation at the surface, and destruction in the interior, of AABW; this dense abyssal water mass acts as a reservoir with which lighter density classes can mix. This description of the circulation is consistent with the constraints on a closed overturning circulation argued for in Chapter 3, with the circulation and surface transformation patterns described in Chapter 4, and with the Tally's [2013] proposed GOC structure.

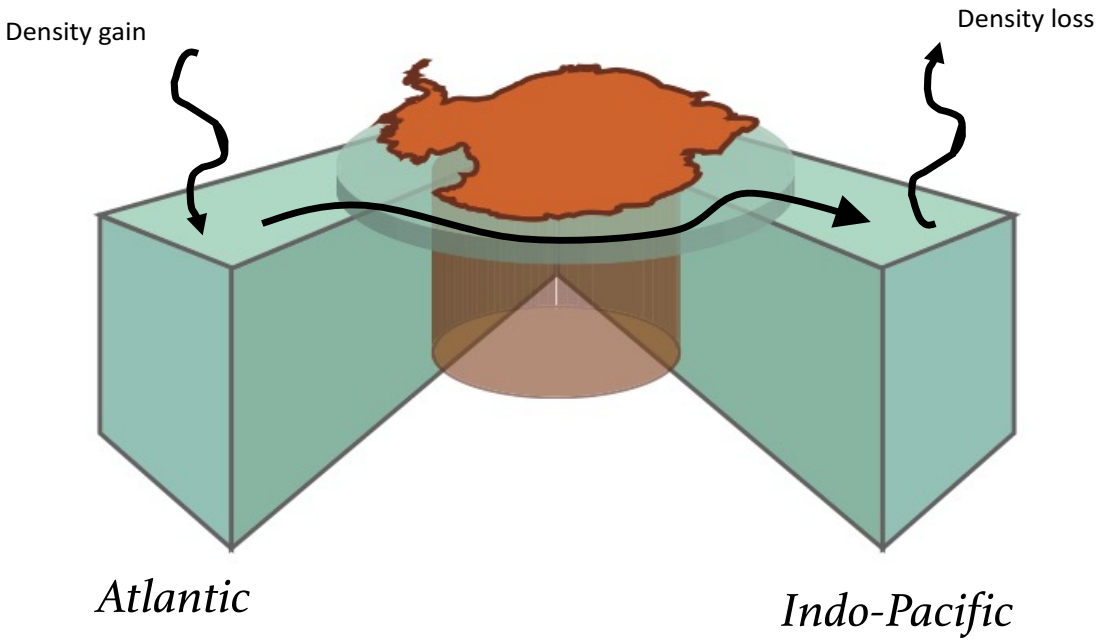

Figure 5.2.5: A schematic depiction of the mass transport pattern that, it is proposed, may be required of the ocean system because the geometry of the global ocean.

5.2.3 Closing Remarks: Revisiting Walin

Walin [1982] introduced the Water Mass Transformation Framework to understand the ocean's thermal circulation, or, as he called it, the ocean's "Hadley Cell." He argued that the meridional distribution of heat fluxes into and out of the ocean could be used to infer a meridional ocean circulation, one which eroded meridional temperature gradients. Here I propose an amendment to Walin's inference, an amendment that relies on the tools provided in his seminal study. Because of the confinement of ocean basins, the ocean's "Hadley Cell" must work to erode not only meridional, but zonal differences in surface forcing arising from Earth's complex continental geometry (this zonal transport is depicted schematically in Fig. 5.2.5). This interpretation of the ocean's role in the climate system is consistent with the many studies documenting how the circulation transports heat northward across the Equator in the Atlantic [Frierson et al., 2013, Donahoe et al., 2013]; however, it also emphasizes an equally important requirement that heat be transported southward out of the Indo-Pacific. Much work is left to be done to substantiate this proposal, including a detailed analysis of the

interactions of the ocean's thermal and hydrological cycles, which must together enable this transport. Yet, despite the work left to come, this dissertation has shown that to appreciate the role of the Global Overturning Circulation in the climate system, we must acknowledge its complex thermodynamic interactions with the atmosphere over its global domain.

Bibliography

Abernathey, R., J. Marshall, and D. Ferreira
2011. The Dependence of Southern Ocean Meridional Overturning on Wind Stress. *Journal of Physical Oceanography*, 41(12):2261–2278.

Abernathey, R. and C. Wortham
2015. Phase Speed Cross Spectra of Eddy Heat Fluxes in the Eastern Pacific. *Journal of Physical Oceanography*, (2010):150218133543002.

Abernathey, R. P., I. Cerovecki, P. R. Holland, E. Newsom, M. Mazloff, and L. D. Talley
2016. *Water-mass transformation by sea ice in the upper branch of the Southern Ocean overturning*, volume 9.

Abraham, J. P., C. M. Domingues, J. T. Fasullo, J. Gilson, G. Goni, S. A. Good, and J. M. Gorman
2013. A Review of Global Ocean Temperature Observations: Implications for Ocean Heat Content Estimates and Climate Change. *Reviews of Geophysics*, 51(3):450–483.

Armour, K. C., C. M. Bitz, and G. H. Roe
2013. Time-Varying Climate Sensitivity from Regional Feedbacks. *Journal of Climate*, 26(13):4518–4534.

Armour, K. C., J. Marshall, J. R. Scott, A. Donohoe, and E. R. Newsom
2016. Southern Ocean warming delayed by circumpolar upwelling and equatorward transport. *Nature Geoscience*, 9(7):549–554.

Ballarotta, M., S. Drijfhout, T. Kuhlbrodt, and K. Döös
2013. The residual circulation of the Southern Ocean : Which spatio-temporal scales are needed? *Ocean Modelling*, 64:46–55.

Banks, H. T. and J. M. Gregory
2006. Mechanisms of ocean heat uptake in a coupled climate model and the implications for tracer based predictions of ocean heat uptake. *Geophysical Research Letters*, 33(7):3–6.

Bitz, C. M. and L. M. Polvani
2012. Antarctic climate response to stratospheric ozone depletion in a fine resolution ocean climate model. *Geophysical Research Letters*, 39(20).

Bitz, C. M. and G. H. Roe
2004. A Mechanism for the High Rate of Sea Ice Thinning in the Arctic Ocean. *J. Climate*, 17:3623–3632.

Broecker, W.
1991. The Great Ocean Conveyor. *Oceanography*, 4(2):79–89.

Bryan, F.
1987. Parameter Sensitivity of Primitive Equation Ocean General Circulation Models.

Bryan, F. O., G. Danabasoglu, N. Nakashiki, Y. Yoshida, D.-H. Kim, J. Tsutsui, and S. C. Doney
2006. Response of the North Atlantic Thermohaline Circulation and Ventilation to Increasing Carbon Dioxide in CCSM3. *Journal of Climate*, 19:2382–2397.

Bryan, F. O., P. R. Gent, and R. Tomas
2014. Can Southern Ocean Eddy Effects be Parameterized in Climate Models? *Journal of Climate*, 27(2012):411–425.

Cerovečki, I., L. D. Talley, M. R. Mazloff, and G. Maze
2013. Subantarctic Mode Water Formation, Destruction, and Export in the Eddy-Permitting Southern Ocean State Estimate. *Journal of Physical Oceanography*, 43(7):1485–1511.

Cummins, P. F., G. Holloway, and E. Gargett
1990. Sensitivity of the GFDL Ocean General Circulation Model to a Parameterization of Vertical Diffusion.

Czaja, A.
2009. Atmospheric Control on the Thermohaline Circulation. *Journal of Physical Oceanography*, 39(1):234–247.

Danabasoglu, G., S. C. Bates, B. P. Briegleb, S. R. Jayne, M. Jochum, W. G. Large, S. Peacock, and S. G. Yeager
2012. The CCSM4 ocean component. *Journal of Climate*, 25:1361–1389.

Danabasoglu, G. and J. Marshall
2007. Effects of vertical variations of thickness diffusivity in an ocean general circulation model. *Ocean Modelling*, 18(2):122–141.

Danabasoglu, G. and J. C. McWilliams
1995. Sensitivity of the global ocean circulation to parameterizations of mesoscale tracer transports.

Doney
1998. Surface Ocean Fluxes and Water-Mass Transformation Rates in the Coupled NCAR Climate System Model *. (Bryan):1420–1441.

Dufour, C. O., L. L. Sommer, J. D. Zika, M. Gehlen, J. C. Orr, P. Mathiot, and B. Barnier
2012. Standing and transient eddies in the response of the Southern Ocean meridional overturning to the Southern annular mode. *Journal of Climate*, 25(20):6958–6974.

Emile-Geay, J.
2003. Warren revisited: Atmospheric freshwater fluxes and âĂIJWhy is no deep water formed in the North PacificâĂİ. *Journal of Geophysical Research*, 108(C6):3178.

Enderton, D. and J. Marshall
2009. Explorations of AtmosphereâĂŞOceanâĂŞIce Climates on an Aquaplanet and Their Meridional Energy Transports. *Journal of the Atmospheric Sciences*, 66(6):1593–1611.

Farneti, R., T. L. Delworth, A. J. Rosati, S. M. Griffies, and F. Zeng
2010. The Role of Mesoscale Eddies in the Rectification of the Southern Ocean Response to Climate Change. *Journal of Physical Oceanography*, 40(7):1539–1557.

Farneti, R., S. M. Downes, S. M. Griffies, S. J. Marsland, E. Behrens, M. Bentsen, D. Bi, A. Biastoch, C. Böning, A. Bozec, V. M. Canuto, E. Chassignet, G. Danabasoglu, S. Danilov, N. Diansky, H. Drange, P. G. Fogli, A. Gusev, R. W. Hallberg, A. Howard, M. Ilicak, T. Jung, M. Kelley, W. G. Large, A. Leboissetier, M. Long, J. Lu, S. Masina, A. Mishra, A. Navarra, a. George Nurser, L. Patara, B. L. Samuels, D. Sidorenko, H. Tsujino, P. Uotila, Q. Wang, and S. G. Yeager
2015. An assessment of Antarctic Circumpolar Current and Southern Ocean Meridional Overturning Circulation during 1958âĂŞ2007 in a suite of interannual CORE-II simulations. *Ocean Modelling*, 93:84–120.

Farneti, R., S. Dwivedi, F. Kucharski, F. Molteni, and S. M. Griffies
2014. On Pacific Subtropical Cell Variability over the Second Half of the Twentieth Century. *Journal of Climate*, 27(18):7102–7112.

Ferrari, R. and D. Ferreira
2011. What processes drive the ocean heat transport? *Ocean Modelling*, 38(3-4):171–186.

Frierson, D. M. W., Y.-T. Hwang, N. S. Fučkar, R. Seager, S. M. Kang, A. Donohoe, E. a. Maroon, X. Liu, and D. S. Battisti
2013. Contribution of ocean overturning circulation to tropical rainfall peak in the Northern Hemisphere. *Nature Geoscience*, (October):1–5.

Fukamachi, Y., S. R. Rintoul, J. A. Church, S. Aoki, S. Sokolov, M. A. Rosenberg, and M. Wakatsuchi
2010. Strong export of Antarctic Bottom Water east of the Kerguelen plateau. *Nature Geoscience*, 3(5):327–331.

Garabato, A. C. N., K. L. Polzin, B. a. King, K. J. Heywood, and M. Visbeck
2004. Widespread Intense Turbulent Mixing in the Southern Ocean. *Science*, 303:210–213.

Garabato, A. C. N., D. P. Stevens, A. J. Watson, and W. Roether
2007. Short-circuiting of the overturning circulation in the Antarctic Circumpolar Current. *Nature*, 447(7141):194–197.

Garrett, C.
1995. Transformation in the red sea.

Gebbie, G. and P. Huybers
2012. The Mean Age of Ocean Waters Inferred from Radiocarbon Observations: Sensitivity to Surface Sources and Accounting for Mixing Histories. *Journal of Physical Oceanography*, 42(2):291–305.

Gent, P. R.
2015. Effects of Southern Hemisphere Wind Changes on the Meridional Overturning Circulation in Ocean Models. *Annual Review of Marine Science*, Pp. 1–34.

Gent, P. R. and G. Danabasoglu
2011. Response to increasing Southern Hemisphere winds in CCSM4. *Journal of Climate*, 24(19):4992–4998.

Gent, P. R. and J. C. McWilliams
1990. Isopycnal Mixing in Ocean Circulation Models.

Gent, P. R., S. G. Yeager, R. B. Neale, S. Levis, and D. a. Bailey
2010. Improvements in a half degree atmosphere/land version of the CCSM. *Climate Dynamics*, 34:819–833.

Gnanadesikan, a.
1999. A Simple Predictive Model for the Structure of the Oceanic Pycnocline. *Science*, 283(5410):2077–2079.

Gnanadesikan, A., M.-a. Pradal, and R. Abernathey
2015. Isopycnal mixing by mesoscale eddies significantly impacts oceanic anthropogenic carbon uptake. *Geophys. Res. Lett.*, (May).

Gordon, A. L.
2001. Bottom water formation. In *Encyclopedia of Ocean Sciences*, J. Steele, K. Turekian, and S. Thorpe, eds., number 1995, Pp. 334–340.

Gregory, J. M.
2000. Vertical heat transports in the ocean and their effect on time-dependent climate change. *Climate Dynamics*.

Griffies, S. M., R. C. Pacanowski, and R. W. Hallberg
2000. Spurious Diapycnal Mixing Associated with Advection in a z-Coordinate Ocean Model. (Levitus 1982):538–564.

Griffies, S. M., M. Winton, W. G. Anderson, R. Benson, T. L. Delworth, C. O. Dufour, J. P. Dunne, P. Goddard, A. K. Morrison, A. Rosati, A. T. Wittenberg, J. Yin, and R. Zhang
2015. Impacts on Ocean Heat from Transient Mesoscale Eddies in a Hierarchy of Climate Models. *Journal of Climate*, 28(3):952–977.

Hallberg, R. and A. Gnanadesikan
2006. The Role of Eddies in Determining the Structure and Response of the Wind-Driven Southern Hemisphere Overturning: Results from the Modeling Eddies in the Southern Ocean (MESO) Project.

Hansen, J., G. Russell, A. Lacis, I. Fung, and D. Rind
1985. Climate Response Times: Dependence on Climate Sensitivity and Ocean Mixing. *Science*, 229:857–859.

Held, I. M., M. Winton, K. Takahashi, T. Delworth, F. Zeng, and G. K. Vallis
2010. Probing the Fast and Slow Components of Global Warming by Returning Abruptly to Preindustrial Forcing. *Journal of Climate*, 23(9):2418–2427.

Henning, C. C. and G. K. Vallis
2005. The Effects of Mesoscale Eddies on the Stratification and Transport of an Ocean with a Circumpolar Channel.

Heuzé, C., K. J. Heywood, D. P. Stevens, and J. K. Ridley
2013. Southern Ocean bottom water characteristics in CMIP5 models. *Geophysical Research Letters*, 40(7):1409–1414.

Hill, C., D. Ferreira, J. M. Campin, J. Marshall, R. Abernathey, and N. Barrier
2012. Controlling spurious diapycnal mixing in eddy-resolving height-coordinate ocean models - Insights from virtual deliberate tracer release experiments. *Ocean Modelling*, 45-46:14–26.

Howe, N. and A. Czaja
2009. A New Climatology of AirâĂŞSea Density Fluxes and Surface Water Mass Transformation Rates Constrained by WOCE. *Journal of Physical Oceanography*, 39(6):1432–1447.

Ito, T. and J. Marshall
2008. Control of Lower-Limb Overturning Circulation in the Southern Ocean by Diapycnal Mixing and Mesoscale Eddy Transfer. *Journal of Physical Oceanography*, 38(12):2832–2845.

Iudicone, D., G. Madec, and T. J. McDougall
2008. Water-mass transformations in a neutral density framework and the key role of light penetration. *Journal of Physical Oceanography*, 38:1357–1376.

Jacobs, S. S.
2004. Bottom water production and its links with the thermohaline circulation. *Antarctic Science*, 16(4):427–437.

Jayne, S. R.
2009. The Impact of Abyssal Mixing Parameterizations in an Ocean General Circulation Model. *Journal of Physical Oceanography*, 39(7):1756–1775.

Jochum, M. and C. Eden
2015. The connection between Southern Ocean winds, the Atlantic Meridional overturning circulation, and Indo-Pacific upwelling. *Journal of Climate*, 28(23):9250–9257.

Johnson, G. C.
2008. Quantifying Antarctic Bottom Water and North Atlantic Deep Water volumes. *Journal of Geophysical Research: Oceans*, 113(August 2007):1–13.

Kirkman IV, C. H. and C. M. Bitz
2011. The Effect of the Sea Ice Freshwater Flux on Southern Ocean Temperatures in CCSM3: Deep-Ocean Warming and Delayed Surface Warming. *Journal of Climate*, 24(9):2224–2237.

Kirtman, B. P., C. Bitz, F. Bryan, W. Collins, J. Dennis, N. Hearn, J. L. Kinter, R. Loft, C. Rousset, L. Siqueira, C. Stan, R. Tomas, and M. Vertenstein
2012. Impact of ocean model resolution on CCSM climate simulations. *Climate Dynamics*, 39(6):1303–1328.

Kostov, Y., K. C. Armour, and J. Marshall
2014. Impact of the Atlantic Meridional Overturning Circulation on Ocean Heat Storage and Transient Climate Change. *Geophysical Research Letters*.

Kuhlbrodt, T., J. M. Gregory, and L. C. Shaffrey
2014. A process-based analysis of ocean heat uptake in an AOGCM with an eddy-permitting ocean component. *Climate Dynamics*, P. submitted.

Langehaug, H. R., P. B. Rhines, T. Eldevik, J. Mignot, and K. Lohmann
2012. Water mass transformation and the North Atlantic Current in three multicentury climate model simulations. *Journal of Geophysical Research: Oceans*, 117(11):1–22.

Lavergne, C. D., J. B. Palter, E. D. Galbraith, R. Bernardello, and I. Marinov
2014. Cessation of deep convection in the open Southern Ocean under anthropogenic climate change. (March).

Levitus, S., J. I. Antonov, J. Wang, T. L. Delworth, K. W. Dixon, and a. J. Broccoli
2001. Anthropogenic warming of Earth's climate system. *Science*, 292:267–270.

Lozier, M. S.
2010. Deconstructing the Conveyor Belt. *Science*, 328(5985):1507–1511.

Lumpkin, R. and K. Speer
2007. Global Ocean Meridional Overturning. *Journal of Physical Oceanography*, 37(10):2550–2562.

Marsh, R., A. Nurser, A. Megann, and A. New
2000. Water mass transformation in the Southern Ocean of a global isopycnal coordinate GCM. *Journal of Physical Oceanography*, 30(5):1013–1045.

Marshall, J., K. C. Armour, J. R. Scott, Y. Kostov, U. Hausmann, D. Ferreira, T. G. Shepherd, C. M. Bitz, and P. T. R. S. A
2014. The ocean ' s role in polar climate change : asymmetric Arctic and Antarctic responses to greenhouse gas and ozone forcing The ocean âĂŹ s role in polar climate change : asymmetric Arctic and Antarctic responses to greenhouse gas and ozone forcing. *Philosophical Transactions of the Royal Society A*.

Marshall, J., D. Jamous, and J. Nilsson
1999. Reconciling thermodynamic and dynamic methods of computation of water-mass transformation rates. *Deep-Sea Research Part I: Oceanographic Research Papers*, 46(4):545–572.

Marshall, J. and T. Radko
2003. Residual-Mean Solutions for the Antarctic Circumpolar Current and Its Associated Overturning Circulation. *Journal of Physical Oceanography*, 33(11):2341–2354.

Marshall, J. and K. Speer
2012. Closure of the meridional overturning circulation through Southern Ocean upwelling. *Nature Geoscience*, 5(3):171–180.

Maykut, G. a.
1982. Large-scale heat exchange and ice production in the central Arctic. *Journal of Geophysical Research*, 87(C10):7971.

McDougall, T. J. and C. J. R. Garrett
1992. Scalar conservation equations in a turbulent ocean. *Deep Sea Research Part A, Oceanographic Research Papers*, 39(11-12):1953–1966.

Morrison, A. K., A. M. Hogg, and M. L. Ward
2011. Sensitivity of the Southern Ocean overturning circulation to surface buoyancy forcing. *Geophysical Research Letters*, 38(14):n/a–n/a.

Munday, D. R., H. L. Johnson, and D. P. Marshall
2013. Eddy Saturation of Equilibrated Circumpolar Currents. *Journal of Physical Oceanography*, 43(3):507–532.

Munk, W. H.
1966. Abyssal recipes. *Deep Sea Research and Oceanographic Abstracts*, 13(4):707–730.

Newsom, E. R., C. M. Bitz, F. O. Bryan, R. Abernathey, and P. R. Gent
2016. Southern Ocean Deep Circulation and Heat Uptake in a High-Resolution Climate Model. *Journal of Climate*, P. 160204142426002.

Nicholls, K. W., S. Østerhus, and K. Makinson
2009. ... over the continental shelf of the southern Weddell Sea, Antarctica: A review. *... of Geophysics*, (2007):1–23.

Nikurashin, M. and G. Vallis
2011. A Theory of Deep Stratification and Overturning Circulation in the Ocean. *Journal of Physical Oceanography*, 41(3):485–502.

Nikurashin, M. and G. Vallis
2012. A Theory of the Interhemispheric Meridional Overturning Circulation and Associated Stratification. *Journal of Physical Oceanography*, 42(10):1652–1667.

Nilsson, J., P. L. Langen, D. Ferreira, and J. Marshall
2013. Ocean Basin Geometry and the Salinification of the Atlantic Ocean. *Journal of Climate*, 26(16):6163–6184.

Orsi, a., G. Johnson, and J. Bullister
1999. Circulation, mixing, and production of Antarctic Bottom Water. *Progress in Oceanography*, 43(1):55–109.

Pradal, M.-A. and A. Gnanadesikan
2014. How does the redi parameter for mesoscale mixing impact global climate in an earth system model? *Journal of Advances in Modeling Earth Systems*, 6:513–526.

Purkey, S. G. and G. C. Johnson
2010. Warming of Global Abyssal and Deep Southern Ocean Waters between the 1990s and 2000s: Contributions to Global Heat and Sea Level Rise Budgets*. *Journal of Climate*, 23(23):6336–6351.

Purkey, S. G. and G. C. Johnson
2013. Antarctic Bottom Water Warming and Freshening: Contributions to Sea Level Rise, Ocean Freshwater Budgets, and Global Heat Gain*. *Journal of Climate*, 26(16):6105–6122.

Radko, T. and I. Kamenkovich
2011. Semi-Adiabatic Model of the Deep Stratification and Meridional Overturning. *Journal of Physical Oceanography*, 41(4):757–780.

Radko, T., I. Kamenkovich, and P.-Y. Dare
2008. Inferring the Pattern of the Oceanic Meridional Transport from the AirâĂŞSea Density Flux. *Journal of Physical Oceanography*, 38(12):2722–2738.

Raper, S., J. M. Gregory, and R. J. Stouffer
2002. The Role of Climate Sensitivity and Ocean Heat Uptake on AOGCM Transient Temperature Response. *Journal of Climate*, 15:124–130.

Redi, M.
1982. Oceanic isopycnal mixing by coordinate rotation.

Rugenstein, M. a. a., M. Winton, R. J. Stouffer, S. M. Griffies, and R. Hallberg
2013. Northern High-Latitude Heat Budget Decomposition and Transient Warming. *Journal of Climate*, 26(2):609–621.

Schanze, J. J. and R. W. Schmitt
2013. Estimates of Cabbeling in the Global Ocean. *Journal of Physical Oceanography*, 43(4):698–705.

Shakespeare, C. J. and A. McC. Hogg
2012. An Analytical Model of the Response of the Meridional Overturning Circulation to Changes in Wind and Buoyancy Forcing. *Journal of Physical Oceanography*, 42(8):1270–1287.

Sinha, B., A. T. Blaker, J. J.-M. Hirschi, S. Bonham, M. Brand, S. Josey, R. S. Smith, and J. Marotzke
2012. Mountain ranges favour vigorous Atlantic meridional overturning. *Geophysical Research Letters*, 39(2).

Smith, R. D., M. E. Maltrud, F. O. Bryan, M. W. Hecht, and L. Alamos
2000. Numerical simulation of the North Atlantic Ocean at 1/10 degrees. *Journal of Physical Oceanography*, 30(7):1532–1561.

Snow, K., A. M. Hogg, S. M. Downes, B. M. Sloyan, M. L. Bates, and S. M. Griffies
2015. Sensitivity of abyssal water masses to overflow parameterisations. *Ocean Modelling*, 89:84–103.

Speer, K., H.-J. Isemer, and A. Biastoch
1995. Water Mass Formation from Revised COADS Data.

Speer, K. and E. Tziperman
1992. Rates of Water Mass Formation in the North Atlantic Ocean. *Journal of Physical Oceanography*, 22(1):93–104.

Stewart, a. L., R. Ferrari, and a. F. Thompson
2014. On the Importance of Surface Forcing in Conceptual Models of the Deep Ocean. *J. Phys. Oceanogr.*, 44(3):891–899.

Stewart, A. L. and A. F. Thompson
2012. Sensitivity of the ocean's deep overturning circulation to easterly Antarctic winds. *Geophysical Research Letters*, 39(18).

Stewart, A. L. and A. F. Thompson
2013. Connecting Antarctic Cross-Slope Exchange with Southern Ocean Overturning. *Journal of Physical Oceanography*, 43(7):1453–1471.

Stewart, A. L. and A. F. Thompson
2015. Eddy-mediated transport of warm Circumpolar Deep Water across the Antarctic Shelf Break. *Geophys. Res. Lett.*, 42:432–440.

Stössel, A., M. M. Stössel, and J.-T. Kim
2007. High-resolution sea ice in long-term global ocean GCM integrations. *Ocean Modelling*, 16(3-4):206–223.

Talley, L. D.
2013. The official magazine of the oceanography society. 26(1):80–97.

Thomas, L. N. and C. J. Shakespeare
2015. A New Mechanism for Mode Water Formation involving Cabbeling and Frontogenetic Strain at Thermohaline Fronts. *Journal of Physical Oceanography*, P. 150805113336000.

Thompson, A. F. and A. C. Naveira Garabato
2014. Equilibration of the Antarctic Circumpolar Current by Standing Meanders. *Journal of Physical Oceanography*, 44(7):1811–1828.

Thompson, A. F. and A. L. Stewart
. A multi-basin residual-mean model for the global overturning circulation.

Toggweiler, J. R. and B. Samuels
1995. Effect of drake passage on the global thermohaline circulation. *Deep-Sea Research Part I*, 42(4):477–500.

Togweiller
. Effect of Sea ice on AABW salinity.

Urakawa, L. S. and H. Hasumi
2012. Eddy-Resolving Model Estimate of the Cabbeling Effect on the Water Mass Transformation in the Southern Ocean. *Journal of Physical Oceanography*, 42(8):1288–1302.

Urakawa, L. S. and H. Hasumi
2014. Effect of numerical diffusion on the water mass transformation in eddy-resolving models. *Ocean Modelling*, 74:22–35.

Walin, B. G.
1982. On the relation between sea-surface heat flow and thermal circulation in the ocean. *Tellus*, 32:187–195.

Warren, B. A.
1983. Why is no deep water formed in the North Pacific ? Pp. 327–347.

Willmott, A. J., D. M. Holland, and M. A. Morales Maqueda
2007. Polynya Modelling. In *Polynyas: Windows to the World*, W. Smith and D. Barber, eds.

Winton, M., W. G. Anderson, T. L. Delworth, S. M. Griffies, William J. Hurlin, and A. J. Rosati
2014. Has coarse ocean resolution biased simulations of transient climate sensitivity? *Geophysical Research Letters*, 41:8522–8529.

Winton, M., K. Takahashi, and I. M. Held
2010. Importance of Ocean Heat Uptake Efficacy to Transient Climate Change. *Journal of Climate*, 23(9):2333–2344.

Wolfe, C. L. and P. Cessi
2011. The Adiabatic Pole-to-Pole Overturning Circulation. *Journal of Physical Oceanography*, 41(9):1795–1810.

Wolfe, C. L. and P. Cessi
2015. Multiple regimes and low-frequency variability in the quasi-adiabatic overturning circulation. *Journal of Physical Oceanography*, (2005):150417113154006.

Xie, P. and G. K. Vallis
2012. The passive and active nature of ocean heat uptake in idealized climate change experiments. *Climate Dynamics*, 38:667–684.

Xu, X., P. B. Rhines, and E. P. Chassignet
2016. TemperatureâĂŞSalinity Structure of the North Atlantic Circulation and Associated Heat and Freshwater Transports. *Journal of Climate*, 29(21):7723–7742.

Zhang, Y. and G. K. Vallis
2013. Ocean Heat Uptake in Eddying and Non-Eddying Ocean Circulation Models in a Warming Climate. *Journal of Physical Oceanography*, 43(10):2211–2229.

Zika, J. D., M. H. England, and W. P. Sijp
2012. The Ocean Circulation in Thermohaline Coordinates. *Journal of Physical Oceanography*, 42(5):708–724.